DESIGN & SIMULATION OF THE ENGINE OUT VIRTUAL NOX AND SOOT SENSOR FOR DIESEL ENGINES

by

Mahesh S. Shewale

A Dissertation

Submitted to the Faculty of Purdue University

In Partial Fulfillment of the Requirements for the degree of

Doctor of Philosophy

School of Mechanical Engineering

West Lafayette, Indiana

May 2022

THE PURDUE UNIVERSITY GRADUATE SCHOOL
STATEMENT OF COMMITTEE APPROVAL

Dr. Ali Razban, Co-Chair

Department of Mechanical & Energy Engineering, IUPUI

Dr. Galen King, Co-Chair

School of Mechanical Engineering

Dr. Gregory Shaver

School of Mechanical Engineering

Dr. Maher Rizkalla

Department of Electrical & Computer Engineering, IUPUI

Approved by:

Dr. Nicole Key

In memory of my beloved dad...

Mr. Shivaji Ramchandra Shewale

ACKNOWLEDGMENTS

I would like to express my deepest appreciation to Dr. Ali Razban, who has not only supported me throughout this journey but also enhanced my vision to look over the horizon. I'm extremely grateful to my doctoral committee members, Dr. Galen King, Dr. Gregory Shaver and Dr. Maher Rizkalla for their constant support and constructive feedback on my work. I'm also deeply indebted to Dr. Mohamed Razi Nalim for his continuous support and suggestions that have improved the quality of this work significantly.

I'd sincerely thank Jerry Mooney, Linda Wright, Monica Stahlhut, Susan James at IUPUI and Cathy Elwell at West Lafayette for their administrative support and advise. I'm also thankful to Michael Golub and Robert Meagher (CNC) for their efforts in providing required software support. I'd like to express my gratitude to my colleague, Vaibhav Ahire for his continuous support in this work.

This journey wouldn't have been possible without the support of my wife, Preeti who has unconditionally sacrificed many things in this journey. Last but not the least, my family and friends in India as well as USA have been always supportive during my PhD.

TABLE OF CONTENTS

LIST OF TABLES

LIST OF FIGURES

LIST OF SYMBOLS

Notations

A	Area (m^2)
BSR	Blade speed ratio
c_p	Specific heat capacity at constant pressure (J/kgK)
c_v	Specific heat capacity at constant volume (J/kgK)
C_D	Coefficient of discharge
C_A	Area contraction coefficient
C_V	Velocity coefficient (m^2)
J	Inertia (kgm^2)
n_{cyl}	Number of cylinders
n_e	Engine rotational speed (rpm)
n_t	Turbine rotational Speed (rpm)
$(O/F)_s$	Stoichiometric oxygen-to-fuel ratio
p	Pressure (Pa)
P	Power (W)
q_{HV}	Heating value of fuel (J/kg)
r_c	Compression ratio
R	Gas constant (J/kgK)
T	Temperature (K)
u	Control input
V	Volume (m^3)
W	Mass flow rate (kg/s)
x_{egr}	EGR fraction
X_O	Oxygen mass fraction
γ	Specific heat capacity ratio
η	Efficiency
λ_O	Oxygen-to-fuel ratio (m^2)
Π	Pressure ratio (m^2)

ρ	Density (kg/m^3)
τ	Time constant (s)
ϕ_c	Volumetric flow coefficient
ϕ	Equivalence ratio
ψ	Energy transfer coefficient
ω	Rotational speed (rad/s)
z	Piston position from TDC (m)
l	Length of connecting rod (m)
a	Crank radius (m)
θ	Crank angle ($^\circ$)
s	Instantaneous pin position (m)
V_c	Clearance volume (m^3)
B	Cylinder bore diameter (m)
P_{motor}	Motoring pressure (Pa)
T_{motor}	Motoring Temperature (K)
x_b	Mass burnt fraction
$\tau_{\mathrm{i}g}$	Ignition delay (s)
Q_{hr}	Total heat release (kJ)
Q_{ht}	Heat transferred (kJ)
U	Internal energy (kJ)
h	Enthalpy (kJ)
$V_{b,\mathrm{i}}$	Reaction zone volume (m^3)
$m_{b,\mathrm{i}}$	Burnt stoichiometry mass (kg)
C_{rad}	Radiation constant (m^2)

Subscripts

a	air
amb	ambient
c	compressor

d	displaced
e	exhaust
$[\ ]_e$	Concentration at equilibrium
egr	exhaust gas recirculation
ei	engine cylinder in
em	exhaust manifold
eo	engine cylinder out
f	fuel
ig	indicated gross
im	intake manifold
m	mechanical
t	turbine
$totem$	total exhaust manifold
$totim$	total intake manifold
vgt	variable geometry turbine
vol	volumetric
δ	fuel injection
rad	radiation
ad	adiabatic
NO	NOx
$comb$	combustion
$motor$	motoring
hr	heat release
ht	heat transfer
$prod$	Products
$react$	Reactants

ABBREVIATIONS

AHRR	Apparent Heat Release Rate
ANN	Artificial Neural Network
ATS	After Treatment System
BTS	Bureau of Transportation Statistics
CAA	Clean Air Act
CI	Compression Ignition
CO	Carbon Monoxide
CO_2	Carbon Dioxide
DPF	Diesel Particulate Filter
ECU	Engine Control Unit
EGR	Exhaust Gas Recirculation
EO	Engine Outm
EOI	End of Injection
EPA	Environmental Protection Agency
ESC	European Steady State Cycle
ETC	European Transient Cycle
FHWA	Federal Highway Administration
FTP	Federal Test Procedures
GT Suite	Gamma Technologies Suite
HC	Hydrocarbon
HCN	Hydrogen Cyanide
HDE	Heavy Duty Engines
HDV	Heavy Duty Vehicles
HiL	Hardware in Loop
HRR	Heat Release Rate
IC	Internal Combustion
IMEP	Indicated Mean Effective Pressure
IVC	Intake Valve Close

IVO	Intake Valve Open
JANAF	Joint Army-Navy-NASA-Air Force
LL	Liquid Length
LOL	Lift-Off Length
LPF	Low Pass Filter
MARE	Mean Absolute Relative Error
MFB	Mass Fractions Burnt
MiL	Model in Loop
N_2	Nitrogen molecule
N_2O	Nitrous Oxide
NASA	National Aeronautics and Space Administration
NO	Nitric Oxide
NOx	Nitrogen Oxides
OBD	On-board Diagnostics
OH	Hydroxide
OICA	Organisation Internationale des Constructeurs d'Automobiles
ROHR	Rate of Heat Release Rate
SCR	Selective Catalytic Reduction
SiL	Software in Loop
SOC	Start of Combustion
SOI	Start of Injection
TDC	Top Dead Center
UHC	Unburnt Hydrocarbon
UNECE	United Nations Economic Commission for Europe
US	United States
VGT	Variable Geometry Turbine
VMT	Vehicle Miles Travelled
VNT	Variable Nozzle Turbine
VOC	Volatile Organic Compounds

VVA	Variable Valve Actuation
VVT	Variable Valve Turbine
WHSC	World Harmonized Stationary Cycle

ABSTRACT

The automotive field has been into a transitioning phase since stringent emission norms have been imposed by various authorities all over the world. To comply with these regulations, automotive manufacturers are coming up with new technologies and components. On the other side, there are certain issues related to the performance of various sensors used to measure engine-out emissions. Novel concepts related to combustion like the Miller cycle and low-temperature high exhaust gas recirculation (EGR) fraction are highly tested on new vehicles. These new concepts heavily depend on in-cylinder parameters like chemical composition, temperature, pressure, and flame characteristics. This leads to a complex and non-transparent engine control systems as diesel combustion itself is a complex phenomenon.

This research work aspires to establish a physics-based control-oriented diesel engine combustion model to estimate in-cylinder states like a mass burnt fraction (MFB), rate of heat release (ROHR), and cylinder pressure traces based on crank angle degree (CAD). Further, comprehensive prediction models are to be designed for NOx and soot based on these states. Additionally, the impact of exhaust gas recirculation (EGR) and turbo fractions on mass exchange in the cylinder during combustion also needs to be covered to make the model more realistic. A chemical kinetics model for diesel combustion based on reactants and products involved in the combustion chemistry needs to be developed to determine the concentrations of products formed during the constant pressure and constant volume adiabatic process. This analysis is focused on the prediction of nitric oxides (NOx) and soot based on the Extended Zeldovich mechanism and Hiroyasu Kadota approach respectively.

EGR significantly reduces the post flame NOx formation by introducing burnt and unburnt fractions from the exhaust gases. These gases reduce the oxygen concentration during the combustion and ultimately reducing the flame temperatures. An appropriate control strategy is to be developed to control the EGR fractions to maintain the NOx levels within the legislative limits. Additionally, fuel consumption and turbo control are needed for the optimized NOx control and fuel economy without affecting the engine performance.

The proposed soot prediction model is established based on component level approach using MATLAB-Simulink as a programing tool. Some of the different subsystems involved

in this model are – properties of injector nozzle, rate of heat release, in-cylinder temperature and pressure history, injection velocity of fuel jet and rate of fuel flow during the engine cycle.

The conventional approach of state space design has been adopted to derive mathematical models for both NOx and soot models. As NOx model has multiple input and outputs, it is further simplified and linearized to obtain SISO system. A state feedback controller is designed for NOx model and PI controller for soot model based on the system requirements.

Model validation is to be done by comparing the results to the high-fidelity GT-Power model controlled with the appropriate controller designed in the work. This GT-Power model has been developed for considering Cummins 6.7L diesel engine as a benchmark and results have been obtained for the same. The conceptual results prove the approach selected for modeling is correct as they agree with the theory behind it.

The obtained results from both uncontrolled predictive model and controlled model have been compared with GT-Suite reference data for both NOx and soot in steady state and transient test cases. The controlled response shows good response with reference data with an accuracy around 2% and shows root mean square errors within acceptable limits below 0.5.

The developed model for both NOx and soot integrated with control system approach has significant advantage over the reference model developed in GT-Suite. The time taken by GT-Suite model is significantly higher and thus are not suitable for real time application. On the contrary, the proposed approach uses a real time prediction of engine out emission and can readily be used in vehicles with minor modifications.

1. INTRODUCTION

Majority of the automotive field throughout the world is embracing new strict vehicle emission norms that demand reduction in exhaust constraints. The purpose of these norms is to minimize engine out and tailpipe emissions from automobiles in action in maximum standard driving conditions and to enhance air quality as well as human health. The important aspect to consider is if vehicle emits less pollutants when it is new and during most of its working lifespan. On the other hand, several studies have concluded that a majority of the vehicles generate pollutants on larger scale during on-road operating conditions than when they are actually tested in lab [1].

Numerous features may cause a rise like this in emissions like engine design parameters, operational mode, and fuel properties. The emission controller architecture may not be correctly derived or can have certain drawbacks in certain operating conditions [1]. Sometimes the manufacturers may utilize different parts add production level than the ones used for approval testing. Furthermore, the control of engine out and tailpipe emission gases deteriorates over the lifespan because of extended maintenance. if poor quality components and parts are used emission levels for that particular automobile can increase in uncontrolled manner. Few of the actual test cases are difficult or put more efforts on engine systems than the ones used during approval testing. These conditions may include very hot or cold weather, improper roads, higher elevations, improper driving etc. The primary architecture of few pollution control methods May be developed to work under restricted test scenarios inside the laboratory. Improper design of approval testing for on road driving conditions can permit such designs. A more detailed and clear reason is by using defeat devices that can avoid or falsify the emission norms. A properly designed automobile emission control program must fulfill all of these manufacturing related problems.

Since last few years, U.S. Clean Air Act (CAA) was established in 1963 And regulatory authorities from U.S. Environmental Protection Agency (EPA) and the California Air Resources Board (CARB) have established thorough and complicated norms and recall procedures. These norms consist of multiple subprograms to identify and check the violation of emission regulations. Engine companies are continuously pushed by policymakers and the

automotive market to come up with engine and related products to be more environment friendly and more fuel efficient. To comply with these demands engine systems turn out to be more complicated with additional actuators and therefore more variables are needed to be calibrated. As the resources and time needed for calibration increases exponentially with respect to the increase in number of variables, the control design for these systems is becoming a hurdle in further development procedures [2]. To maintain a competitive environment and follow with the norms engine systems must make optimum utilization of their complex and high-cost actuators. Another problem is with the reduction of emission targets a bigger section of total drive cycle pollutants is due to the sudden changes during transient operation. The reason for the generation of these spikes being the sudden rise in in cylinder conditions due to sudden change in fuel input. In earlier years, it was sufficient for the engine systems to be calibrated for steady speeds but in future careful attention and more resources need to be utilized on the transient behavior of engine as it may lead to an increase in emissions and deteriorate the performance of the engine over the long run.

Several methods for calibration of engine systems have been developed like model-based calibration and design of experiments which rely on a lot of statistical data to be processed. One of the solutions towards the challenge is in calibration can be to add more sensors to the engine. Due to this addition of more sensors, more data flows in and focus may be shifted from offline calibration to real time control with closed loop feedback system. As an alternative to detailed pre-calibrated maps fine tuning off actuator configuration that can enhance the performance of engine parameters can be done in real time. To that intent sensors that can offer data on system level objectives such as fuel consumption and pollutant control are required. Nowadays real time control of engine system and its components relies significantly on indirect measurements like the flow rate of mass inside exhaust manifold. Physical sensors for NOx measurement are located at different positions in the engine system as well as after treatment devices. However these sensors are located downstream of turbine where the pressure and temperature are observed to be less. As a result, they can only record low pass filtered, cylinder averaged data throughout an engine cycle and there is a need of instantaneous signal output. The sensors used for soot measurement have recently

being utilized at tailpipe end but their response and accuracy is observed to be significantly insufficient for having real time control of engine system and makes it more complex [2].

To comply with the latest regulations in diesel engines a very intricate after treatment technologies have been established. Few to name are selective catalytic reduction (SCR) and lean NOX trap (LNT). SCR control architecture demands for sentencing of NOx upstream as well as downstream of the SCR unit. This is required to find out the exact quantity of urea to be inserted and also to prevent ammonia slip. Physical sensors that are normally utilized for this application deliver direct sensing of relative air fuel ratio and have a critical impact on the control architectural design for SCR. However in cases where these physical sensors are either too expensive or unrealistic, virtual sensors can be employed. In this scenario, a sensor is generally placed at the outlet of SCR to log the amount of NOx and ammonia slip And at the same time the control architecture for the injection of urea quantity is designed using virtual sensor to determine NOx at SCR inlet.

The virtual sensors are based on fast running real time mathematical models with quick dynamic response and also have offline estimation capabilities. These are a good choice to minimize hardware complexity of the engine management system and can be very efficiently used in cases where direct measurement of non-measurable signals is not possible. Another case where it can be employed is where the existing physical sensor cannot guarantee the required sensing attributes. Therefore, there is need to develop these sorts of mathematical models that would explain the entire engine operation concerning desired outputs when certain inputs are provided.

The involvement of thermochemical and fluid dynamic processes is the reason for the modeling of engine system to be complicated task. Therefore on board processing and control algorithms should be fast enough to ensure the required performance. The current state of the art work majorly depends on calibration maps or regression models that requires huge datasets to be stored in the memory [3].

Unlike spark-ignited engines where the flammable air fuel mix is primarily uniform, diesel combustion process varies. The diesel fuel is injected from the nozzle orifice into the combustion cylinder and further undergoes the compression stroke. The emission gases as a result of this combustion process depend on existing conditions not only during the combustion

phase but also during the expansion stroke and specifically before the opening of the exhaust valve. Different properties of air fuel mixture like engine design, expansion time, combustion temperatures, fuel ignition quality, ignition delay play a critical role in the pollutant formation mechanisms [4]. Specifically, the concentration of various species in the reactants and products of the combustion have a significant impact on their own generation and variation in exhaust gases. Products of incomplete combustion such as particulate matter generated in initial stages of combustion usually get oxidized in final stage of the engine drive cycle. Further combustion is assisted by different factors like sufficient residence time for oxidation, higher in cylinder temperatures, end mixing of on board hydrocarbons with remaining air. In many cases initially when nitric oxide is generated it does not breakdown further but there are more chances for increasing its concentration during remaining drive cycle if the temperatures remain higher [5]. So to contemplate the mathematical representation and analysis of this entire phenomenon, comprehensive predictive models are needed to be developed. It is necessary to represent all the processes and their relationships starting right from air-fuel mass entering into intake manifold till the oxidized mass going out from exhaust manifold at the end of the cycle.

Figure **fig1p1** shows the origination zones of unburned hydrocarbons (HC) and NO in direct-injected diesel engines. The concentration of species produced in both the premixed (uncontrolled) and diffusion (mixing controlled) combustion phases are displayed.

1.1 NOx Modeling Approaches

Combustion processes for certain fuels do not include nitrogen. In these cases, NOx the theme is generated by four distinct mechanisms that draw nitrogen from air as mentioned below:

- Fenimore or prompt mechanism
- N2O-intermediate mechanism
- NNH mechanism
- Thermal or Zeldovich mechanism

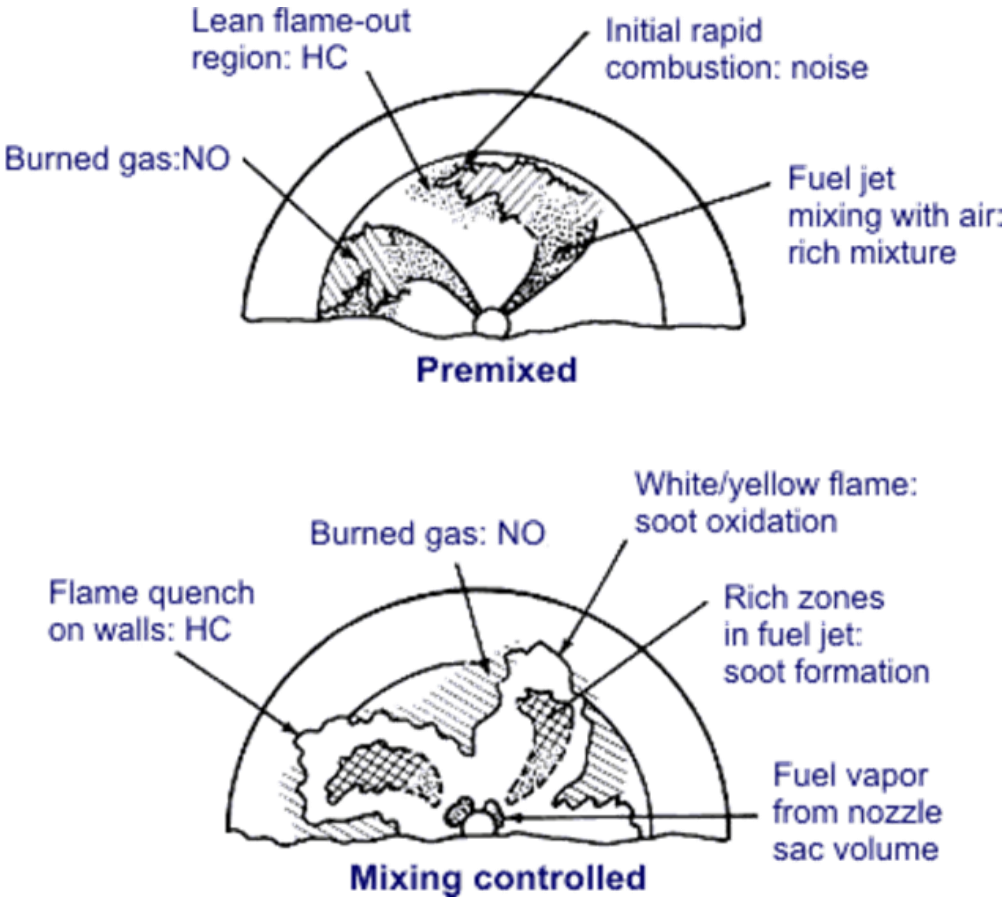

Figure 1.1. Pollutant formation mechanisms in DI combustion system [6]

1.1.1 Fenimore Mechanism

This mechanism considers the chemical interaction of hydrocarbon molecules during the combustion process. Fenimore discovered that some part of NO what's quickly formed around the flames zone in premixed laminar flame way before there is delay in production of NO that utilize the thermal production mechanism. He denoted this quickly generated NO as prompt NO. the common method of this mechanism is being initially HC radicals react with nitrogen molecules to produce amino compounds. These compounds are further transformed to intermediary compounds that eventually result in NO. Neglecting the fact that methods that result in CH radicals to initialize this method, the entire process can be shown as

$$CH + N_2 \Leftrightarrow HCN + N$$
$$C + N_2 \Leftrightarrow CN + N$$

For the combustion zones where equivalence ratios are found to be fewer than 1.2, the chemical conversion of hydrogen cyanide, HCN, to produce NO follows the shown cycle:

$$HCN + O \Leftrightarrow NCO + H$$
$$NCO + H \Leftrightarrow NH + CO$$
$$NH + H \Leftrightarrow N + H_2$$
$$N + OH \Leftrightarrow NO + H$$

For equivalence ratios higher than 1.2, other routes open up and the chemistry turns out to be more intricate. Miller and Bowman [7] concluded that the above system is no longer rapid, and that NO is reused to HCN, preventing NO generation. Figure 1.2 schematically illustrates the processes involved.

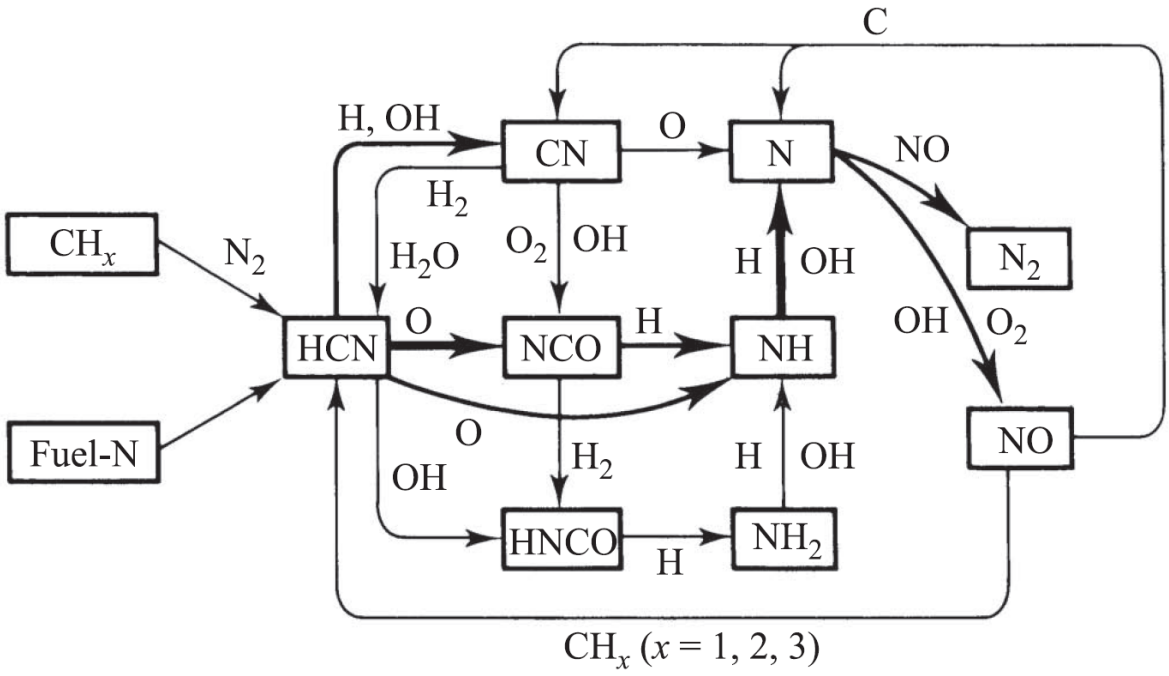

Figure 1.2. Production of NO associated with the Fenimore prompt mechanism [5]

1.1.2 N_2O Intermediate Mechanism

This mechanism is extremely critical in lean combsution zone applications ($\phi < 0.8$) especially at low-temperature circumstances. The three sequential steps of this method are

$$\mathrm{O + N_2 + M \Leftrightarrow N_2O + M}$$
$$\mathrm{H + N_2O \Leftrightarrow NO + NH}$$
$$\mathrm{O + N_2O \Leftrightarrow NO + NO}$$

This approach turns out to be important in NO control system design that uses lean premixed combustion, which is utilized by gas-turbine manufacturers.

1.1.3 NNH Mechanism

The NNH method for NO generation is a newly realized reaction route. The two important stages in this mechanism are

$$\mathrm{N_2 + H \Leftrightarrow NNH}$$
$$\mathrm{NNH + O \Leftrightarrow NO + NH}$$

This path is especially vital in the combustion of hydrogen and for hydrocarbon fuels with higher carbon-to-hydrogen ratios.

1.1.4 Zeldovich or Thermal Mechanism

This method comprises of two chain reactions as

$$\mathrm{O + N_2 \Leftrightarrow NO + N}$$
$$\mathrm{N + O_2 \Leftrightarrow NO + O}$$

which can be extended by combining the reaction

$$\mathrm{N + OH \Leftrightarrow NO + H}$$

This group of chemical reactions can be regarded as the extended zeldovich mechanism. Generally, this approach is coupled with the chemical interactions in the combustion process with the help of O_2, O, and OH species. But in certain cases where the combustion of fuel and air mixture completes before NO formation becomes critical, these two processes can be disintegrated. Here, in case if the related timescales are adequately longer, we can conclude that N_2, O_2, O, and OH concentrations are their equilibrium and N atoms are in steady state. these considerations significantly make easier the intricacy in estimation of NOx.

The simplified expression for rate of NO formation can be expressed as shown in equation 1.1

$$\frac{d[NO]}{dt} = k_1^+[O]\,[N_2] + k_2^+[N]\,[O_2] + k_3^+[N][OH] - k_1^-[NO][N] - k_2^-[NO][O] - k_3^-[NO][H] \quad (1.1)$$

where k_1^+, k_2^+, k_3^+ are forward rate constants and k_1^-, k_2^-, k_3^- are backward reaction rate constants. A similar expression for d[N]/dt can be written as

$$\frac{\mathrm{d}[N]}{\mathrm{d}t} = k_1^+[O][N_2] - k_2^+[N][O_2] - k_3^+[N][OH] - k_1^-[NO][N] + k_2^-[NO][O] + k_3^-[NO][H] \quad (1.2)$$

Since $[N]$ is much smaller than the concentration of other species, it is assumed to be equal to zero. Therefore, the modified expression for NO formation rate is

$$\frac{d[NO]}{dt} = 2k_1^+[O]\,[N_2]\,\frac{1 - \frac{[NO]^2}{K[O_2][N_2]}}{1 + \frac{k_1^-[NO]}{\left(k_2^+[O_2] + k_3^+[OH]\right)}} \quad (1.3)$$

Where

$$K = \left(\frac{k_1^+}{k_1^-}\right)\left(\frac{k_2^+}{k_2^-}\right)$$

At equilibrium,

$$
\begin{aligned}
R_1 &= k_1^+ [O]_{\mathrm{e}} [N_2]_{\mathrm{e}} = k_1^- [NO]_{\mathrm{e}} [N]_{\mathrm{e}} \\
R_2 &= k_2^+ [N]_{\mathrm{e}} [O_2]_{\mathrm{e}} = k_2^- [NO]_{\mathrm{e}} [O]_{\mathrm{e}} \\
R_3 &= k_3^+ [N]_{\mathrm{e}} [OH]_{\mathrm{e}} = k_3^- [NO]_{\mathrm{e}} [H]_{\mathrm{e}}
\end{aligned}
\tag{1.4}
$$

As a conventional rule, the thermal approach is less significant below 1800 K. Contrary to the instances where the oxidation of fuel takes place, NO is produced it relatively slower by thermal mechanism and thus, this type of NO formation mechanism is usually known to be produced in the post flame part of the combustion process.

1.1.5 Tradeoff between NOx Formation Mechanisms

The thermal or Zeldovich mechanism is significant in the combustion process at higher temperatures width more the range of equivalence ratios, whereas the Fenimore approach is it specifically critical in rich fuel combustion only. It is observed that N_2O intermediate mechanism has a critical impact on NO generation in very lean, and low temperature processes. The NNH method is a comparatively newer identified and needs to be explored more from chemistry perspectives. Several observations mention the significant contribution of first three approaches in both premix uncontrolled and diffusion controlled phases. The combined contribution of all four pathways his important for lead premixed combustion in a jet stirred reactors.

1.2 Soot Prediction Modeling Approaches

Particulate matter or commonly known as soot is one of the major emission parameters in case of diesel engines. These particles very small in size have proven to be a significant hazard to human health. These very tiny elements can penetrate deep into the tissues of human lungs and can cause serious health problems. As nitrogen oxides and particulate matter cannot be simply minimized without sacrificing the performance of the engine, they are considered to be the most critical pollutants. This proposed approach can work as a standalone system for calculating the amount of soot generated from the diesel engine or as a subsystem in a bigger level control architecture.

In upcoming sections, the outline of different steps off soot generation is discussed. Usually, the net suit generated follows six distinct steps [8]. These steps are mentioned below.

- Fuel pyrolysis
- Nucleation
- Surface growth
- Coalescence
- Agglomeration
- Oxidation

The first five steps are collectively considered as soot formation phase and this excludes the last step of oxidation. The suit formation phase follows a sequential phenomenon as mentioned above whereas the oxidation phase takes place constantly because of the availability of oxygen molecules inside the cylinder. In diesel engines, these formation and oxidation phases occur in distinct location inside the cylinder. Moreover, throughout the combustion procedure, formation leads initially, and soon after oxidation occurs. The size of elementary atoms varies in the range of 20–70 nm. After the combustion is complete, the particles are clustered ahead and get to the size of 0.02–2 mm.

Amongst the semiempirical methodologies, the Hiroyasu and Kadota method presents possibility for several more advancements. The Hiroyasu and Kadota [9] model establishes the soot formation and the soot oxidation separately as shown in equation 1.5 below.

$$\begin{aligned} \tfrac{dm_{\text{Soot}}}{dt} &= \tfrac{dm_{\text{Formation}}}{dt} - \tfrac{dm_{\text{Oxidation}}}{dt} \\ \tfrac{dm_{\text{Formation}}}{dt} &= A_f \cdot m_{fg} \cdot p^{0.5} \cdot \mathrm{e}^{-\left(\frac{E_{Sf}}{RT}\right)} \\ \tfrac{dm_{\text{Oxidation}}}{dt} &= A_0 \cdot m_s \cdot \tfrac{p_{O_2}}{p} \cdot p^{1.8} \cdot \mathrm{e}^{-\left(\frac{E_{so}}{RT}\right)} \end{aligned} \tag{1.5}$$

In both the expressions for formation and oxidation, this approach takes into account multiple factors like an empirical scaling constant A, in cylinder conditions like temperatures and pressures, concentration of species.

In other methods used for soot modeling, this concept of Hiroyasu and Kadota [9] has been modified with additional parameters that consider injection turbulence [10] and the soot chemistry [11] utilizing the phi-T map from Akihama et al [12]. The turbulence at

injector nozzle tip is expressed as a function of rate of fuel injected in diffusion controlled phase for the formation and characteristic mixing scale for the oxidation phase. The phi-T map gain uses the Arrhenius type of expression In the relation to predict the amount of soot. In Kirchen et al. [13], this approach has been modified that denote few key states and the model can real time communicate with signals coming in from ECU. All these efforts or modifications have a major drawback that they do not consider in cylinder pressure which is a major factor in soot estimation.

Kozuch [14] and Bayer and Foster [15] have proposed a soot estimation model based on hiroyasu method. In Bayer and Foster [15], the calculation of AFR that highly impacts soot formation is determined by using liftoff length. This method implies that relative air fuel ratio for soot formation depends heavily on the air being entrained back into the flame. In Kozuch [14], appropriate air fuel ratio is determined by using a partial function of the fuel enhancement in the soot supporting diffusive flame. There is a good example of a fast running two step model established by Westlund and Aangstrom [16] and it calculates the amount of soot formation by utilizing air fuel ratios, EGR rate and the injection turbulence. The oxidation phase here is characterized by Nagle and Strickland-Constable [17]. In these approaches the calculation time that use calibration maps is usually around 150ms four single cycle. This is significantly higher for real time control algorithms in high speed diesel engines. The approach adopted by Schaeffler et al. [18] uses the experimental approach for this two-step model also known as grey box models. The overall engine operating conditions and properties that have a significant impact on soot generation are supplied with exponential terms both for suit formation and oxidation and are multiplied further to predict suit advancement as a tailpipe quantity. Each of these methods, except Kirchen et al.'s [13], requires integration with real time processes over the entire engine cycle and as a reason, this increases the computation time significantly.

The liquid fuel is injected with the help of injector nozzle directly into the combustion chamber just ahead of expected instant of combustion, as the piston moves towards the final instance of the compression stroke. The liquid jet after lift of length disperses into small drops, atomizes and mixes with warm and high pressure air mass in the cylinder. At this instance, the pressure and temperature of surrounding air is significantly higher than the

auto ignition temperature of fuel. Due to this reason, impulsive ignition of fuel droplets text place after a small delay. This delay between start of injection and the start of heat release is known as ignition delay. After this ignition delay interval, further combustion procedure is generally divided between two phases. In the first stage, the fuel injected mixes with air inside the combustion chamber and ignites quickly. This part of the combustion process is usually denoted as premixed stage and is related to the higher rates of heat release for a smaller duration. This heat release in restricted time frame depends significantly on-air fuel mixture initialized throughout that particular interval.

Dec J. E. [19] discussed the production and characteristic properties of a quasi-steady diesel fuel jet, as indicated in figure 1.3. It should be noted that this approach is relevant for large diameter and quiescent cylinder combustion processes or for a free jet off fuel injected that doesn't have any boundaries.

During the start of fuel injection, it starts to infiltrate the combustion cylinder and high-temperature air is entrained back into the fuel jet spray. The hot air vaporizes the fuel and In the initial instances of fuel injection through nozzle orifice, it begins to penetrate into the combustion cylinder and surrounding air which is at higher temperatures tries to re-enter back into the fuel jet spray. This hot air when mixed with fuel, vaporizes the fuel droplets after denoted axial distance commonly known as liquid length. There is a reduction in this liquid length after start of combustion but remains constant until the end of injection. After this liquid length, the air fuel mixture in the rich premixed zone remains to maintain its higher temperature until it is converted into the cluster. The resultant products due to this rich combustion process spread widely and tend to mix radially outside until they reach the surrounding gases inside the cylinder. At the instances where these rich clusters and remaining gases in the cylinder mix with each other to yield a stoichiometric mixture, then there is a formation of diffusive flame. This flame front covers the injected fuel jet in a thin and turbulent fashion that further extends upstream towards the nozzle. Now here liftoff length plays a very critical role. As demonstrated by Siebers & Higgins [20], the lift off length controls the amount of oxygen reentering back into the fuel jet spray and thus the stoichiometric AFR of the rich zone. In the subsequent phases that occur in the final stages,

soot is oxidized and NOx is generated on the outer periphery of the diffusive flame at higher temperatures in the vicinity where oxygen and nitrogen molecules are abundantly available.

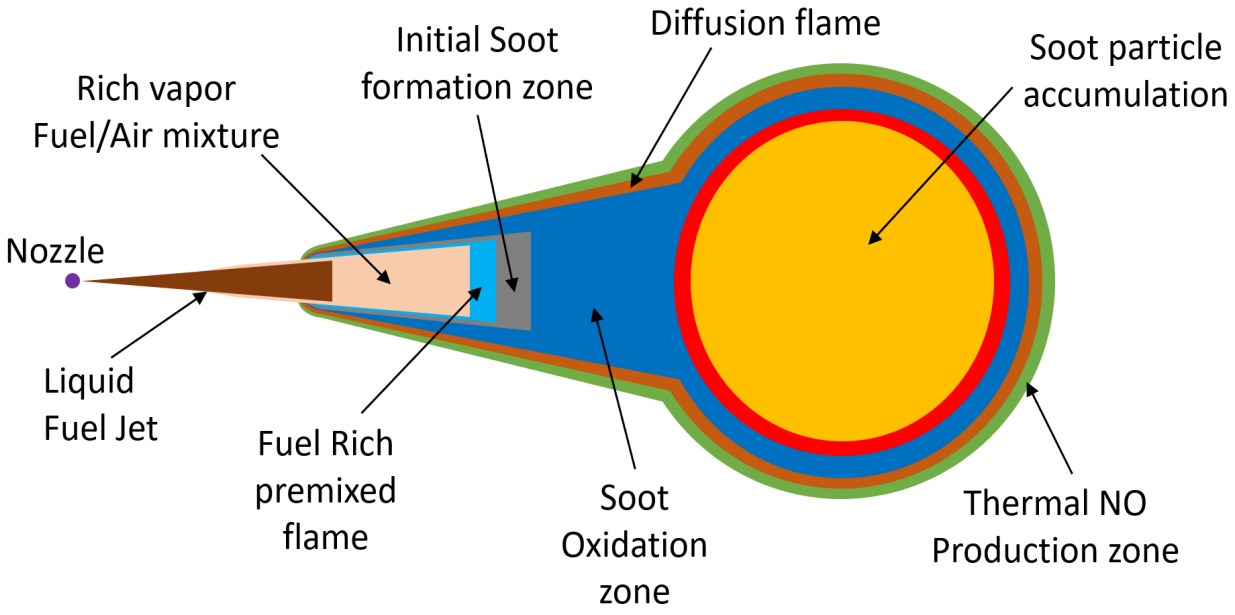

Figure 1.3. Quasi-steady Diesel combustion plume

Early pyrolysis of fuel normally recognizes an extremely rich combustion zone. The products of this chemical reaction are produced in larger quantities that eventually become the precursors of soot such as unburned hydrocarbons, radicals of C_3H_3, C_2H_2, and C_2H_4. The primarily developed particles of soot grow in size with the help of agglomeration, surface growth and direct deposit method. As they come in contact with surrounding air which is already at higher temperatures, these soot particles, precursors and species are all burnt off. The initial phase of pyrolysis of diesel fuel droplets occurs in fuel rich zones and this primary reaction occurs downstream of the liquid length. In addition to these processes, studies have detected the occurrence of area where small and tiny soot particles start to form [19]. The atoms for these precursors initialize and increase in size as they move further down in the direction of turbulent fuel jet spray. In the subsequent phases as these particles are introduced with remaining oxygen inside the cylinder, the oxidation of these particles takes place.

Siebers Higgins [20] invented that the lift of length was a critical factor in deriving the equivalence ratio in rich primary reaction zones. And when the air is reentered into the fuel spray, it is the only source for oxygen for the primary reaction and after that, the diffusive flame envelope restricts further entrainment of gases back into the flame. If the lift of length is higher, it allows for additional air to be reentered back into the flame and it also reduces the equivalence ratio in primary reaction zone. This reduction in equivalence ratio results in less amount of hydrocarbons in exhaust gases. When the combustion phenomenon starts to cool down due to less availability of oxygen inside the combustion chamber, most of this soot atoms produced throughout engine cycle are also oxidized [5]. In the final steps during the combustion cycle, there is a competition that occurs in rapidly cooling temperature zones because of the cooling due to volume expansion and thus the rate of soot oxidation also increases. The soot mass still remaining after this final step of combustion process is expelled out of the combustion cylinder through exhaust manifold of the engine.

1.3 Closure on the Chapter

The significance and understanding of NOx and soot formation mechanisms is vital in case of their prediction modeling which is studied throughout this chapter. Various mechanisms were studied both for NOx and soot generation and the tradeoffs were discussed. Based on this comparison, it was beneficial to use Extended Kalman approach for NOx generation and Hiroyasu & Kadota model for soot generation. To explore more into the motivation of these topic, it is necessary to know the existing work done and problems that occur with existing sensors. An effort has been done to explore this in next chapter.

2. LITERATURE REVIEW

Increasing demands for strict emission and on-board diagnostics (OBD) norms are the main motive behind utilization of engine out NOx and soot data. This data can also be used as an input different subsystem model specifically designed for after treatment systems. For this purpose, it is essential to physically place sensors before after treatment devices and it makes this a complex and costly task. To overcome these problems virtual sensors are used which are mathematical calculations as an integration of physical and chemical processes taking place inside the combustion cylinder and related components. These virtual sensors are flexible and can estimate the desired output by utilizing certain input signals that are already available from ECU or previously developed calibration maps. Virtual sensors can either replace physical sensors or they can be used with physical sensors in parallel.

Different approaches to mathematically derive emissions that heavily depend on certain number of engine parameters have been discussed in the literature. The complexity of these approaches Varies from highly detailed CFD models to very simple experimental input output correlations. If the requirement is to use these models in control architecture with real time feedback, the analytical complexity must be very small and the input given to the model has to be accessible based on the data coming from sensors with fast sampling rate and higher accuracy.

The sensors used to measure cylinder pressure in test cells provide signals with high degree of chronological order and accuracy during the combustion process in specific setups only. These physical sensors have been used since long time in different research centers and different studies indicate that there may be a possibility to use these sensors in production level engines. To analyze the market survey of these sensors it is critical to find out the possible advantages and disadvantages in the type of signal output they deliver.

The base logic for a virtual NOx sensor significantly relies on the numerical analysis for the NOx generation inside combustion chamber. As far as the production level automotive ECUs are concerned a base layout of NOx formation methods is derived [21]. Depending on the level of accuracy required, they can be further divided as black box, grey box or physics-based models. The physics based NOx approaches uses two or more zones to calculate in

cylinder pressure, temperature and concentration of species of products. This pressure signal calculated works as input to the main prediction model [22], [23]. Therefore, these virtual sensors require the actual pressure sensor to be placed inside combustion chamber for real time estimation of NOx. Elbert et al. [24] proposed a concept based on zero-cylinder pressure sensor. In this approach, offline estimation of in cylinder pressure is done by using other in cylinder parameters to effectively calculate online burning rates with respect to Wiebe function. The approach based on physical phenomenon allows fast offline prediction but they are not suitable for ECU applications because off the high latency. And that's the reason physics based models how excellent predictive capabilities. On the other hand, grey box models have certain assumptions that are highly inspired from physical models but optimize ECU performance. In these models, the engine parameters are generally estimated as a function of time and not for crank angle scale. The highest degree of prediction accuracy is obtained by black box models add state rely heavily on different sources of information such as artificial neural networks, polynomial equations, calibration maps and actual data from sensors. In this case, the resources and time required for calibration of predictive model are very expensive and it is commercially not viable to spend so much for a limited purpose.

2.1 Current Modeling Approaches

In order to predict engine emissions by utilizing the in-cylinder conditions, a method is proposed that uses a detailed data from the combustion process. The idea of using in cylinder pressure and temperature to find out different engine parameters like emissions have been discussed in several research efforts earlier, mutually applying experimental data-based models, and physical models. Seykens et al. [25] described a similar sort of method in which combustion cylinder pressure was considered to be an input to calculate engine out NOx and soot. Wilhelmsson et al. suggested a physical two-zone approach for NOx estimation relying on cylinder pressure information. Traver et al. [26] specified a collection of physical variables obtained from the cylinder pressure data (such as ignition delay, combustion duration, peak pressure) and trained a neural network to forecast HC, CO, CO_2 and NOx emissions from

these physical signals. Çebi et al. [27] too utilized a set of variables obtained from the cylinder pressure data, and a parametric experimental calculation to calculate the PM emissions.

Two mathematically derive the engine and its subsystems mean value models are a novel approach for control-oriented objectives. This approach has proven to be a good optimum balance between computational efforts and the degree of accuracy [28]. In this approach, the dynamic characteristics of engine during transient operation expressed by ordinary governing differential equations. As the actuators in engine system do not significantly impact in controlling the rapid dynamic behavior in the conversion phase, it is usually assumed as quasistatic in this approach. In transient test cases, the torque generated by engine is correlated with the actual amount of fuel flowing into the cylinder at any particular engine speed. Contrary to this statement, there are few boundary conditions in the combustion stage and they can affect the engine out emissions significantly during the transient operation. These include the rate of emission formation, EGR rate and boost pressure. Until date, a prediction approach based on control oriented modeling has not been established that can estimate the engine out emissions.

The CFD and phenomenological prediction models are typically crank angle based and explain the in-cylinder processes in detailed fashion. For transient operating conditions, the predictive models must run on a very faster and real time scale. This is a main constraint in case of phenomenological and CFD models as they have high computational costs and time. So, they are not suitable for real time application. On the other hand, time based experimental and regression models are very efficient in terms of computation efforts and time. As a reason, they are best suitable 4 real time implementations on actual vehicle. The outcome of such a dynamical analysis may be quantified in the form of either a state-space model or a (preferably low-order) transfer function. Eventually, it can be used for controller synthesis and black-box models are classic illustrations of this style of models. Because the internal configuration of the system is unfamiliar, the input/output performance is derived with either an Artificial Neural Network (ANN) approach or with a polynomial method. The primary drawback of these black box models is that it requires huge number of test cycle data to train the model and predict required parameters. This dependency on a particular data set limits the flexibility of the model to be implemented on other type of engines or

even other test cases. There is a workaround to overcome this problem and that is use of a phenomenological model that can estimate the data required to calibrate these black box models. This proves to be a very promising solution for further analysis but the degree of accuracy of phenomenological calculations cannot be guaranteed and computation effort increases significantly.

Other solution under consideration is the utilization of green box modeling methods that also employs few physical correlations. Using a statistical model for engine out emissions straight forward polynomial expression is developed. This model uses the required process parameters and signals. This method can be utilized for different applications or different engines as physics-based model inputs are used. Using the correlations of actual air fuel ratio, the engine out emissions are predicted for transient test cases by using static calibration base maps along with correction gains. An ANN approach is presented [26] to predict gaseous exhaust emissions levels from a Navistar T444 direct injection diesel engine based on certain variables. These variables belong to the steady state data collected for peak pressure, maximum rate of heat release and temperature. This ANN approach is tested for accuracy during transient test cases. Del Re and Langthaler suggested Structure identification (SI) algorithm that can be used to predict nitrogen oxide engine out emissions using the signals directly from ECU. This model comprised of the dynamics of intake and exhaust manifolds as well as the sensor performance.

2.2 NOx Sensor Issues

Commercial NOx sensors for automotive applications are primarily Yttria-Stabilized Zirconia (YSZ) electrochemical sensors of the amperometric type [29]. Figure 2.1 illustrates the basic operating principle [30]. The sensor employs two or three electrochemical units in adjoining cavities. The initial cavity separates oxygen molecule out of the sample, so that it does not impact the NOx detection in the second cavity. The demand to eliminate O_2 permits this sort of NOx sensor to provide a double use; it can additionally identify exhaust O_2 amounts.

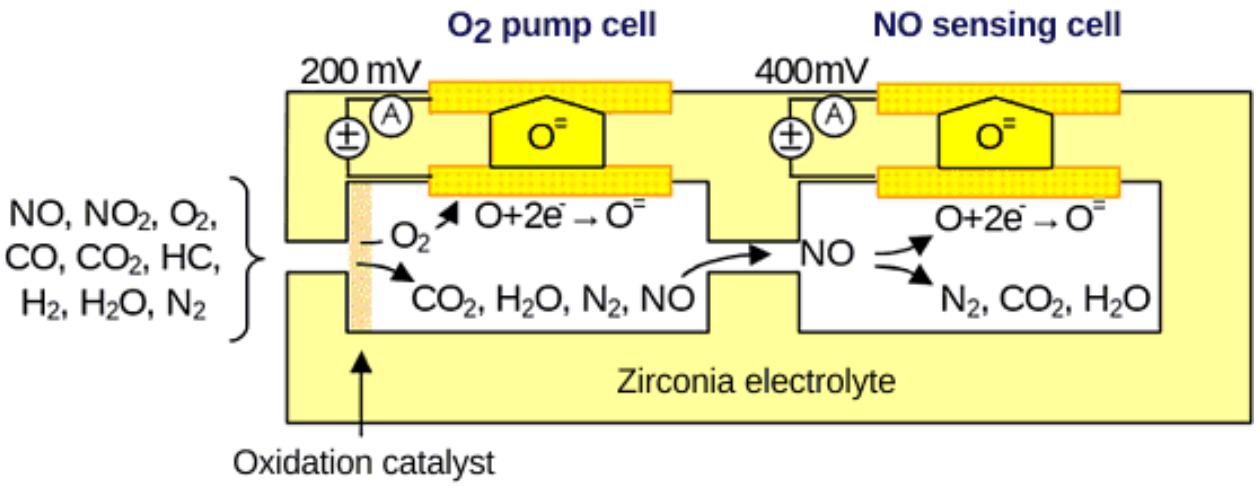

Figure 2.1. Schematic representation of an amperometric NOx sensor [30]

The O_2 in the first chamber is lowered and the resultant O ions are pushed via the zirconia electrolyte by using a voltage of around -200 mV to -400 mV. The current is proportionate to the O_2 concentration. The residual gases disperse into the second chamber where a reduction catalyst produces NOx to break down into N_2 and O_2. As with the first chamber, a voltage of -400 mV used to the electrode separates the resultant O_2 which is then injected out of the cell; the pumping current of the second chamber is relational to the quantity of oxygen from the NOx breakdown. An additional electrochemical element can be employed as a Nernstian lambda sensor to help out control the NOx recognition sensor.

Diesel NOx sensory devices have dual intent, they are utilized to sense both the oxygen level in the exhaust and NOx (NO and NO_2) amount. The data acquisition takes place in two distinct compartments in the sensor, and the exhaust gases run consecutively across one and then into the other. Gases stream from the exhaust flow all through a diffusion barrier to get to the first cavity, which "extracts" the available oxygen out utilizing a Nernst cell (simple oxygen sensor). The electric current for driving this initial Nernst cell is employed to determine exhaust oxygen amount (lambda). In certain sensors like LML Duramax, oxygen

quantity in the exhaust gases is delivered directly to the electronic control module (ECM) by NOx sensor to help out in regeneration process of diesel particulate filter (DPF) [31].

With the available oxygen eliminated, the NOx is then put to transfer out of a different diffusion barrier and into the second measurement cavity. At this moment, the NOx molecules confront a catalytic component, which splits them into nitrogen and oxygen gases. A second Nernst cell is then utilized to drain the newly produced oxygen outside of the cavity, and this electric current is utilized to determine the NOx concentrations in the exhaust flow. The remaining nitrogen fumes then stream out through an exit port in the second cavity.

Similar to oxygen sensors, NOx sensors will not perform unless they are at the appropriate temperature necessary which is typically about 800°C, so they have an included heater that is also unit operated. The power source to the NOx sensor unit is important for appropriate sensor functioning. If system voltage is less, an internal voltage enhancing unit in the glow plug control module (GPCM) will compensate the tradeoff to guarantee appropriate NOx sensor functioning.

In the case of a cold start, humidity in the exhaust system can affect with NOx sensor performance. Here, the ECU will not initiate the NOx sensor heaters until exhaust temperatures achieve a particular level and condensed humidity is vaporized. This can cause in a lag of up to 5 minutes prior to both NOx sensors are entirely in operation [31].

2.2.1 Cross-Sensitivities

NOx sensors centered on YSZ ceramics are responsive to ammonia and additional nitrogen compounds. The sensitivity of existing NOx sensors reduces in the mentioned order: $NO > NH_3 > NO_2$ [32]. The cross-sensitivity to ammonia is a result of the oxidation of ammonia to nitrous oxide in the initial cavity of the sensor. The cross-sensitivity is particularly strong at low concentrations. Inside the concentration limit which usually varies from 0-200 ppm, the signal from NO and NH_3 are nearly identical. While the cross-sensitivity to NH_3 makes it challenging to distinguish between NOx and ammonia slip downstream of the SCR

catalyst, signal processing methods have been extensively developed to make it possible for ECU to determine if NH_3 interference with the NOx measurement is significantly resolved.

2.2.2 Accuracy and Response Time

The operation of NOx sensors has witnessed fast development throughout the early days following the introduction of the technique [33]. This objective has been surpassed, as many industrial sensors possess NOx sensitivity on the range of 10 ppm. However, the technology appears to have reached a plateau—sensitivities of ±5 ppm NOx that were targeted by development projects [34] have not yet been achieved.

The smaller the NOx amount of the exhaust, the more problematic is the interpretation of the output data. The precision of many sensors is obtained around 10 ppm NOx at a 0 ppm NOx concentration. At 100 ppm, the car edition accuracy is roughly ±10%. The commercial vehicle versions can achieve a better than ±10% accuracy at NOx levels of 500 ppm or higher.

Also the sluggish response period of NOx sensors—yet over 0.75 s—could profit from enhancement for dynamic purposes. According to some specifications, a step response from 33% to 66% of the signal impulse is possible within 550 ms [35]. In practical use, some sorts of response—specifically a step from a high-level to a low NOx concentration—can only be displayed with a time lag.

2.2.3 Thermal Shock and Poisoning

Field knowledge collected after the release of the Smart NOx sensor in Euro IV and Euro V applications revealed that the sensor could be susceptible to thermal transients and chemical pollution [36]. Inadequate durability of industrial NOx sensors has been an exceptionally significant problem in heavy-duty engines, where the essential durability, operational time and mileage are greater compared to the passenger car use.

Spot cooling because of tiny water drops falling and vaporizing over the exterior of the sensor could be a significant cause of component cracks and thermal shock malfunction. The possibility for this kind of destruction is especially extreme in a cold start, when the exhaust

gas temperature is lower than the dew point of water. Hence, it is required to hold up until this stage is done and the exhaust gas is free of moisture prior to the sensor can be placed into action. After implementing of the operational voltage, the sensor goes through a preheat stage and warms the sensor tip to roughly 85°C. As the circuit senses the so-called dew point end trigger via CAN bus, the ceramic on the ceramics is reheated to 800°C in several stages. This procedure needs almost 45 seconds of time.

Amongst chemical pollutants, solvable salts of magnesium—a component appearing in some lubrication oil additives, and in various aftertreatment elements—were observed to trigger a worsening of the sensor output data. Magnesium poisoning is irreversible and results to long-lasting impairment of the sensor [37].

The origin of contamination could additionally be the sensor materials used. Denso stated that a damage to the sensor output was initiated by transmission of Au from the oxygen pump electrode—material for which is Pt/Au—on the top of the NO detection electrode (Pt/Rh), and by element deposition on the electrode [38]. Sulfur, on the other side, is not an issue throughout the operational lifespan of the sensor. As the surface is warmed to 800°C, the binding force of sulfur and its mixtures are too small to produce contamination.

NGK/Continental stated on the progress of an advanced sensor, integrating a new envelope offering safeguard against liquid drops and self-diagnostic tasks to account for chemical pollution [39]. Nevertheless, the potential level of protection from liquid drops is restricted by the loss of dynamic output of the sensor.

2.2.4 Complexity and Cost

Additional downside of amperometric NOx sensors is their more expense because of the multiple cavity layout and the necessity for intricate electronic circuit to identify nanoampere current ranges.

The shortcomings of the amperometric sensors motivate the development of alternative technologies, including impedancemetric and potentiometric NOx sensing approaches [40], [41].

2.3 Soot Sensor Issues

Various types of soot or particulate matter sensors have been developed to estimate the amount of soot in a diesel particulate filter (DPF) or to detect excessive particulate matter emissions downstream of a DPF in instance of a filter malfunction. The forecast of soot amount in the filter primarily relies on a differential pressure information, but also additional methods like radio frequency (RF) sensors have additionally been established. Sensors for DPF fault identification consist of accumulating sort of sensors utilizing a resistive electrode, and electric charge centered mechanisms.

2.3.1 Resistive Soot Sensor

In the resistive electrode sensor, a pair of flat electrodes affixed to a ceramic carrier as shown in figure 2.2 is located in the tip of the sensor, which is located in the exhaust pipe and exposed to the gas stream. As the exhaust flow passes into the sensor, soot particles are dumped on and stuck between the electrodes by thermophoresis—particle transportation from the warmer exhaust flow to the comparatively colder electrodes. Along with the buildup of soot, conductive routes are developed among the two electrodes and the cumulative conductivity of the system enhances, causing in a rise of electric current (sensor signal). These conductive soot shapes are occasionally mentioned to as soot dendrites, because of their split, tree-shaped structure.

The first stage is ‘‘deadband,’’ in which the resistance stays constant for the duration necessary for the sensing component to be electrically linked by accumulated soot. In next stage When suit is deposited in between two electrodes, a soot bridge is formed through the resistance which is primarily in ranges of 10Mohm steadily declines with time because of rise in accumulated soot quantity [43].

After the heating stage is over, the resistance stays pretty constant at particular small amount over 0.1Mohm even though the rise in the accumulation quantity, and then remaining suit is burnt off at higher temperatures above 600°C with the help of electrical heating. The time duration between start of this cycle until the termination of second phase is collectively known as response time as shown in figure 2.3.

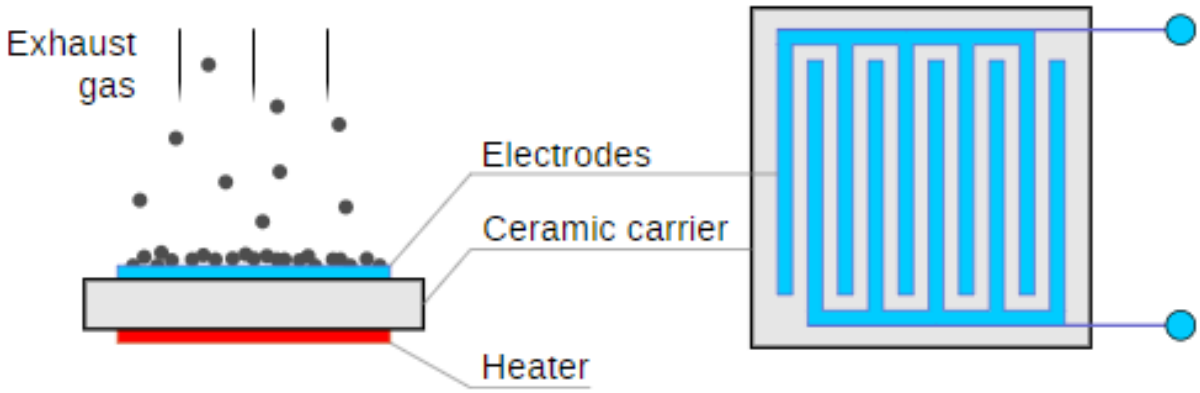

Figure 2.2. Schematic of a resistive electrode for soot sensing [42]

The engine exhaust gas comprises of isolated soot fragments and bigger particles containing flaky structures that are removed from the exhaust manifold walls and water droplets coming out from diesel particulate filter. As this big particles go inside the sensor cavity, the space in between two electrodes is reduced, the current starts flowing and the resistance decrease suddenly.

In order to minimize random signals, different sorts of flow approaches have been presented [44]. A detailed CFD analysis was carried out to trace the path of these particles. The study concludes that as the velocity of the stream increases, less are the chances of soot particles to reach to the substrate. Similar sort of experimentation to find out the path of particle for different shield cap layouts was discussed in Hopka et al [45].

The resistive electrode demands to be regenerated regularly to permit the elimination of the accumulated soot on the electrode, so to permit a constant soot observing procedure. Thus, heating parts are incorporated in the interior the sensor arrangement to facilitate such regeneration via raising the sensor electrode temperature. As a prolonged drive cycle is required to gather adequate soot, particularly with bigger engines where the identical quantity of soot is diluted in a bigger quantity of exhaust gas, the duration of FTP-75 test

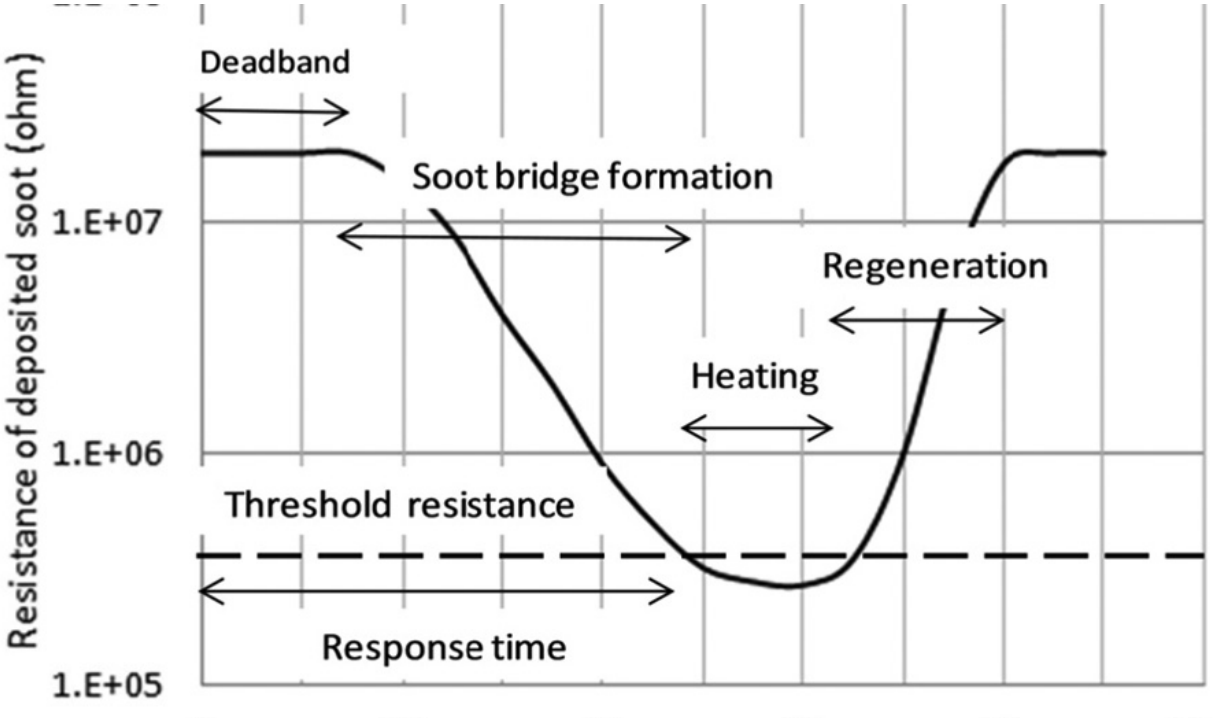

Figure 2.3. Response of deposited soot resistance to soot accumulation and regeneration [43]

is not enough to measure the PM, which causes OBD compliance problems [46]. The data acquisition usually commences after a sensor regeneration, that is finished as the sensor recognizes a dew point. A potential alteration could be to permit the sensor to collect soot across numerous drive cycles.

Another issue with the accumulating sensor is its increasing variability at higher gas flow rates, as the soot dendrites attached to the electrode may become blown off [46]. It was demonstrated through testing that little modifications to few dendrites impacted the adjacent dendrites via adjustments to the electric field, adding to variability.

2.3.2 Electrostatic Capacitance Soot Sensor

The fuel rich combustion zone results in generation of soot particles. As these soot particles pass through diffusive combustion flame, which is at elevated temperatures, they come in contact with abundantly available ions and electrons that are generated due to chemical ionization processes. As a reason, some of these particles become positively charged. When

an electric field is implemented in the vicinity of the outer periphery of sensing component, these positively charged soot particles are expelled away from the sensor tip. This is the main idea behind accumulating type of soot sensors that use electrostatic capacitance to detect soot deposited on the surface [47]. The electric heater and electrodes in zigzag manner are used for regeneration in the same way as of resistive soot sensors. These extra set of electrodes is located into the sensor cavity that requires high voltage power supply near the electrodes used for suit detection. The electrodes used for sensing of soot detects the electrostatic capacitance between them and increases with increase in deposited soot amount. These type of sensors have excellent attributes like the capacitance of the electrodes are very slightly depends on temperature. And as a result, they are very sensitive to the quantity of soup deposited with respect to the resistive soot sensor.

Although these sensors how a good degree of performance, they are not used but OEMs due to its high cost and higher power supply required for the operation [48].

2.3.3 RF-based Soot Sensor

The working principle for these type of sensors in real time application in case of soot deposition in the diesel particulate filter has been well discussed in Sappok et al [49]. This involves the utilization of metallic filter housing for RF resonant cavity. When the soot fragments are deposited on the filter, it changes dielectric properties of the resonant space and the frequency of resonance decreases which is inversely proportional to the quantity of suit deposited [50].

This sensor output remains unchanged by the rate of exhaust gas flow but it responds to change in temperature. This is due to the dielectric properties of the particle that alter with respect to change in the temperature. This type of sensor provides direct measurement of soot deposited in diesel particulate filter and the time derivative of this data provides direct measurement of engine out suit in certain cases where the soot oxidation in diesel particulate filter is reduced [51].

Let's consider a case where quantity of soot deposited increases in a particular test case and the soot quantity calculated from engine out emissions has a significant trade off. In

this case, the diesel particulate filter can be assumed to have undergone a breakthrough. Therefore, this type of sensor is expected to account for control of DPF regeneration and simultaneously analyze the breakdown scenario [52]. These types of sensors are needed to be tested in more detail for long term operation of the sensor tip and overall cost of the sensor.

This technique is only appropriate to non-conducting filter media—conducting materials efficiently prevent the signal from piercing the filter. Considering of common DPF media, RF sensors can be utilized with cordierite and aluminum titanate filters, but they may not be relevant to SiC which is slightly conducting.

2.4 Controller Architectures and Implementation

Prediction models when they are integrated with physical phenomenon models have significant impact in determination of engine out emissions in the control architecture of the engine. When using these models for real time applications. Multiple methods can be adopted to attain optimum model fitness such as different data analysis techniques and filter design methods. Guzzella et al. [53] proposed using the test data based on calibration maps and designing an auto tuning PID controller. In this work, a first order filter was used for the optimal control of fuel quantity and engine speed. In order to further enhance this work, auto tuning of gains was proposed and the results of this work were compared with another developed LQG controller. However, in order to minimize delays in the controller response, they also integrated a Smith predictor. This ensures achievement of desired response while keeping the errors at a minimum level. Another approach was developed around 2000, that included self-tuning of PID controller gains by adopting an algorithm based on fuzzy logic. The methodology inspired but this technique was implemented on F100 chip, and the control variables were to set to be flux and load of air. The outcomes of this research work highlighted that this regulation of PID gains enhanced the spectrum of dynamic behavior of the designed controller for wide range of loads [54]. Wahlström et al., 2009 [55] carried out a detailed study focused on minimizing pumping losses and fuel utilization. In this work, two different types of controllers were compared. The first controller architecture contained a comprehensive mathematical model of the system that included integration of PID controller

and selectors for maxima and minima. This approach attained and fulfilled all the objectives targeted for that control system but on the other side, because of change in signs of DC gains, the pumping losses were drastically raised by 26%. Second type of controller was designed by using PID controller in integration with another nonlinear compensator. This work was successful in minimizing errors in EGR structure but on the other side the pumping losses were worsened. With respect to these studies they recommended the first controller design approach if the system is highly nonlinear and has a dynamic output in the feedback.

A novel control architecture depending on multivariable analysis was suggested by Arnold et al. in 2006. The objective of this architecture was to optimize certain parameters of air handling system like pressure in intake manifold and mass of intake air. Further, a PID controller was designed, the results before and after implementation of this controller were compared for desired transient response and considerable enhancement in performance of the system was observed. This approach was proposed to be implemented on real car ECUs for real time processing applications [56]. In certain cases, the control architecture do not require feedforward loop or internal physical models to control the air path system. This was proven to be more beneficial technique in terms of processing time and response of the controller ask compared to the embedded controllers already available. In this method, in order to simplify the model, novel approach to integrate linearized dynamic feedback for tracking diesel engine performance integration with EGR and VGT was with proposed. With this simplification of the model, the order of mean value model was reduced from eight to three [57].

Other approaches were proposed around 2010 in order to simplify the models. Certain techniques like inversion of model and reduction of degrees of freedom were suggested based on feedforward control for a diesel engine integrated with EGR and VGT [58]. Most recently, artificial neural networks (ANN) are being established by researchers all over the world that can estimate the output of diesel engine in terms of performance and emission gases under particular set of operating conditions and also take the type of fuel into account [68-70]. These methods are also utilized for OBD fault diagnostics and for deriving the calibration maps under different test case scenarios [59]. These are considered to be a type of empirical models as they are designed to operate under certain conditions only. However, they are

found to be more resourceful in other control architectures that heavily depend on the applications such as adaptive algorithms, supervisory control and predictive model methods.

Multiple prediction approaches have been studied that consist of data processing algorithms using multiple order filter integration techniques. Different type of controllers such as PID, feedforward, fuzzy logic or a combination of few of these is discussed in detail. The actual implementation of these controllers heavily relies on multiple factors such as the intricacy of the process and the desired response. This is beneficial because the processing time is reduced, and the control signal required for actuation takes less time. The use of latest methods such as ANN and implementation in engine control architecture to train the prediction models and further calibration is also discussed here. Yap et. al. [60], proposed a layer by layer optimization network as a part of algorithm based on supervised learning. This was proven to have enhanced processing time. The layout of this network is shown in figure 2.4. This logic includes 3 distinct layers. Every neuron in the hidden layer is connected to every neuron in the input layer. These employ interconnection with the help of weighing factors.

Recurrent neural network (RNN) models possess the advantage of having the dynamic behavior of the controlled system being manipulated by a simulated environment. Figure 2.5 shows the scheme of the RNN model used for virtual sensors where and u are output and control input, respectively. These RNNs are developed from static multi-layered perception feed-forward networks. To introduce the dynamic effect, feedforward connections are added among the neurons. The control structure described here is referred to as a nonlinear output error (NOE) model. Training and test data sets have been derived from experimental data and measured on a compact commercial engine during engine transients by imposing throttle and load perturbations. To enhance RNN generalization, the input variables have been uncorrelated by perturbing the fuel injection around the stoichiometric amount.

2.5 Recent Modeling and Control Strategies

Since last few decades, novel techniques have been implemented as a result of strict emission norms established globally by various governing authorities. At the same time

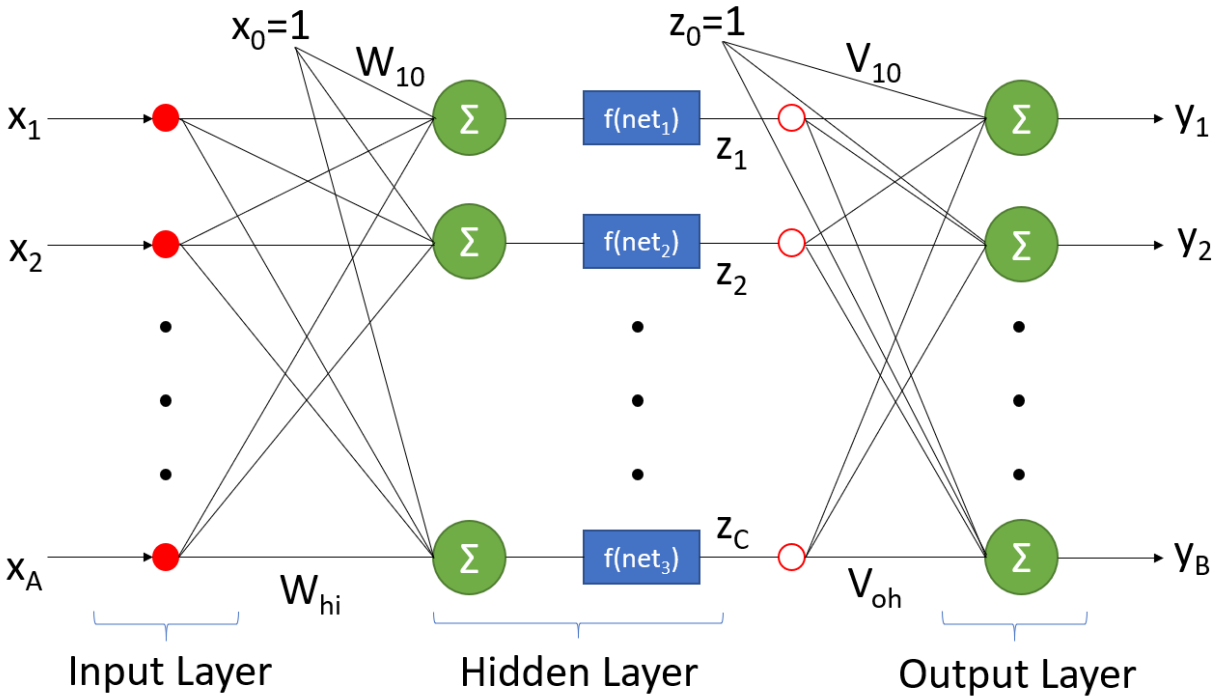

Figure 2.4. Architecture of OLL in a layer-by-layer optimization

considerable research has been carried out to enhance the prediction capabilities of the estimation models. Different type of controllers and optimization techniques are integrated with this prediction models and the validation of this control architecture is done with respect to experimental data. The sensitivity and system stability of this control oriented models relies on the method of system identification and desired response.

The parameters in this type of analysis can be considered to be any type of variable such as a calculation based on physical models or an actual physical sensor output. This section describes multiple efforts carried out towards advancements in modern diesel engines that are focused on increasing the overall efficiency and minimize the tailpipe emissions. Few of the problems discussed in this section are:

a. The accuracy of predictive models

b. Method of controller design and optimization techniques

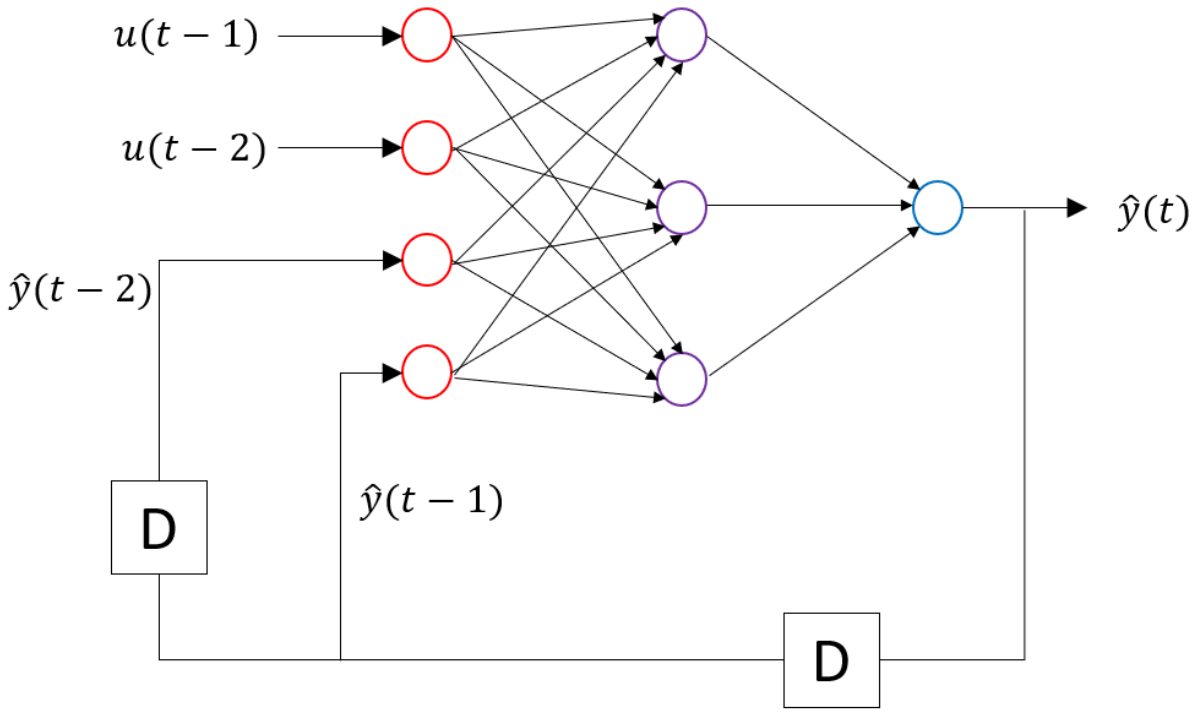

Figure 2.5. Structure of NOE RNN used in virtual sensors

c. The stability of controller

d. Verification and validation through globally practiced driving cycles

If the objective is to optimize the rate of fuel flow inside the cylinder and minimize NOx, the control of airpath in intake manifold along with turbocharger and EGR is an important aspect. Min et. al. [61] suggested an approach that can estimate certain unobservable in cylinder states As a result of air fuel mass exchange and thermodynamic processes. A least square optimization algorithm was employed for these state predictions. Here, a time constant was inserted to account for transport delay and temperature changes. The model output achieved quantity of fuel within 5% accuracy. Another effort was made depending on the air intake calculations that could evaluate the efficiency of EGR system with respect to certain emission boundaries. This approach requires the presence of actual physical sensor

to determine oxygen fraction and does not include physical modeling of the subsystems [62]. Neither Min et.al. nor Tan et. al. used this approach for any type of engine out emissions like NOx or soot and did not integrate it with any controller architecture. Wang et. al. [63] described state feedback controller design involving multiple degrees of freedom. In this study, the reference data was obtained with the help of a calibration map and used to control the optimum amount of fuel injected in pressure based intake manifold model. The derived controller displays required robustness and quick settling time throughout all test case scenarios, but it cannot be readily used as a base level architecture as there are no physics based calculations involved.

In order to represent physical systems numerically, system identification needs to be done. Various methods having established for this purposes that can analyze intricate physical systems. One of these methods is Hammerstein-Weiner approach and was used by Neilsen et. al. to demonstrate a high level nonlinear mathematical model of the diesel engine system including turbocharger and EGR that could optimize fuel injection quantity and timing [64]. In order to control the EGR fraction, controller based on nonlinear adaptive logic was designed that could instantaneously predict the states of cylinder under consideration for designated test cases. Even though it regulates the EGR valve, there is still need of control algorithms that could precisely predict few of in cylinder parameters such as rate of heat release, concentration of species and pressure. No efforts have been put into the engine out emission prediction that could be used for real time feedback control. To overcome the drawbacks in the dynamic behavior of system like overshoot, The prediction models are needed to be integrated with additional control architectures. Hong et. al. [65] implemented PI controller for turbo charger and EGR control that could effectively account for the nonlinear dynamic behavior of these subsystems during the transient operation. The constants required for this controller very obtained from the nonlinear governing expressions for VGT and EGR for European test cycle operating points. The implementation of this controller enhanced the transient response of the system and decreased the overshoot from 64% to 12% for step input. However, the tuning of controller gains is a redundant process if it has to be tested on different engines and thus time consuming.

One of the other methods suggested by Yang et. al.[66] is to analyze the flow of air in intake and exhaust manifolds considering EGR and turbocharger with the help of electrical turbo assist (ETA) in a closed loop controller feedback system. This type of method was derived using system identification toolbox in MATLAB and sophisticated calibration maps and test data obtained from the engine was used. A simple mathematical model for multiple degrees of freedom was developed. The stability of these systems is also validated by providing different disturbance signals and by tuning of controller gains at specific test conditions. Since this model is extensively dependent on calibration maps, it fails to account for any uncertainties outside the fitness boundaries of the model. To overcome this problem, there is a need of designing an observer for real time control and error tracking that could reject these disturbances [67]. The methods described above are highly dependent on feedback controller and they fail to account for predicted or estimated cylinder states and these further affect the stability of the controller. Precise estimation of states of the engine system and it's connectivity with engine out emissions coupled with physical and chemical kinetic calculations are important aspect in controller architecture for modern diesel engines. The controller design needs to be simplified and model order needs to be reduced to handle this complex system with flexibility and effectiveness.

Shoaib Ahmed et al [68] developed a model which was well intended for light and heavy-duty engines only. So, it missed the medium duty range of diesel products. This approach was based on a 2-zone thermodynamic model that considers both burned and unburned gas areas. This provides basis to attain a higher degree of prediction by utilizing MATLAB and ADVISOR as tools. Here, equivalence ratio again is a critical factor in NOx generation and this approach lacks the consideration of time temperature history in zones where AFR varies. This research work also states the need of attaining low emissions while keeping low fuel utilization. Pol Masclans Abelló et. al. [69] established a new approach named Cycle Analysis by Ordered Power (CAbOP) in which different emission parameters that are derived using three different simulators. These simulators consider re-structuring of time domain data that utilizes mechanical power at the wheel. The raw measurement data recorded from real experimental drive cycles. This data lacks the signals from nay unmeasurable states like

in-cylinder conditions. As a result, there is a need for a detailed physics based derived model to better understand the combustion process and predict the amount of emissions generated.

A novel approach that considers properties of diesel combustion flame at higher stoichiometric fuel fractions and its effect on soot formation is derived [70]. It captures the detailed data from both formation and oxidation phases that occur as a result of diffusive flame. This approach is a robust, simple and can be applied in numerous applications. The prediction method estimates soot amount as a result of equivalence ratio and distance from fuel injector nozzle. This work mentions need of additional empirical data capture for soot volume fraction in elevated stoichiometric fuel fractions for validation. But there is need to predict net soot generated with respect to crank angle as the cylinder goes through various strokes. This is dependent on various factors like in cylinder conditions and flame parameters which need to be addressed while modeling. Feng Jiang et. al. [71] developed a mathematical model for gasoline engine using GT-Power and MATLAB-Simulink interface and was used for an optimization purpose. The subsystems of this model considered were combustion system, pressure wave and optimization models for intake manifold. The main assumption for this work was air and exhaust gas were considered to be ideal gases. And therefore, the gas exchange properties depend on in-cylinder temperature and species composition. The integration of MATLAB and GT-Suite was well demonstrated in this work but lacks the need of appropriate controller to minimize the tradeoff between predicted and reference data.

High fidelity prediction models for soot bear considerably higher computational resources [72]. Therefore, high precision soot modeling is a numerically difficult task for simulation in case of diesel engines. Here, a neural network method displays a good possibility for application in many cases as it can precisely predict soot properties the requirement of any governing equations. They used initial cases of neural networks to calculate soot concentration based on a detailed CFD model result. These CFD results were considered as an input to train neural network-based models that recognize the fundamental relations between gas phase characteristics and soot amount generated. As the prerequisite for this approach is CFD model results, the resources in terms of computational cost and time are higher and thus, it is not suitable for real time control of the engine system.

Ibrahim Khalil Umar et. al. [73] developed a new neuro fuzzy ensemble (NF-E) model for estimation of particulate matter concentration on hourly basis. This involves a critical selection of related input variables for base model. The adaptive neuro fuzzy inference system (ANFIS) includes a nonlinear kernel for determination of ensemble output data. The efficiency of this approach could be distinguished with certain advanced modeling methods like neural network and need a physics based non linear governing equations for accurate prediction. Integration of empirical data and CFD model output was utilized to predict emission and performance of RCCI engine [74]. This also ensures elimination of high cost and time-consuming experimental validation procedures. But this approach needs a huge set of previous experimental data to train the predictive models and not suitable for real time control of the system.

M.I. Rumaling et. al. [75] presented the development of PM10 prediction model by using nonlinear autoregressive with exogenous input model. The algorithms used were NAR and NARX that predicted real time-based results for PM but they fail to predict a detailed crank angle based results that better explain the soot formation and oxidation phenomenon. A mathematical derivation to display marine diesel engine's rotational velocity and implementation of PID controller was presented [76]. Here, the researchers introduced this PID controller to regulate this marine diesel engine with the help of python language. The results of this python script were compared with another PID controller designed using MATLAB-Simulink interface. Here, the earlier developed python script was used for real time control of the engine but again this approach lacks the support of physics based model for better accuracy of the output results.

Cheng Ke at. al. [77] developed a nonlinear model predictive controller (NMPC) based on nonlinear autoregressive model with exogenous input neural network (NARXNN). This NMPC controller is derived using NMPC toolbox in MATLAB. The co-simulation model in integration with GT-Power and MATLAB-Simulink is developed. This model is tested for unit step input and reference tracking performances. From the results, the step response of NMPC is better than PID controller and the tradeoff for reference tracking simulation is around 15% which still needs to be minimized in order to ensure accurate prediction.

2.6 Research Gaps and Objectives

For a typical diesel engine, there is increase in engine out emissions over the entire operational lifetime. As the advancements in engine design are considered, engine systems become complicated with additional sensors and actuators as they need more resources as well as time towards system integration and calibration. Usually, NOx sensors are positioned downstream of turbine. They offer low pass filtered, cylinder averaged data over the entire engine cycle and not the instantaneous signal. A common disadvantage among soot sensors is less accuracy and delayed response time.

With respect to recent approaches, there is a need of direct sensing of parameters where sensors cannot be installed physically. As a solution there is a need of detailed mathematical model to predict these emissions. The existing soot models also lack the inclusion of cylinder pressure that leads to less accurate results. The engine out emissions are significantly influenced during transient operation by boundary conditions of combustion process like EGR rate. On the other side other prediction approaches like CFD methods have high computational cost and are not suitable for transient test cases that run much faster than real time processes.

From the controller perspectives, various controllers have been designed for different subsystems of the engine system. However, the proposed approach is a system level approach and requires appropriate controllers that employ flexible and sophisticated access to system states. Based on the above work done by various researchers, it is necessary to address issues like NOx and soot prediction. The proposed model needs to be developed as a tool that predicts the engine out emissions of diesel engines with flexibility, modularity and also eliminates the issues with physical sensors. The main motive behind this research work is based on following factors:

- Eliminating the physical sensors to minimize cost
- Faster response time specially to avoid cold start condition effects

2.6.1 Diesel Engine Combustion Model

a. Manifold Models for intake and exhaust mass flows considering EGR and Turbo effects.

b. Cylinder Model for the combustion and mass exchange/mixing modes

c. ROHR model for pressure, mass burnt fraction and temperature prediction.

d. Chemical Kinetics Equilibrium solver for adiabatic temperature and composition.

2.6.2 NOx Prediction Model

a. Zeldovich mechanism based on temperature and composition

b. Extended Zeldovich mechanism with additional temperature related correlations based on the Zeldovich reaction for NOx formation.

2.6.3 Soot Prediction Model

a. Development of fuel injection and spray model

b. Determination of flame parameters and thermodynamic properties

c. Rates of soot formation and oxidation

2.6.4 Controller Design and Optimization

a. System Identification determine the states and system dynamics.

b. Suitable Controller Strategy for EGR.

2.6.5 Validation with GT-Suite Model and Model Correction

Model validation for correction by comparing it with GT power results.

2.7 Closure on the Chapter

Various types of NOx and soot sensors have been reviewed and discussed for their issues in this chapter. It is evident that existing sensors are costly for certain applications, and they lack faster response in certain atmospheric conditions like cold weather. Therefore, there is need to come up with predictive mathematical models that could replace these sensors with above problems resolved. Next chapter discusses about this mathematical model approach for NOx prediction and intermediate and few primary results obtained have been presented.

3. NOx MODELING

The literature discussed in previous chapter leads to a necessity of detailed NOx prediction approach which is discussed in this chapter. Different subsystems like combustion cylinder, intake and exhaust manifolds, EGR and turbocharger have been considered and their mathematical governing equations have been integrated. Determination of in-cylinder characteristics like mass flow rates, in-cylinder pressure temperatures, rate of heat release, chemical equilibrium and species concentration play a vital role in the determination of engine out NOx and have been discussed in detail. The time temperature history of the in-cylinder areas like rich, stoichiometric and lean zones also contributes to NOx formation and has been discussed in detail.

3.1 Model Architecture

Nitrogen oxides (NOx) can be reduced by increasing the intake manifold EGR fraction x_{egr}. However, x_{egr} depends in complex ways on the actuation of the EGR and VGT. It is therefore required to have organized control of the EGR and VGT to achieve the legislated emission constraints for NOx and smoke [78]. While designing and validating a controller for this system, it is advantageous to have a mathematical model that explains the dynamic behavior of the system and the non-linear outcomes that are crucial for control of mass flows. These vital attributes denote that system has non-minimum phase behaviors, overshoots, and sign reversals. The model explains the dynamics in the manifold pressures, turbocharger, EGR, and actuators with some states to acquire quick simulation periods. Figure 3.1 shows the overview of NOx model that involves inputs and outputs from each sub-system contributing to the local and global estimated variables.

The system is divided into three milestones: Engine Plant, Reference Generator from operating points and GT-power results, and a suitable controller. It covers the flow of object models and their respective usage in the system. Figure 3.2 indicates the detailed block diagram of NOx estimation based on Extended Zeldovich mechanism. The details of subsystems involved have been discussed in further sections.

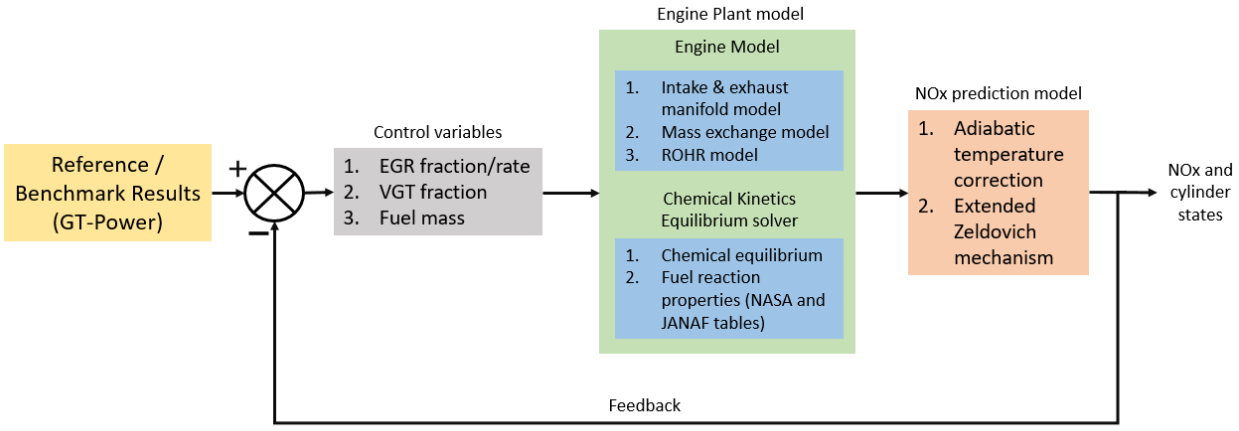

Figure 3.1. NOx model approach

3.2 Cylinder and Mass Exchange Model

The cylinder model subsystem is created to better demonstrate exchange of fuel and air mass injected into each engine cycle. This considers the influence of different components included in cylinder block and engine assembly throughout the entire engine cycle. While deriving this model, different systems were considered like intake and exhaust manifolds, EGR and VGT valves as separate subsystems. Figure 3.2 depicts the overall architecture of this system. It consists of 3 distinct control inputs and five states that are of prime importance to the system. The operation of engine is a function of engine speed obtained from operating cycles and performance curve. So the final model is shown in state space form as shown in equation 3.1 below.

$$\dot{x} = f\left(x, u, n_{\mathrm{e}}\right) \tag{3.1}$$

Where x is a state vector as shown in equation 3.2,

$$x = \left(p_{im}, X_{\mathrm{oim}}\,, p_{\mathrm{em}}\,, X_{\mathrm{oem}}\,, p_c\right)^T \tag{3.2}$$

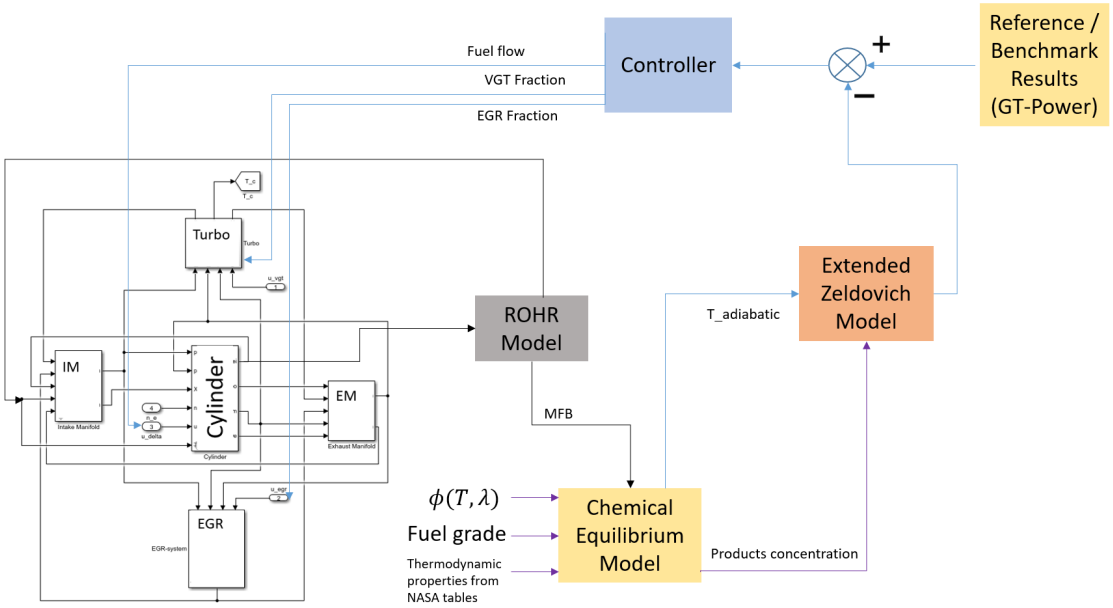

Figure 3.2. Integration of subsystems for control-oriented NOx model

And p_{im} and p_{em} are intake and exhaust manifold pressure. X_{Oim} and X_{Oem} are the oxygen mass fractions at intake and exhaust manifolds, and w_t is the turbine speed. Oxygen mass fraction states are the critical states as they are needed for the oxygen to fuel ratio λ_O.

And the u is a control vector as shown in equation 3.3,

$$u = (u_{egr}, u_{vgt}, u_{\delta})^{\mathrm{T}} \tag{3.3}$$

Where u_{egr}, u_{vgt}, u_{δ} are the EGR valve position, VGT is the actuator position, and Fuel-injected, respectively. u_{egr} and u_{vgt} change from 0 to 100 percent for closed and open positions, respectively. W_{ei}, W_{eo}, W_{egr}, W_c are the mass fractions through engine intake valve, from engine outlet valve, from EGR outlet, and compressor outlet respectively.

3.2.1 Manifolds

The manifold models are created as dynamic mathematical calculations each for intake and exhaust manifolds that predict two critical parameters like pressure and oxygen mass fraction in them. With respect to ideal gas law, a usual isothermal model is developed based

on mass conservation and assumes that manifold temperature stays constant and does not vary significantly. Thus, the governing equations for both these manifolds can be expressed in equation 3.4 below.

$$\begin{aligned} \frac{d}{dt}p_{\text{im}} &= \frac{R_a T_{\text{im}}}{V_{\text{im}}}\left(W_c + W_{\text{egr}} - W_{\text{ei}}\right) \\ \frac{d}{dt}p_{\text{em}} &= \frac{R_a T_{\text{em}}}{V_{\text{em}}}\left(W_{\text{eo}} - W_t - W_{\text{egr}}\right) \end{aligned} \tag{3.4}$$

The thermodynamic processes is split in two phases: 1) ideal-gas constant for air is R_a and the specific heat capacity ratio for air is γ_a, 2) the ideal-gas constant for exhaust gas is R_{e} and the specific heat capacity ratio is γ_{e}. The temperature in intake manifold T_{im} is believed to be steady and equivalent to the temperature in the intercooler. The temperature in exhaust manifold T_{em} will be discussed in subsequent sections and V_{im} and V_{em} are the volumes of intake and exhaust manifolds respectively. The mass flows in compressor, EGR, intake and exhaust manifolds W_c, W_{egr}, W_{ei}, W_{eo}, and W_t will be discussed in next sections.

There are two sets of thermodynamic properties: 1) air has the ideal-gas constant R_a and the specific heat capacity ratio γ_a, 2) the exhaust gas has the ideal-gas constant R_{e} and the specific heat capacity ratio γ_{e}. The intake manifold temperature T_{im} is assumed to be constant and equal to the cooling temperature in the intercooler, the exhaust manifold temperature T_{em} will be described further, and V_{im} and V_{em} are the manifold volumes. The mass flows W_c, W_{egr}, W_{ei}, W_{eo}, and W_t will be described in further sections.

The extent of EGR fraction in the intake manifold is described as in equation 3.5

$$x_{\text{egr}} = \frac{W_{egr}}{W_c + W_{\text{egr}}} \tag{3.5}$$

EGR additionally includes oxygen which impacts the oxygen-to-fuel fraction inside the cylinder. This outcome is included by deriving the oxygen concentrations in intake and exhaust manifolds as X_{Oim} and X_{Oem} respectively. These fractions are defined with respect to equation 3.6.

$$X_{\text{Oim}} = \frac{m_{\text{oim}}}{m_{\text{totim}}}, X_{\text{Oem}} = \frac{m_{\text{Oem}}}{m_{\text{totem}}} \tag{3.6}$$

where m_{Oim} and m_{Oem} are the oxygen mass quantities in the intake and exhaust manifold respectively. Here, m_{totim} and m_{totem} are the total masses in the intake and exhaust manifolds respectively. Differentiating X_{Oim} and X_{Oem} with respect to time and using the law of mass conservation[40] yields the differential equations as in 3.7.

$$\begin{aligned} \frac{d}{dt}X_{\mathrm{Oim}} &= \frac{R_a T_{\mathrm{im}}}{p_{\mathrm{im}} V_{im}} \left(W_c \left(X_{Oc} - X_{Oim}\right) + W_{egr} \left(X_{Oem} - X_{Oim}\right)\right) \\ \frac{d}{dt}X_{\mathrm{Oem}} &= \frac{R_{\mathrm{e}} T_{em}}{p_{em} V_{em}} \left(W_{eo} \left(X_{O\mathrm{e}} - X_{Oem}\right)\right) \end{aligned} \tag{3.7}$$

where X_{Oc} is the steady oxygen fraction in the compressor, i.e. air with X_{Oc}=23.14%, and $X_{O\mathrm{e}}$ is the oxygen fraction in the exhaust manifold entering through the engine cylinders. A distinct methodology to consider oxygen in the EGR gas is to prove the burned gas ratio in the control volume is a general practice for states in many research efforts [55]–[57].

3.2.2 Cylinder

Three submodels illustrate the performance of the cylinder; as follows:

- A model that explains flow of fuel and gas that enters and exits the cylinder, the oxygen-to-fuel ratio, and the oxygen fraction in the composition going out from the cylinder.
- A detailed mathematical model for exhaust manifold temperature;
- An engine torque model

Flow Inside the Cylinder

The flow of air from intake manifold into the combustion chamber W_{ei} is explained with the help of volumetric efficiency η_{vol} [5] of the cylinder as shown in equation 3.8.

$$W_{\mathrm{ei}} = \frac{\eta_{\mathrm{vol}}\, p_{\mathrm{im}} n_{\mathrm{e}} V_d}{120 R_a T_{\mathrm{im}}} \tag{3.8}$$

where p_{im} and T_{im} are the pressure and temperature inside the intake manifold, n_{e} is the engine speed, and V_d is the displaced volume by the cylinder. The volumetric efficiency is expressed by equation 3.9,

$$\eta_{\text{vol}} = \text{c}_{\text{vol1}} \sqrt{p_{\text{im}}} + \text{c}_{\text{vol 2}} \sqrt{n_{\text{e}}} + \text{c}_{\text{vol 3}} \tag{3.9}$$

The flow of fuel W_f inside the cylinder is governed by control variable u, that denoted the quantity of fuel injected in milligrams per cycle and cylinder as shown by below equation 3.10.

$$W_f = \frac{10^{-6}}{120} u_\delta n_{\text{e}} n_{cyl} \tag{3.10}$$

where n_{cyl} is the number of cylinders in the engine setup. The mass balance expression in equation 3.11 gives the flow rate out from the cylinder.

$$W_{eo} = W_f + W_{\text{ei}} \tag{3.11}$$

The fraction of oxygen-to-fuel ratio λ_O in the cylinder is described by equation 3.12 as

$$\lambda_O = \frac{W_{eo} X_{O\text{im}}}{W_f (O/F)_s} \tag{3.12}$$

where $(O/F)_s$ is the stoichiometric fraction at the ideal combustion of the oxygen quantity to the fuel quantity. It is equivalent to the AFR that is a general choice of operational variable in the past research work [57], [58], [79], [80].

During and after compression stroke, the oxygen starts burning in the vicinity of diesel droplets. To avoid smoke in diesel engines, λ_O>1. And the O_2 fraction farther from the cylinder can then be defined as the unburned oxygen fraction by equation 3.13 as,

$$X_{O\text{e}} = \frac{W_{\text{ei}} X_{O\text{im}} - W_f (O/F)_s}{W_{eo}} \tag{3.13}$$

Exhaust Manifold Temperature

This subsystem includes of the estimation of the temperature of exhaust coming out of cylinder and a relation for the heat losses in the exhaust manifold. The modeling approach for cylinder-out temperature T_{e} is taken from previous research [70]. This method is dependent

upon ideal-gas Seliger cycle (or limited pressure cycle [5]) estimation given by equation 3.14 as

$$T_{\mathrm{e}} = \eta_{SC}\Pi_{\mathrm{e}}^{\left(1-\frac{1}{\gamma_a}\right)} r_c^{1-\gamma_a} x_p^{\left(\frac{1}{\gamma_a}-1\right)} \times \left(q_{\mathrm{in}} \left(\frac{1-x_{cv}}{c_{pa}} + \frac{x_{cv}}{c_{Va}} \right) + T_1 r_c^{\gamma_a - 1} \right) \tag{3.14}$$

where η_{sc} is a compensation gain for non-ideal cycles and x_{cv} is the fraction of fuel utilized during constant-volume combustion process. The remaining fuel, i.e. $(1 - x_{cv})$ is consumed during constant-pressure combustion phase. This approach also considers the following factors: the pressure ratio given by equation 3.15 as

$$\Pi_{\mathrm{e}} = \frac{p_{em}}{p_{\mathrm{im}}} \tag{3.15}$$

The pressure ratio after combustion and before combustion in the Seliger cycle expressed by equation 3.16 as

$$x_p = \frac{p_3}{p_2} = 1 + \frac{q_{\mathrm{in}} X_{cv}}{c_{Va} T_1 r_c^{\gamma_a - 1}} \tag{3.16}$$

This air fuel charge has specific energy contents expressed by equation 3.17 as

$$q_{\mathrm{in}} = \frac{W_f q_{HV}}{W_{\mathrm{ei}} + W_f} \left(1 - x_r\right) \tag{3.17}$$

When inlet valve closes at the end of intake stroke, the temperature at this instant is given by equation 3.18 as

$$T_1 = x_r T_{\mathrm{e}} + \left(1 - x_r\right) T_{\mathrm{im}} \tag{3.18}$$

The residual gas fraction given by equation 3.19 as

$$x_r = \frac{\Pi_{\mathrm{e}}^{1/\gamma_a} x_p^{-1/\gamma_a}}{r_c x_v} \tag{3.19}$$

and the volume fraction between after combustion and before combustion in the Seliger cycle is demonstrated by equation 3.20 as

$$x_v = \frac{v_3}{v_2} = 1 + \frac{q_{\mathrm{in}} \left(1 - x_{cv}\right)}{c_{pa} \left[\left(\frac{q_{\mathrm{in}} x_{cv}}{c_{Va}} \right) + T_1 r_c^{\gamma_a - 1} \right]} \tag{3.20}$$

As the calculations above are non-linear and rely on each other, the cylinder-output temperature is computed numerically by applying a fixed-point iteration which begins with the initial values $x_{r,0}$ and $T_{1,0}$. Then the equations are utlized in each iteration k.

The reduction in temperature because of heat losses in exhaust pipes is mathematically derived in similar fashion as model 1 discussed in reference [24], and it is expressed as a function of mass flow rate coming out from the cylinder as in equation 3.21.

$$T_{em} = T_a + (T_{\mathrm{e}} - T_a) \exp \frac{h_{tot} \pi d_{pipe} l_{pipe} n_{pipe}}{W_{\mathrm{eo}} C_{pe}} \tag{3.21}$$

where T_a is the ambient temperature, h_{tot} the total heat transfer coefficient, d_{pipe} the pipe diameter, l_{pipe} the pipe length and n_{pipe} the number of pipes.

3.3 Heat Release rate model

The validation of developed emission model is done with the help of rate of heat release profiles that are obtained from in-cylinder pressure and temperature conditions. These in-cylinder condition profiles have all the history that includes engine operating variables like rate of fuel consumption and further formation of emissions. The proposed work highlights on mathematical modeling of rate of heat release with respect to crank angle degrees (CAD) scale. This ROHR relies heavily on multiple factors like rate of fuel mass entering into the cylinder and species concentration in the air charge. Speed and torque demand on the engine decide these fuel injection flow rates and other relevant instances such as start of injection (SOI), end of injection (EOI), which is further followed by ignition delay predicted with the help of a correlation that is not considered in this work. TO find out this ignition delay, certain parameters like injection duration and AFR are critical. The mass of air entering into the cylinder affects AFR for the first engine cycle. In the second cycle when EGR and VGT actuators come into effect, the chemical composition of the species in this charge changes and it changes the local AFR as well. This well determines the start of combustion (SOC) instance and the total duration of combustion decides the rate of heat release and mass burnt fractions. Using these variables, we can determine in-cylinder pressure and temperature base on ROHR. Below figure 3.3 describes the input and output parameters

from this ROHR model. The mass burnt fraction is the result of fuel injection quantity as well as timing, air quantity, AFR and heat is liberated during the combustion phase. The volumetric expansion as a result of this heat release is responsible for sudden pressure increase inside the cylinder. These in-cylinder conditions are further useful for determining emissions which are relevant to the reaction rates at different instances during the engine cycle.

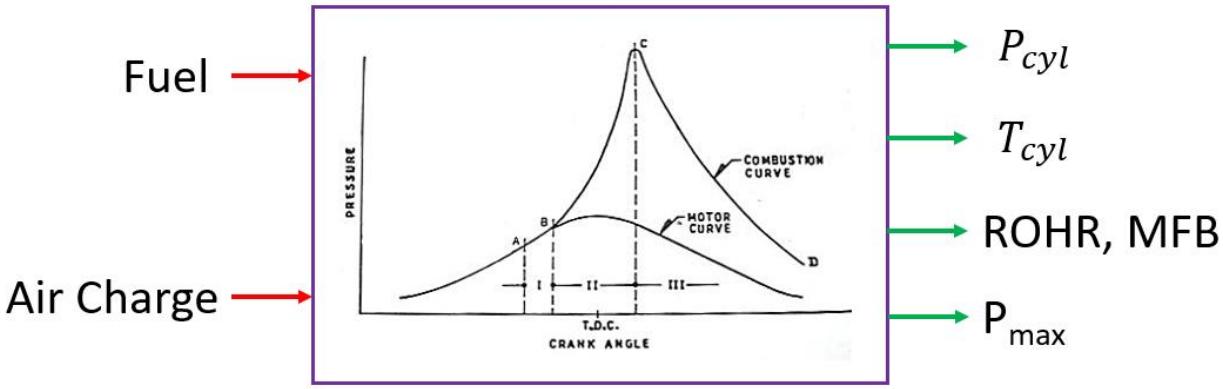

Figure 3.3. Heat release rate model parameters

Rate of heat release model is initialized with deriving the motoring curve relied on the thermodynamic ideal cycle. The instantaneous change in cylinder volume is calculated and in-cylinder instantaneous pressure is also predicted based on ideal gas laws.

3.3.1 Engine Geometry

The geometric volume of cylinder and relative speed of piston are calculated by using basic design calculations of the engine and crank assembly, as follows. The relative instantaneous location of piston relative to top dead center (TDC) is calculated by equation 3.22,

$$z = l + a - s \tag{3.22}$$

where, l is the length of connecting rod and a is the crank radius and s is axial distance between center of the piston and center of the crankshaft determined as follows by equation 3.23,

$$s = a\cos\theta + \sqrt{l^2 - a^2\sin^2\theta} \tag{3.23}$$

where, $\theta$is instantaneous crank angle position.

The instantaneous relative location of piston is a result of crank angle $\theta$and is expressed by equation 3.24,

$$z(\theta) = l + a(1 - \cos\theta) - \sqrt{l^2 - a^2\sin^2\theta} \tag{3.24}$$

The clearance volume, V_c of the cylinder is expressed as the volume of combustion cylinder with respect to the relative position of the piston and the cylinder volume as a result of piston position is given by equation 3.25,

$$V(\theta) = V_c + \frac{\pi B^2 z(\theta)}{4} \tag{3.25}$$

Where B is the diameter of cylinder (bore). This expression is further employed to calculate ROHR inside the cylinder during combustion as a result of cylinder pressure.

3.3.2 Engine Thermodynamic Cycle

A conventional 4 stroke diesel engine consists of four distinct strokes expressed by half engine rotation for 180 CAD. First stroke is intake stroke in which fresh air and fuel are injected into the cylinder. This is followed by second stroke known as compression stroke in which air fuel mixture reaches to an instant where the chemical energy of fuel is converted to useful work as a result of combustion process. In the final moments of compression stroke, this composition of air and fuel burns and it defines the start of next stroke also known as expansion stroke. This stroke results into actual work output for the engine based on speed and torque requirements. At the last moments of expansion stroke, the hot gases resulted from combustion process are pushed out from the cylinder during the exhaust stroke. In this stroke, the cylinder is prepared for next engine cycle and ready for new air fuel charge to

be entered. This entire engine cycle consists of two full angular rotations of the crankshaft. During combustion and expansion stroke the chemical energy of fuel is converted into useful mechanical work as shown by equation 3.26 below.

$$W = \int_{-2\pi}^{2\pi} P(\theta) dV(\theta) \tag{3.26}$$

3.3.3 Ideal Gas Cycle for Determining the Motoring Curve of Engine

Any internal combustion engine follows ideal gas law. the in cylinder pressure is derived on crank angle degrees scale for 720 degrees per cycle and it completes two full rotations of the crankshaft. This model also considers some critical parameters like valve timing, engine speed, intake pressure and engine geometry. The engine strokes discussed in earlier section automatically discussed below in the order of occurrence.

Using the ideal gas law in cylinder condition like pressure and volume are mathematically calculated as a function of crank angle degrees using equation 3.27,

$$P_{\text{motor}} = \left[\frac{V\left(\theta_{\text{ref}}\right)}{V(\theta)}\right]^{k} \times P\left(\theta_{\text{ref}}\right) \tag{3.27}$$

Where, P_{motor} is the motoring pressure with respect to the crank angle (CAD), $V(_{ref})$ is the reference volume at initial reference CAD, $V()$ is the volume at CAD, $P(_{ref})$ is the initial reference pressure (atm pressure here with turbo boost) and k is the adiabatic constant equal to 1.33. Further Temperatures can be found out using ideal Gas law in equation 3.28,

$$PV = mRT \tag{3.28}$$

It was observed from these motoring curves that after addition fuel there was a sudden peak in both temperature and pressure indicating start of combustion.

As discussed before, the heat release rate delivers the main input to the emission formation models, but also delivers many additional variables that are of great importance for combustion control.

The in-cylinder pressure history can be predicted based on the earlier determined rate of heat release profile. Using this data other critical factors in the combustion process can be derived for example, peak pressure during combustion, indicated specific fuel consumption and maximum pressure.

When the rate of heat release is known, it is possible to determine in cylinder averaged temperature. This is a very critical parameter while finding out thermal loading. Furthermore, one of the important parameter in exhaust gas is temperature and can be well predicted.

3.3.4 Wiebe Function

One of the approaches in engine modeling is to find out mass burnt fraction as a result of crank angle degrees by utilizing Wiebe function. It is given by equation 3.29.

$$MFB, x_b = \left\{ 1 - \mathrm{e}^{\left(-a\left(\frac{\theta-\theta_{SOC}}{\Delta\theta}\right)\right)^{m+1}} \right\} \tag{3.29}$$

Where $a = 5$, $m = 2$, θ is instantaneous crank angle, θ_{SOC} is the start of combustion angle calculated from total combustion duration $\Delta\theta = 30°$.

This function is usually adopted to describe the entire combustion phenomenon. The result of this function is mass fraction burnt where zero mass fraction indicates the start of combustion and then rises exponentially to 1 indicating the termination of combustion process. The crank angle degrees difference between these two instances is the total duration of combustion.

3.3.5 Cumulative Heat Release Rate (CHRR)

The processes taking place inside combustion chamber follow first law of thermodynamics and are utilized to determine rate of heat release in equation 3.30,

$$dQ_{hr} = dU + dQ_{ht} + dW \tag{3.30}$$

Assuming a 15% heat loss through the walls, thus only 85% of the total heat released is used for producing the work. To predict engine out emissions first we need to calculate the instantaneous pressure add exhaust valve and corresponding temperatures. These exhaust gas temperatures can be well derived by utilising cumulative rate of heat release with respect to crank angle degrees scale as shown below in equation 3.31,

$$\frac{dQ}{d\theta} = \frac{dU}{d\theta} + P\left(\frac{dV}{d\theta}\right) = \frac{\gamma}{(\gamma-1)P(\theta)\left(\frac{dV}{d\theta}\right)} + \frac{1}{(\gamma-1)V(\theta)\left(\frac{dP}{d\theta}\right)} \tag{3.31}$$

To determine this heat release rate, we need to take into account mass burn fraction by using Wiebe's function which is given by equation 3.32.

$$Q = x_b \times m_f \times LHV \tag{3.32}$$

Where m_f is fuel quantity at that instantaneous crank angle degrees and this is predicted with the help of optimised air fuel ratio, the outputs off cylinder and mass exchange model as discussed in previous section. Next, this species concentration in the reactants for both fuel and air utilised in chemical equilibrium solver and are result of mass burnt fraction. The relevant information for emission formation and its duration is obtained from the instance of maximum pressure. All these cylinder phenomenon observe the ideal gas law during all strokes. Also all the combustion cycles during the commotion stroke are associated with rate of heat release as a function of quantity of fuel utilised during that instantaneous crank angle degrees.

3.4 Chemical Equilibrium Model

For a perfect combustion of diesel fuel, the chemical reaction involving air and fuel as reactants and resulting products are balanced in the equilibrium state. This conversion of products from reactants as a result of complete combustion is shown in following equation 3.33.

$$C_xH_y + (t)(a)\,(O_2 + 3.76N_2) \rightarrow xCO_2 + \frac{y}{2}H_2O + (t \times 3.76 \times N_2) + (t-1)\left(x + \frac{y}{a}\right)O_2 \quad (3.33)$$

When fuel C_xH_y chemically reacts with air at stoichiometric fractions, the products as a result of this reaction are formed and maintain the chemical equilibrium. the products as a result of about reaction heavily rely on fraction 't' and it defines local air fill ratios and mass burnt fractions also.

With respect to first law of thermodynamics, the total enthalpy of products should be equal to the total enthalpy of reactants as shown in equation 3.34 below.

$$h_{\text{reat}}\ (T_{\text{react}}\ , P) = h_{\text{prod}}\ (T_{\text{prod}}\ , P) \quad (3.34)$$

The parameters required for zeldovich mechanism like adiabatic temperature are determined for this constant pressure and constant volume process. JANAF and NASA tables are used to refer enthalpy of formation four products and reactants. To find out adiabatic temperature, and iterative algorithm based on Newton raphson method is adopted that minimizes the enthalpy difference between reactants and products. Further calculation to find out emissions also requires the concentration of species in products. This subsystem is analyzed with respect to crank angle degrees with the help of local air fuel ratios and mass burnt fraction.

3.5 NOx Prediction Model

This work highlights on the determination of nitrous oxides based on extended zeldovich mechanism. The chemical kinetic behavior of NOx generation includes the serial occurrence of reactions that are majorly regarded as oxidation of N_2 to NOx. This includes two types of nitrous oxides, NO (Nitric Oxides) and NO_2 (Nitrogen Oxides). NO is significantly observed during the usual engine operations as compared to NO_2 occurring at light load test cases. This current work predominantly highlights the estimation of NO emissions only. According to Extended Zeldovich mechanism, rate of NO formation is given by following equation 3.35.

$$\frac{d[NO]}{dt} = \frac{6 \times 10^{16}}{T^{\frac{1}{2}}} \times \mathrm{e}^{\left(\frac{-69090}{T}\right)} \times [O_2]_{\mathrm{e}}^{1/2} [N_2]_{\mathrm{e}} \ \mathrm{mol/cm^3\ S} \tag{3.35}$$

$[O_2]_{\mathrm{e}}$ and $[N_2]_{\mathrm{e}}$ are obtained through chemical equilibrium model and rate of heat release model gives mass burn fraction. T is the adiabatic temperature in kelvin obtained with the help of iterative solver.

3.6 Significance of ϕ- T Map

The idea to develop an additional 3 step model was proposed to better understand the formation of NOx in diesel combustion by considering its time temperature history in 3 different steps as mentioned below.

1. Initially, the injected fuel mixes with limited amount of air in cylinder obtaining rich mixture.
2. Next, it releases certain amount of heat, and it forms stoichiometric mixture that leads to complete combustion. During this time, NOx would be significantly generated during the combustion process at locations of highest temperature.
3. The products of this process mix with remaining air in the cylinder and then temperature goes down.

With respect to recent there is such work that adopts highly oxygenated fuel for diesel engines, Miyamoto et al. [81] how displayed that regardless of the type of oxygenation there is decrease in emissions that depends heavily on the oxygen content in the fuel. Figure 3.4 represents $\phi$and T environments for a quasi-steady diesel jet flame having a two-stage environment of fuel oxidation [82] on the ϕ- T map relating to soot and NO formation constraints in oxygenated fuel reactions. As shown in Fig.3.4, inside diesel fuel jet flame the soot formation should be suppressed while controlling the temperature around this diffused burning process around the jet . This would ensure the reduction in nitrous oxide emissions in premixed fuel rich ignition process [83].

Regarding recent attempts to use highly oxygenated fuels for diesel engines, Miyamoto et al. [68] have demonstrated that the reduction in emissions depends strongly on the oxygen

content in the fuel, regardless of the kinds of oxygenates. Figure 3.4 represents $\phi$and T conditions for a quasi-steady diesel jet flame having a two-stage nature of fuel oxidation (i.e., premixed fuel-rich ignition and diffusion flame) [69] on the ϕ- T map relating to soot and NO formation limits in oxygenated fuel reactions. As shown in Fig. 3.4, $\phi$and T in the premixed fuel-rich ignition process inside a diesel jet flame sheath need to be controlled for the suppression of soot formation, while the control of T in the diffusive burning process around the jet periphery is required for the reduction in NOx emissions [70].

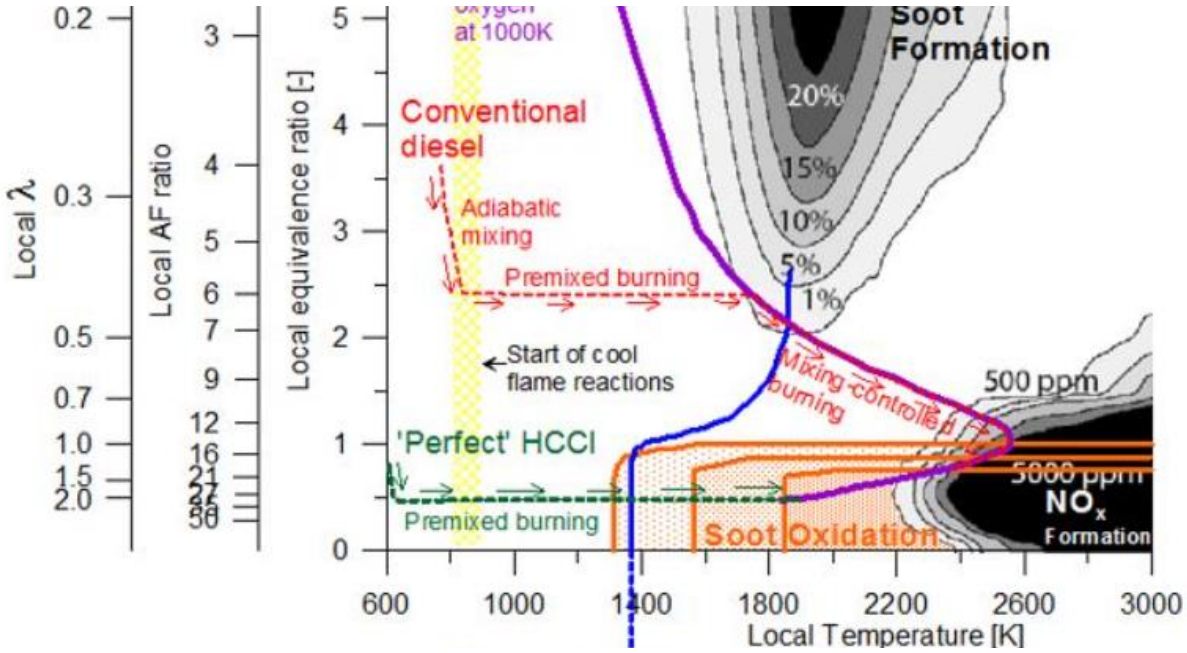

Figure 3.4. ϕ- T map for quasi-steady diesel jet relating to soot and NO formation limits in oxygenated fuel reactions

Siebers and Higgins [20] predicted the amount of ϕas a result of air fuel mixture that forms upstream of liftoff length. This is especially in premixed fuel rich ignition region and considers the axial change of cross-sectional average equivalence ratio inside the spray. The determination of equivalence ratio due to the air entrained before liftoff length can be estimated by equation 3.36 below.

$$\phi = \frac{2(A/F)_{st}}{\sqrt{1 + 16\,(x/x^{+})^{2}} - 1} \tag{3.36}$$

where x is the lift off length of the jet fuel spray and x^+ is the characteristic length scale for the spray influenced by air - fuel densities as well as spray angle and is defined by

$$x^+ = \sqrt{\frac{\rho_f}{\rho_a}} \frac{\sqrt{C_a} d_0}{0.66 \times \tan\left(\frac{\theta}{2}\right)} \tag{3.37}$$

Here, the term d_0 is the orifice diameter, C_a the area contraction coefficient, ρ_f and ρ_a the injected fuel and ambient gas densities respectively, and $\theta$is the spray spreading angles.

With respect to zeldovich mechanism, rate of NO formation is given by equation 3.35. To find out total NO formed during the entire engine cycle, it is essential to determine NO formation reaction zone volume [71]. This heavily relies on the quantity of mass burnt and number of moles of products included information reaction. The volume of reaction zone, $V_{b,\mathrm{i}}$ is given by equation 3.38 as,

$$V_{b,\mathrm{i}} = m_{b,\mathrm{i}} \times \frac{R}{\text{Total number of moles} \times \text{Total molecular wieghts}} \times \frac{T_{\mathrm{comb}}}{P_{\mathrm{i}}} \tag{3.38}$$

where, $m_{b,\mathrm{i}}$ is mass of burnt composition at stoichiometry depending on local equivalence fuel-air ratio, and is given by equation 3.39 as,

$$m_{b,\mathrm{i}} = (MFB_{\mathrm{i}} - MFB_{\mathrm{i}-1})\, m_f + m_a\, (MFB_{\mathrm{i}} - MFB_{\mathrm{i}-1})\, \phi_{local} \tag{3.39}$$

Considering three different local equivalence ratios in each rich, stoichiometric, and lean zone, the reaction zone volume was predicted based on equation 3.38 as shown in figure 3.5 below. Similarly, the temperature plot in all 3 zones can be well predicted iteratively using the same equation and is shown in figure 3.6.

It can be concluded from both figures that the combustion in rich zone starts early as compared to stoichiometric and lean mixture.

The cumulative effect of reaction zone volume is taken into consideration depending on the combustion temperature and respective values of $V_{b,\mathrm{i}}$ were used to determine total NOx formed based on equation 3.40 below.

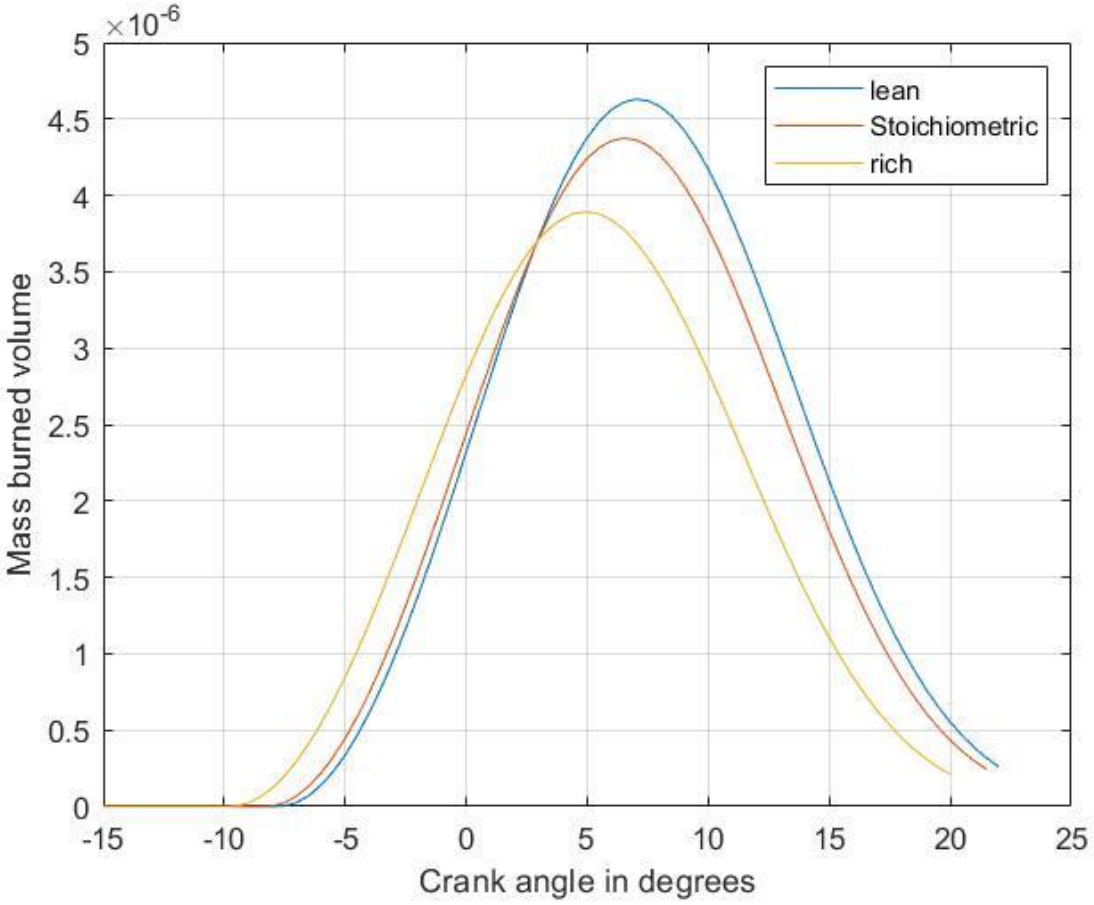

Figure 3.5. Volume of burned mass in cylinder vs crank angle

Thus, total amount NOx generated during one entire combustion cycle is given by,

$$NOx_{cycle,\mathrm{i}} = V_{b,\mathrm{i}} \int_{\mathrm{SOC}}^{EOC} \frac{d[NO]}{dt} d(CAD) \tag{3.40}$$

3.7 Closure on the Chapter

The NOx prediction model based on Extended Zeldovich approach has been presented. The detailed working and integration between mass air exchange model, heat release rate model, heat losses, chemical equilibrium model, EGR and VGT model has been presented. Here, the intermediate results like temperature, HRR and mass burnt fraction we get are in line with the previous literature. A simple crank angle-based prediction for NOx is obtained

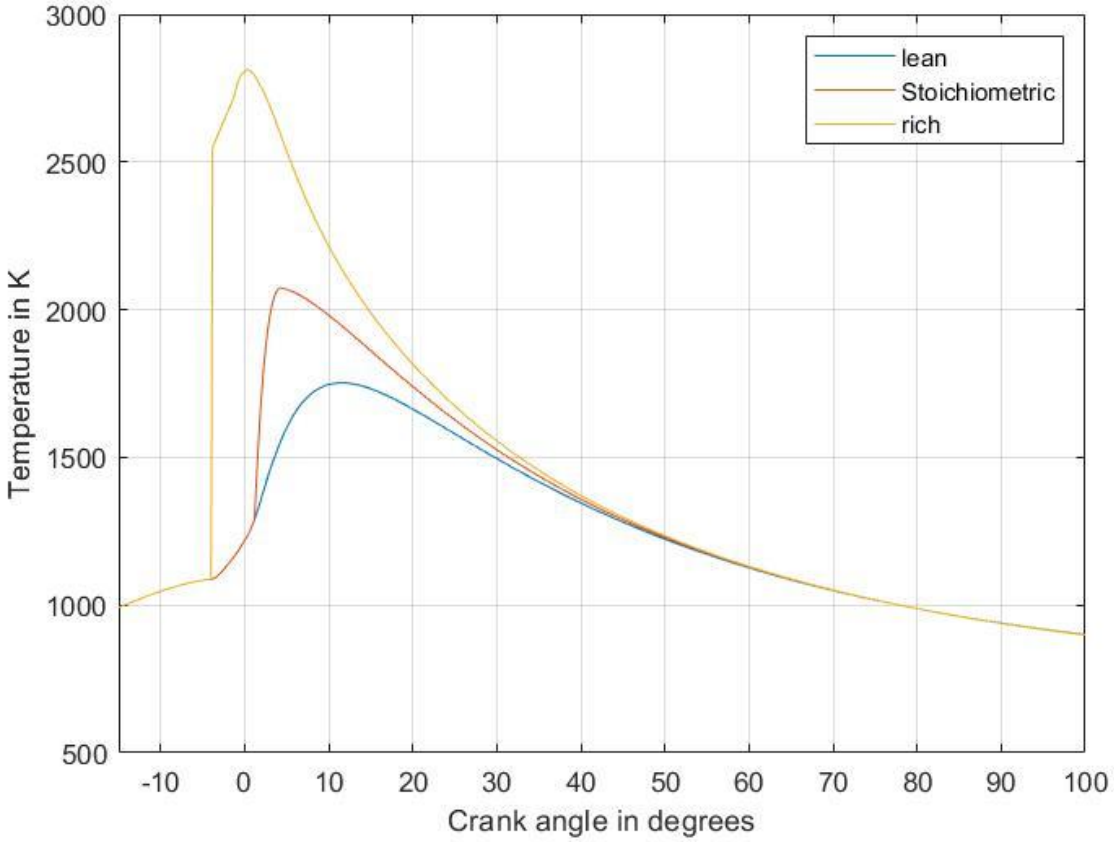

Figure 3.6. Time temperature history considering the 3-step process

and discussed in detail in further chapters. Next chapter presents the detailed development of soot prediction model in which the entire model is discussed along with its subsystems and their integration.

4. SOOT MODELING

Before mathematically describing the mechanism of the formation of soot, it is necessary to understand the concepts involved in this mechanism. There is a strong link between certain physical characteristics of the fuel spray of diesel direct injection and emission of particulate matter or soot. This bond determines the need to first model the physical characteristics of the fuel spray, and then to model properly the particulate emission material of direct injection diesel engines. The model is created using Simulink and simulations data is recorded on crank angle degrees (CAD) scale.

Figure 4.1 shows the flowchart for soot model approach in which various parameters like in-cylinder pressure and temperature have been acquired from the GT-Power model developed. However, some of the parameters are required to be analyzed in detail and hence the net mass of soot cannot be determined at this stage.

4.1 Injection Coefficient

To consider the effect of mass and momentum fluxes of fuel jet leaving from the nozzle orifice, 3 distinct coefficients are used [84]: the first one is the discharge coefficient (C_D), second being the velocity coefficient (C_V), and the third is area contraction coefficient (C_A). Initially the discharge coefficient accounts for the mass flow rate through an injector orifice, whereas the area reduction or velocity coefficient allows the momentum flux to be taken into account. The area contraction coefficient accommodates for flow area loss as result of vapor bubbles as a result of cavitation. All these three coefficients are correlated by the Eq. 4.1. At elevated injection pressures, C_V =1, will only in a few percent overestimated of the momentum flux [85].

$$C_D = C_A \cdot C_V \tag{4.1}$$

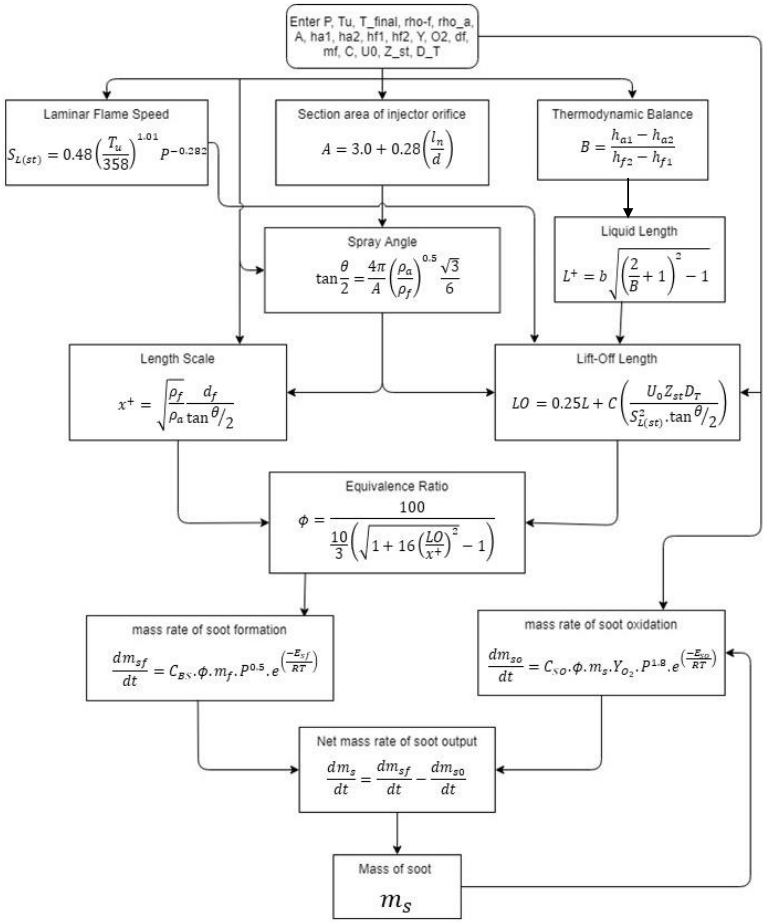

Figure 4.1. Algorithm flowchart for soot model

4.2 Spray Angle

When a fuel liquid jet leaves from the injector nozzle inside the cylinder it diversifies in shower drops those mixes with vapor afterwards. This angle of diversion or expansion depends on multiple factors like dimensions of injector orifice and air fuel densities as shown in figure 4.2. If this angle is more it would result in more amount of gas coming back into the liquid jet as it goes away from the nozzle. the mathematical approach derived by Reitz Bracco [86] to find out spray angle also employs the use of aspect ratio of the nozzle. This ratio is length to diameter ratio of the injector orifice. This model also considers did they Reynolds and Weber numbers and the ratio of air fuel densities throughout the combustion cycle. Orifice area is given by equation 4.2 as

$$A = 3.0 + 0.28\left(\frac{l_n}{d}\right) \tag{4.2}$$

Substituting, we get simplified expression for spray angle as shown in equation 4.3. Several latest fuel injectors operate add sufficient pressures to result in automization nearest to the nozzle tip.

$$\tan\left(\frac{\theta}{2}\right) = \frac{1}{A} \cdot 4\pi \cdot \sqrt{\frac{\rho_a}{\rho_f}} \cdot \frac{\sqrt{3}}{6} \tag{4.3}$$

4.3 Liquid Length

The liquid length it's a distance travelled by the fuel jet before dispersing with the air. Siebers [78] established a scaling law to determine this liquid length. It is based on ideal diesel fuel spray model [86] shown in Fig. 4.2.

The assumptions made by Siebers [85], are also applicable to this approach. These assumptions include perfect air fuel mixing inside jet spray, uniform fuel concentration, uniform velocity, uniform temperature and finally no velocity slip occurs between fuel and reentered gas.

As the liquid jet enters through the nozzle it starts to mix with neighboring gases at a uniform speed and increases the spray angle. therefore we can say that the amount of gas entering back into the jet is directly proportional to the axial distance from the injector nozzle. Siebers Higgins [9] established a length scale (x^+) denoted in equation 4.4. It normalizes axial injection lengths that allow dimensionless parameters to explain the properties of the injecting spray. Here (ρ_a/ρ_f) is the ratio of fuel and gas densities, the letter a is an empirical constant (0.66), and θ is the spray angle.

$$x^+ = \sqrt{\frac{\rho_a}{\rho_f}} \cdot \frac{d_f}{\operatorname{artan}\left(\frac{\theta}{2}\right)} \tag{4.4}$$

When fuel jet enters through nozzle orifice, The flow of fuel is a restricted by the change in cross section and this reduction of useful area is expressed by effective diameter of orifice.

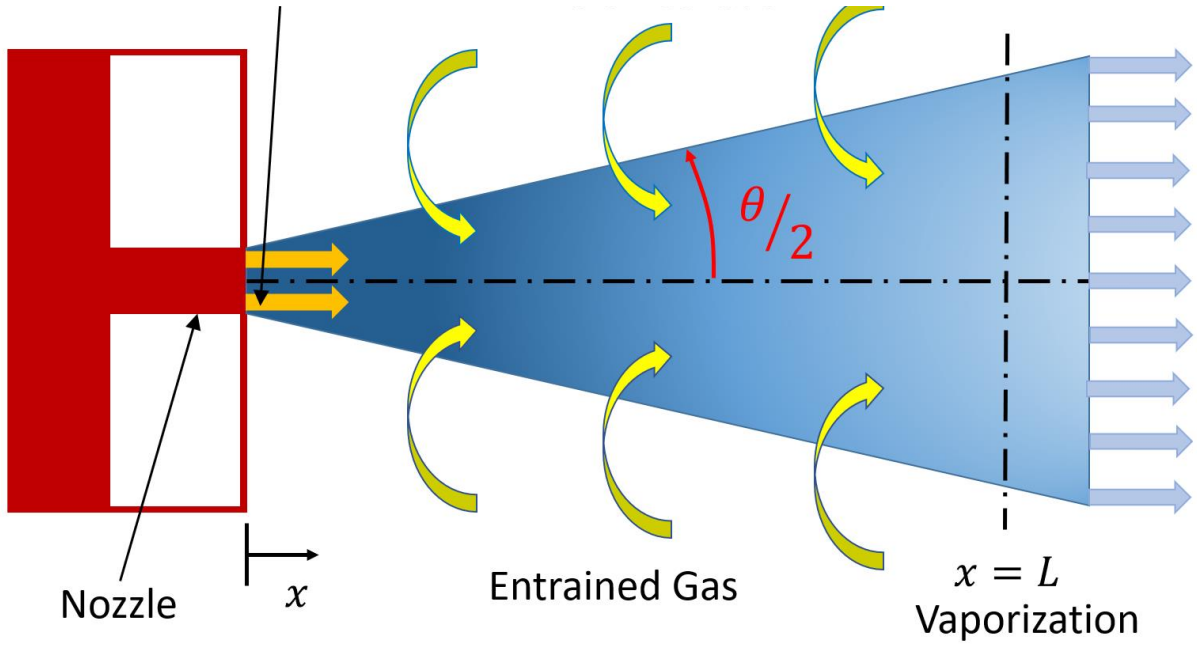

Figure 4.2. Spray Vaporization Model

Equation 4.5 shows the effective area, where C_A is the coefficient of area contraction and d is the physical diameter of the orifice.

$$d_f = \sqrt{C_A} \cdot d \tag{4.5}$$

The equation 4.6 shows the liquid length (L^+) relation based on Siebers [5]. In equation 4.6, b is an experimental constant (0.41), and B is obtained by obtaining thermodynamic balance.

$$L^+ = b \cdot \sqrt{\left(\frac{2}{B} + 1\right)^2 - 1} \tag{4.6}$$

B represents a balance of two different thermodynamic reactions, and it involves and help differences off air and fuel in initial and final phases [85]. The equation 4.7 shows these relations.

$$B = \frac{\varepsilon_a \left(T_2, P_{a2}\right) \cdot P_{f2} \cdot M_f}{\varepsilon_f \left(T_2, P_{f2}\right) \cdot P_{a2} \cdot M_a} = \frac{h_{a1} - h_{a2}}{h_{f2} - h_{f1}} \tag{4.7}$$

Constraining the end state of the liquid fuel to saturated vapor state and considering the final mixture of air and fuel to be in thermodynamic equilibrium, it allows us to use the final temperature of the composition inside cylinder. When initial guess is considered, we can determine the vapor pressure of the fuel and other properties in the in the thermodynamic cycle. The partial pressure of the air can be predicted by deducting the partial pressure of the fuel from the total cylinder pressure, at the guessed temperature. At this phase, we can calculate rest of the properties inside the combustion chamber at any instant. If the two sides of equation 4.7 are not equal a new initial guess is entered and the alterative algorithm again looks for converging solution.

4.4 Lift-Off Length

It is the axial distance from the injected nozzle to the point along spray jet where diffusive flame covers the fuel spray. After this point the air cannot be reentered into the spray. Even though liftoff length depends majorly on liquid length, It also is there is a lot of thermodynamic properties of the fuel. below equation 4.8 shows this relation based on Siebers with Bayer Foster [8], [78].

$$LO = (0.25)L + C\left[\frac{U_0 \cdot Z_{st} \cdot D_T}{S^2_{L(st)} \cdot \tan\left(\frac{\theta}{2}\right)}\right] \tag{4.8}$$

The value of the stoichiometric fuel mixture fraction (Z_{st}) is defined by Peters [87] in the equation 4.9, where R_1 is the fraction of mass of oxygen to fuel at stoichiometric mixture, R_2 is the fraction of mass of fuel-on-fuel flow (typically 1 for pure fuels), and R_3 is the fraction of mass of oxygen in the oxidizer flow (0.232 for air). This ratio is constant for a given type of fuel.

$$Z_{st} = \left(1 + \frac{R_1 R_2}{R_3}\right)^{-1} \tag{4.9}$$

Thermal diffusivity (D_T) is established also by Peters [87] in equation 4.10, as an result of how rapidly the heat of reaction is transferred downstream, to heat the incoming reactants to a temperature suitable for occurrence of the reaction.

$$D_T = \frac{\lambda}{\rho \cdot C_p} \tag{4.10}$$

The in-cylinder temperature and pressure conditions are used to calculate laminar flame speed at stoichiometric air fuel mixture in m/s. This empirical relation was developed by Bradley et al. [88] and shown in equation **??** below. To determine this relation, a 10% n-heptane and 90% iso-octane mixture was considered for study but was found to be useful for similar HC fuels.

$$S_{L(st)} = 0.48 \left(\frac{T_u}{358}\right)^{1.01} \cdot P^{-0.282} \tag{4.11}$$

4.5 Equivalence Ratio

One of the important parameters of primary reaction is the equivalence ratio (ϕ) and it can be derived from liftoff length. With the detailed study of an ideal fuel jet spray model, it can be concluded that the axial distance from injector nozzle tip has a significant impact on the mass of air reentering into the fuel jet spray. Siebers Higgins [20] established equation 4.12 to explain this process of equivalence ratio that heavily depends on lift off length and characteristic length scale. Under the assumption that air cannot be reentered once the fuel spray is encompassed with the diffusion flame, the critical parameter here remains to be lift off length And is a deciding factor for maximum amount of air reentering into the jet spray.

$$\phi = \frac{100}{\frac{10}{3}\left(\sqrt{1 + 16\left(\frac{LO}{x^+}\right)^2} - 1\right)} \tag{4.12}$$

4.6 Soot Model

The ultimate determination of soot mass generated is dependent on different revisions of equations established by Hiroyasu Kadota [89] that primarily consider the difference between the rate soot formation and oxidation. The equation 4.13 displays the net soot generation rate formula used in [90][106].

$$\dot{m}_s = \dot{m}_{sf} - \dot{m}_{so} \tag{4.13}$$

The final amount of net soot model is connected to predict the real time soot generated at instantaneous crank angle throughout the engine cycle. With respect to research efforts of Kazakov Foster [91], in the final stages of combustion, the temperature starts decreasing due to less availability of oxygen and goes below 1000K. After this instant, soot formation stops and the model is reset for the next combustion cycle.

At higher temperature and quick reaction time conditions, generally observed in a combustion cylinder, the entire phenomenon of soot generation may be expressed by an Arrhenius type equation. Equation 4.14 is with reference to Patterson et al. [90], and expresses the rate of soot formation in which different variables are considered such as empirical constants, in-cylinder pressure and temperature, equivalence ratio, mass of fuel, activation energy of soot formation (12500 cal/mol), universal gas constant and temperature of soot formation.

$$\frac{dm_{sf}}{dt} = C_{BS} \cdot \phi \cdot m_f \cdot P^{0.5} \cdot \exp\left(\frac{-E_{Sf}}{RT}\right) \tag{4.14}$$

Equation 4.15 is an Arrhenius type rate equation for the determination of rate of soot oxidation, depending on the work done by Patterson et al. [90]. Here dm_{so}/dt is the rate of soot oxidation, C_{SO} is the empirical constant of soot oxidation, m_s is the mass of soot, Y_{O2} is the fraction of moles of oxygen present in the combustion chamber, P is the instantaneous in-cylinder cylinder pressure, E_{so} is the activation energy of the soot oxidation reaction (14000 cal/mol), R is the universal gas constant, and T is the temperature in the soot oxidation zone.

$$\frac{dm_{sf}}{dt} = C_{BS} \cdot \phi \cdot m_f \cdot P^{0.5} \cdot \exp\left(\frac{-E_{Sf}}{RT}\right) \tag{4.15}$$

Referring to a particular engine and type of fuel, the base soot oxidation constant is designated to be specific. The process of soot oxidation occurs in and around the fuel jet diffusive flame. This flame is considered to be a region where a turbulent ignition flame is started due to mixing of fresh air with partially formed products of early phase rich zone

reactions. This turbulent flame is usually denoted to occur in the vicinity of stoichiometric air fuel conditions [5]. Therefore, fraction of oxygen moles in oxidation zone is considered to be equivalent of that of reactants region in which stoichiometric mixture of air and fuel happens to take place. The temperature in oxidation region is identified in similar fashion to that of utilized for formation model. However, the simplified form of these chemical reactions is known to occur at stoichiometric conditions to better understand ideal combustion conditions that describes the occurrence and propagation of diffusion flame [92]. The statistical parameters used for this model are mentioned in table 4.1 below.

Table 4.1. Parameters Used for Modeling

Parameter	**Value**
C_A	0.86
C_V	1.0
a	0.66
b	0.41
E_{sf}	12500 cal/mol
R	1.9872 cal/gmolK
E_{so}	14000 cal/mol

One of the critical variables in determination of spray angle is air density. To determine air density, cylinder dimensions and initial boundary conditions for ambient air were considered. The fuel jet was injected through orifice at -5 CAD BTDC for a crank angle duration of 7 CAD which is well predicted as shown in figure 4.3. Ideally, this profile is expected to be a pulse. However, as the fuel is injected into the cylinder, it mixes with pressurized air coming in through intake valve and there are slight deviations as shown in figure 4.3.

Figure 4.4 displays the rates of soot formation and oxidation both. As the fuel is injected from -5 CAD BTDC to 2 CAD ATDC, soot formation starts at the same instance and continues to form until 4 CAD ATDC. This is followed by oxidation phase that occurs from 4 to 11 CAD ATDC after which oxidation stops because of lack of oxygen in the combustion cylinder. It is important to note that rate of formation is much higher than that of oxidation. And hence, it becomes proven that net soot generated is always less than that of formation phase [93].

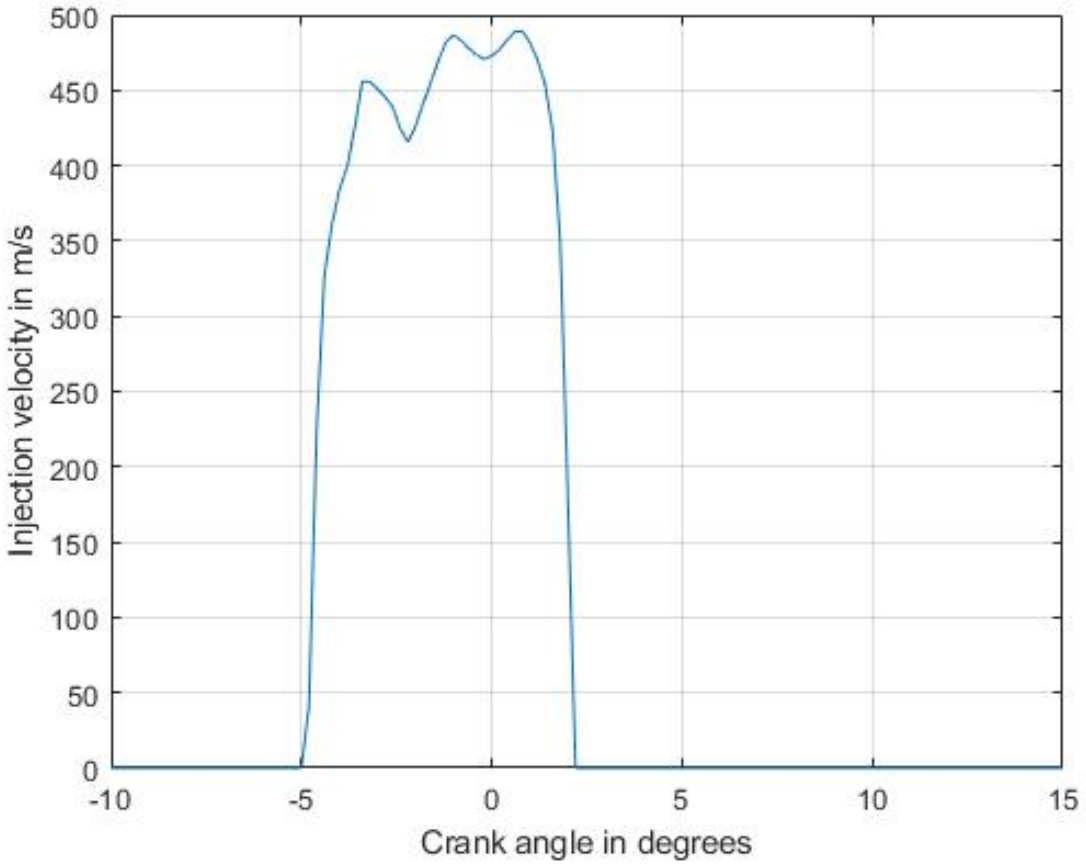

Figure 4.3. Injection Velocity Profile

4.7 Closure on the Chapter

The process of soot formation and oxidation has been discussed in detail using Hiroyasu and Kadota approach. The predicted results for injection velocity and rates of soot formation and oxidation are well validated with the literature. This chapter describes the basis for further state space modeling and controller design discussed in upcoming chapters.

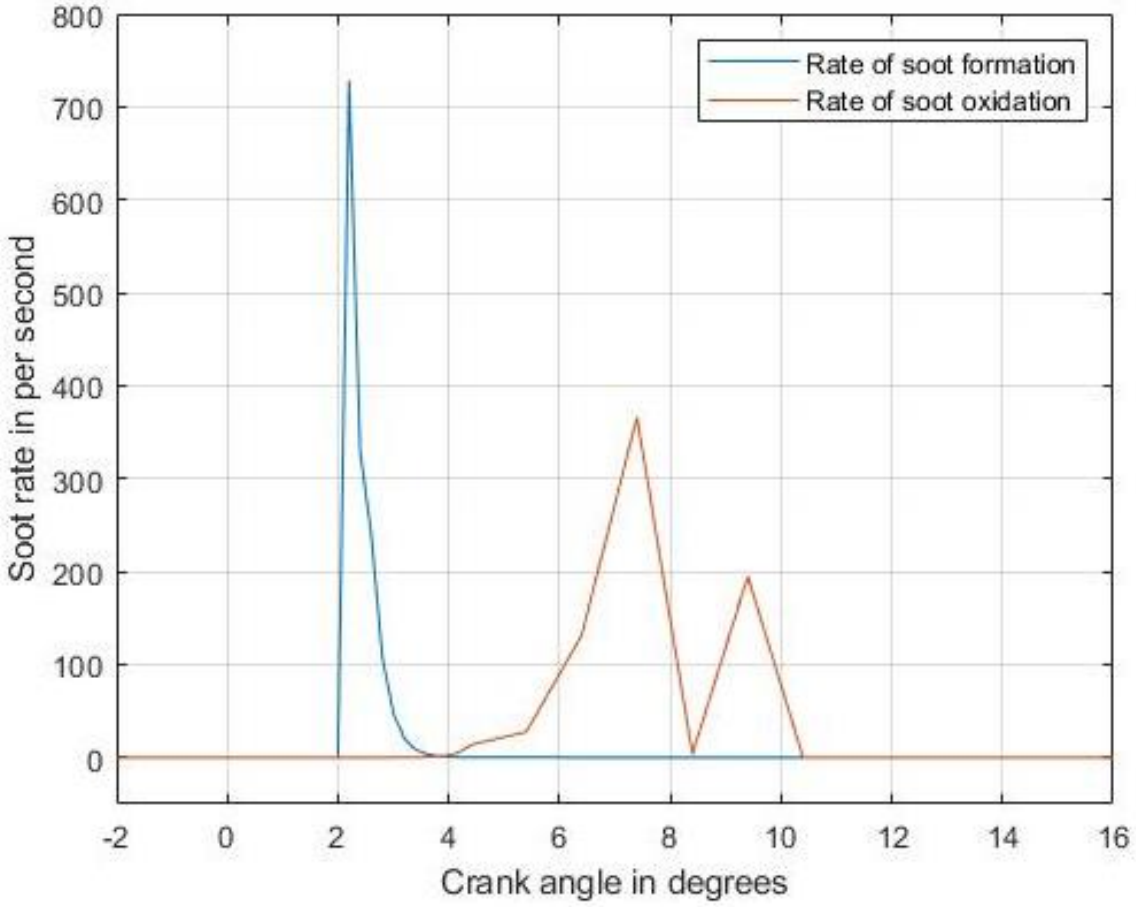

Figure 4.4. Rate of Soot Formation Oxidation

5. STATE SPACE MODELING AND CONTROLLER DESIGN

In order to design a controller for any plant, it is important to derive a mathematical model that expresses the system dynamics based on its states. These states of the system are based on critical components of the system that contribute heavily to the NOx generation. If the system has more degrees of freedom, it can be simplified and reduced to a lower degree provided that there is no significant loss of information and all the relevant data required for the control is recorded. This also reduces computation time and system complexity. Then a system needs to be checked for its controllability in order to ensure all the states of the system are controllable. If this is true, a suitable controller can be designed to fulfil the required performance criteria.

5.1 Derivation of NOx State Space Model

The diesel engine system under consideration contains various subsystems like cylinder, EGR cooler, turbocharger, intake and exhaust manifolds as shown in Chapter 3.

5.1.1 Details of Subsystems in NOx Model

Intake Manifold Parameters

Generally, it is understood that the temperature in intake manifold is remains unchanged with reference to the ideal gas law and conservation of mass and energy. Other parameters like air mass fraction, rate of pressure and mass can be described [94] by equations 5.1 as

$$\begin{aligned} W_{\text{im}} &= W_c + W_{\text{egr}} - W_{cyl} \\ \dot{p}_{\text{im}} &= \frac{\gamma R}{V_{im}} \left[W_c T_{\text{ic}} + W_{\text{egr}} T_{egr} - W_{cyl} T_{\text{im}} \right] \end{aligned} \tag{5.1}$$

Exhaust Manifold Parameters

The exhaust manifold is mathematically derived in similar fashion as of intake manifold and given by equation 5.2 as

$$\begin{aligned} W_{em} &= W_{ec} - W_{egr} - W_t \\ \dot{p}_{em} &= \frac{\gamma R}{V_{em}} \left[W_{cyl} T_{cyl} - W_{egr} T_{em} - W_t T_{em} \right] \end{aligned} \tag{5.2}$$

Turbocharger

It can be concluded for turbocharger [94] as first order inertia system with a time constant as given in equation 5.3 as

$$\dot{p}_c = \frac{1}{\tau_{tc}} \left[\eta_m p_t - p_c \right] \tag{5.3}$$

As shown in equation 5.4 below, with reference to the first law of thermodynamics, the output power of turbine can be estimated [95], [96] as

$$p_t = \eta_t W_t C_{pem} T_{em} \left(1 - \boldsymbol{\pi}_t^{\frac{1-\gamma}{\gamma}} \right) \tag{5.4}$$

In the same way, the mas flow of the compressor outlet can be described as given in equation 5.5 as

$$W_c = \frac{p_c \eta_c}{C_{pim} T_c \left(\boldsymbol{\pi}_c^{\frac{\gamma-1}{\gamma}} - 1 \right)} \tag{5.5}$$

The mass flow of the turbine can be calculated [97] with reference to the equation of continuity of steady flow as

$$W_t = \frac{A_{eff} p_{em}}{\sqrt{R_g T_{em}}} \psi_t \left(p_a, T_{em} \right) \tag{5.6}$$

where

$$\psi_t \left(p_a, T_{em} \right) = \begin{cases} \frac{1}{\sqrt{2}}, 0 \leq \frac{p_a}{p_{em}} \leq 0.5 \\ \sqrt{\frac{2p_a}{p_{em}} \left(1 - \frac{p_a}{p_{em}} \right)}, 0.5 \leq \frac{p_a}{p_{em}} \leq 1 \end{cases} \tag{5.7}$$

A_{eff} is effective flow area of the turbine nozzle.

The compressor output temperature can be defined [98] as

$$T_c = T_a \left[1 + \frac{1}{\eta_c}\left(\boldsymbol{\pi}_c^{\frac{\gamma-1}{\gamma}} - 1\right)\right] \tag{5.8}$$

EGR Valve

A nozzle orifice equation can be used to approximate EGR flow as

$$W_{egr} = \frac{A_{\mathrm{e}gr} p_{em}}{\sqrt{R_g T_{\mathrm{ie}gr}}} \psi_{\mathrm{e}}\left(p_{\mathrm{i}m}, p_{em}\right) \tag{5.9}$$

where

$$\psi_{\mathrm{e}}\left(p_{\mathrm{i}m}, p_{em}\right) = \begin{cases} \frac{1}{\sqrt{2}}, 0 \leq \frac{p_{\mathrm{i}m}}{p_{em}} \leq 0.5 \\ \sqrt{\frac{2p_{\mathrm{i}m}}{p_{em}}\left(1 - \frac{p_{\mathrm{i}m}}{p_{em}}\right)}, 0.5 \leq \frac{p_{\mathrm{i}m}}{p_{em}} \leq 1 \end{cases} \tag{5.10}$$

$A_{egr} = C_d A_{ref}$ is effective flow area of the EGR valve.

EGR Cooler

The engine system consists of two coolers– the intercooler and EGR cooler. Usually, the pressure drop across these coolers is neglected and temperature difference after the cooler can be expressed [99] as

$$\begin{aligned} T_{\mathrm{ic}} &= T_c\left(1 - \eta_{c,c}\right) + \eta_{c,c} T_{\mathrm{cool}} \\ T_{\mathrm{egrc}} &= T_{egrc}\left(1 - \eta_{c,\mathrm{e}}\right) + \eta_{c,\mathrm{e}} T_{\mathrm{cool}} \end{aligned} \tag{5.11}$$

Cylinder

As we are considering a diesel engine in this case, the physical model is comparatively minimal, and cylinder can be assumed as a material exchange medium in between intake and the exhaust manifolds. Assuming that the engine speed is a known quantity, the mass flow into the cylinder can be expressed [100] by velocity equation as

$$W_{cyl} = \frac{n_{\mathrm{e}} V_d p_{\mathrm{i}m}}{120 R_g T_{\mathrm{i}m}} \eta_{vol} \tag{5.12}$$

In spite of the gases remaining in the cylinder after the combustion process that are retained, the estimated rate of mass flowing through exhaust manifold can be calculated as

$$W_{em} = W_{cyl} + W_f \tag{5.13}$$

If the fuel injected in cylinder is completely burned, the fraction of air mass of that remains unburned in exhaust gas can be expressed as

$$X_{O,em} = \frac{X_{O,\mathrm{im}} W_{cyl} - AFR_{st} W_f}{W_{em}} \tag{5.14}$$

The exhaust temperature is a result of various factors including engine speed, excess air and O_2 fraction in the intake manifold. It can be expressed as

$$\begin{aligned} T_{\mathrm{e}} &= T_1 + \Delta T_{\mathrm{e}} \\ \Delta T_{\mathrm{e}} &= f\left(N, \phi_a, X_{\mathrm{im}}\right) \end{aligned} \tag{5.15}$$

Where ϕ_a is the excess air coefficient.

With regards to the above governing equations for the subsystems involved, the entire system can be expressed by below differential equations as

$$\begin{aligned} W_{\mathrm{im}} &= W_c + W_{\mathrm{egr}} - W_{cyl} \\ \dot{p}_{\mathrm{im}} &= \tfrac{\gamma R}{V_{im}} \left[W_c T_{\mathrm{ic}} + W_{\mathrm{egr}} T_{egr} - W_{cyl} T_{\mathrm{im}}\right] \\ \dot{X}_{o,\mathrm{im}} &= \tfrac{W_{egrc}(X_{o,\mathrm{em}} - X_{o,\mathrm{im}}) + W_c(1 - X_{o,\mathrm{im}})}{m_{im}} \\ \dot{p}_{em} &= \tfrac{\gamma R}{V_{em}} \left[W_{cyl} T_{cyl} - W_{\mathrm{egr}} T_{em} - W_t T_{\mathrm{em}}\right] \\ \dot{X}_{o,em} &= \tfrac{W_{cyl}\left(X_{o,cyl} - X_{em}\right)}{m_{em}} \\ \dot{p}_c &= \tfrac{1}{\tau_{tc}} \left[\eta_m p_t - p_c\right] \end{aligned} \tag{5.16}$$

These seven states corresponding to above differential equations express mass, pressure and oxygen concentrations in intake, exhaust manifolds and transient characteristics of the turbocharger.

5.1.2 Model Simplification

The dynamic model described in previous section is critical for NOx prediction as it estimated the O_2 fractions in both manifolds which is an essential parameter in extended Zeldovich mechanism used for NOx estimation in this study. As this model is complex and has comparatively higher dimensions, there will be more constraints while designing a controller for this system. Therefore, in order to simplify this model, it is more appropriate to consider oxygen mass fraction in intake manifold as a control variable for proposed closed loop feedback system [101]. This O_2 mass fraction in can be expressed with reference to mass conservation law as

$$\begin{aligned} \dot{X}_{O,\mathrm{im}} &= \frac{W_{egrc}\left(X_{O,em}-X_{O,\mathrm{im}}\right)+W_c\left(X_{O,a}-X_{O,\mathrm{im}}\right)}{m_{im}} \\ \dot{X}_{O,em} &= \frac{W_{cyl}\left(X_{O,cyl}-X_{em}\right)}{m_{em}} \end{aligned} \tag{5.17}$$

where $X_{O,a}$ is O_2 mass fraction in atmospheric air in intake manifold.

Here, in transient conditions, the temperature of intake and exhaust manifolds does not change. So the flows in them i.e. W_{im} and W_{em} are expressed by using ideal gas equation [102] and those states can be neglected from the system.

Thus, considering other parameters as the state variables, the state vector can be written as $x = [p_{\mathrm{im}}, p_{om}, X_{O\mathrm{im}}, X_{O\mathrm{em}}, p_c]$ and the input variable as $u = X_{O,egr}$ the state space model of the proposed system can be given as

$$\begin{aligned} \dot{p}_{\mathrm{im}} &= -C_1 p_{\mathrm{im}} + C_2 C_d X_{O,\mathrm{egr}} \psi_{\mathrm{e}} p_{\mathrm{em}} + \frac{C_3}{\Pi_c^{\frac{\gamma-1}{\gamma}}-1} p_c \\ \dot{p}_{\mathrm{em}} &= C_4 p_{\mathrm{im}} - \left[C_5 C_d X_{O,\mathrm{egr}} \psi_{\mathrm{e}} + C_6 \psi_t\right] p_{\mathrm{em}} + C_7 W_f \\ \dot{X}_{O,\mathrm{im}} &= C_2 C_d X_{O,\mathrm{egr}} \psi_{\mathrm{e}} \frac{p_{\mathrm{em}}}{p_{\mathrm{im}}} \left(X_{O,\mathrm{em}} - X_{O,\mathrm{im}}\right) + \frac{C_3}{\frac{\gamma-1}{\gamma}} - \frac{p_c}{p_{\mathrm{im}}} \left(X_{O,a} - X_{O,\mathrm{im}}\right) \\ \dot{X}_{O,\mathrm{em}} &= C_4 \frac{p_{\mathrm{im}}}{p_{\mathrm{em}}} \left(X_{O,\mathrm{im}} - X_{O,\mathrm{em}}\right) - C_7 W_f \frac{1}{p_{\mathrm{em}}} \left(X_{O,\mathrm{em}} + AFR_{st}\right) \\ \dot{p}_c &= C_8 \psi_t \left(1 - \Pi_t^{\frac{1-\gamma}{\gamma}}\right) p_{\mathrm{em}} - C_9 p_c \end{aligned} \tag{5.18}$$

where the values $C_{\mathrm{i}}(\mathrm{i}=1,.,9)$ can be considered as constants in certain operating conditions specified and the values of these constants is given by following equations derived within.

$$
\begin{aligned}
C_1 &= \frac{n_{\mathrm{e}} V_d \eta_{\mathrm{vol}}}{120 V_{\mathrm{im}}} \\
C_2 &= \frac{R_g T_{\mathrm{im}}\ A_{\mathrm{ref}}}{V_{\mathrm{im}}\ \sqrt{R_g T_{\mathrm{egrc}}}} \\
C_3 &= \frac{R_g T_{\mathrm{im}}\ \eta_c}{V_{\mathrm{im}}\ T_a C_{p,\ \mathrm{im}}} \\
C_4 &= \frac{n_{\mathrm{e}} V_d T_{\mathrm{em}}\ \eta_{\mathrm{vol}}}{120 V_{\mathrm{em}}\ T_{\mathrm{im}}} \\
C_5 &= \frac{R_g T_{\mathrm{em}}\ A_{\mathrm{ref}}}{V_{\mathrm{em}}\ \sqrt{R_g T_{\mathrm{egrc}}}} \\
C_6 &= \frac{A_{eff} \sqrt{R_g T_{em}}}{V_{em}} \\
C_7 &= \frac{R_g T_{em}}{V_{em}} \\
C_8 &= \frac{\eta_m \eta_t C_{p,em} T_{em} A_{\mathrm{e}ff}}{\tau_{tc} \sqrt{R_g T_{em}}} \\
C_9 &= \frac{1}{\tau_{tc}}
\end{aligned}
\tag{5.19}
$$

The control parameter considered here is oxygen mass fraction in EGR that means output equation can be given as

$$
y = X_{O,\mathrm{im}} \tag{5.20}
$$

5.1.3 Model Linearization

The state space equations consist of above equation 5.18 that are highly non-linear and explain the dynamic behavior of the system. A linearized model can be derived by using Taylor's approximation [93] in the region of operating point (x_0, u_0). In this case, linearized state space system can be expressed by the vector matrix as

$$
\begin{aligned}
\Delta \dot{x} &= A\Delta x + B\Delta u \\
\Delta y &= C\Delta x + D\Delta u
\end{aligned}
\tag{5.21}
$$

where $\Delta x = x - x_0, \Delta u = u - u_0$ and $\Delta y = y - y_0$

A, B, C and D are coefficient matrices of the state space model and can be given as

$$
\begin{aligned}
A = \left(\frac{\partial f}{\partial x^T}\right)_{x_0,u_0} &= \begin{bmatrix} \frac{\partial f_1}{\partial p_{im}} & \frac{\partial f_1}{\partial p_{em}} & 0 & 0 & \frac{\partial f_1}{\partial p_c} \\ \frac{\partial f_2}{\partial p_{im}} & \frac{\partial f_2}{\partial p_{em}} & 0 & 0 & 0 \\ \frac{\partial f_3}{\partial p_{im}} & \frac{\partial f_3}{\partial p_{em}} & \frac{\partial f_3}{\partial X_{o,im}} & \frac{\partial f_3}{\partial X_{O,em}} & \frac{\partial f_3}{\partial p_c} \\ \frac{\partial f_4}{\partial p_{im}} & \frac{\partial f_4}{\partial p_{em}} & \frac{\partial f_4}{\partial X_{o,im}} & \frac{\partial f_4}{\partial X_{o,em}} & 0 \\ 0 & \frac{\partial f_5}{\partial p_{em}} & 0 & 0 & \frac{\partial f_5}{\partial p_c} \end{bmatrix}_{x_0,u_0} \\
B = \left(\frac{\partial f}{\partial u}\right)_{x_0,u_0} &= \begin{bmatrix} \frac{\partial f_1}{\partial X_{O,egr}} \\ \frac{\partial f_2}{\partial X_{O,egr}} \\ \frac{\partial f_3}{\partial X_{O,egr}} \\ 0 \\ 0 \end{bmatrix}_{x_0,u_0} \\
C = \left(\frac{\partial g}{\partial x^T}\right)_{x_0,u_0} &= \begin{bmatrix} 0 & 0 & 1 & 0 & 0 \end{bmatrix}_{x_0,u_0} \\
D = \left(\frac{\partial g}{\partial u}\right)_{x_0,u_0} &= 0
\end{aligned}
\tag{5.22}
$$

As the system is SISO, Δu and Δy have to be scalar. A is 5×5 dimensional matrix, B is 5×1 dimensional matrix, C is 1×5 dimensional matrix and D is a scalar.

5.1.4 Controllability

The objective of this work is to design and implement the controller for NOx reduction. Therefore, it is essential to check if the system is controllable. Characteristic evaluation of the state space model is significant for designing appropriate state feedback controller, and it is the foundation for optimal control. The operating test conditions selected for this study are 1500rpm and 50% EGR valve opening. These values are used to develop the analytical model of the coefficients $C_{\mathrm{i}}(\mathrm{i} = 1, ., 9)$. The relevant data calculated from the developed model is used as an input to this state space model here so that coefficient matrices A and B at the operating point can be obtained as

$$A = \begin{bmatrix} -129.45 & 7.25 & 0 & 0 & 1524.85 \\ 93.87 & -213.56 & 0 & 0 & 0 \\ -3.98 \times 10^{-5} & -8.29 \times 10^{-4} & -16.85 & 1.45 & 0.014 \\ 0.0048 & 1.78 \times 10^{-4} & 51.02 & -51.96 & 0 \\ 0 & 2.35 & 0 & 0 & -34.18 \end{bmatrix}$$

$$B = \begin{bmatrix} 1.06 \times 10^{6} \\ -4.82 \times 10^{6} \\ -95.36 \\ 0 \\ 0 \end{bmatrix} \tag{5.23}$$

The output equation here is a function of oxygen mass fraction in intake manifold. The O_2 mass fraction is a state variable of the system. The output of the system can also be controlled by controlling this state. With respect to the controllability criterion, the system is fully controllable if the controllability matrix $C_M = [\ B \quad AB \quad ... \quad A^{n-1}B\ ]$ is a full rank matrix [95]. Therefore,

$$C_M = \begin{bmatrix} B & AB & A^2B & A^3B & A^4B \end{bmatrix}$$

$$= 10^6 \begin{bmatrix} 1.06 & -172.215 & 13214.1 & 1.05 \times 10^{6} & -810.139 \times 10^{6} \\ -4.82 & 1128.9 & -257245.5 & 56.17 \times 10^{6} & -11.897 \times 10^{9} \\ -95.36 \times 10^{-6} & 5.56 \times 10^{-3} & -1.1822 & 274.7617 & -61199.9 \\ 0 & -0.6352 \times 10^{-3} & -0.30899 & -26.62 & 30485.6 \\ 0 & -11.327 & 3040 & -708433.4 & 156.232 \times 10^{6} \end{bmatrix} \tag{5.24}$$

And rank of C_M is 5 i.e., it is a full rank matrix. Hence, the system is fully controllable.

In similar fashion, to design an observer we need to check if the system is observable. The necessary and sufficient condition for LTI system that can be observed is that observability matrix $O_M = [\ C \quad CA \quad ... \quad CA^{n-1}\ ]^T$ needs to be a full rank matrix [95]. Therefore,

$$O_M = \begin{bmatrix} C \\ CA \\ CA^2 \\ CA^3 \\ CA^4 \end{bmatrix} = \begin{bmatrix} 0 & 0 & 1 & 0 & 0 \\ -39.8 \times 10^{-6} & -829 \times 10^{-6} & -16.85 & 1.45 & 0.014 \\ -65.03 \times 10^{-3} & 0.22387 & 357.901 & -99.7745 & -0.7751 \\ 28.9442 & -50.419 & -11121.1 & 5703.2 & -67.6625 \\ -8453.3 & 10828.6 & 478370.4 & -312466 & 46292.6 \end{bmatrix} \tag{5.25}$$

Rank of O_M is 5 i.e., it is a full rank matrix. Hence, the system is fully observable.

5.1.5 State Feedback Controller Design

Below equation 5.26 expresses the state space model of the system in linearized form. The control parameter Δu is substituted by state variable Δx as

$$\Delta u = \Delta v - K\Delta x \tag{5.26}$$

where Δv is the reference input to the system, K is feedback gain matrix. Hence, the closed loop equation of the system can be written as

$$\begin{aligned} \Delta \dot{x} &= (A - BK)\Delta x + B\Delta v \\ \Delta y &= C\Delta x \end{aligned} \tag{5.27}$$

Here, feedback gain matrix K controls the transient characteristics of the closed loop system with state feedback controller. Here, a quadratic optimal design method with reference to optimal control can be utilized to optimize feedback gain matrix. Let the error vector be

$$\mathrm{e}(t) = \Delta v(t) - \Delta y(t) \tag{5.28}$$

The general form of quadratic performance index [96] is given as

$$J = \frac{1}{2}\mathrm{e}\left(t_f\right) F \mathrm{e}\left(t_f\right) + \frac{1}{2}\int_{t_0}^{t_f} [\mathrm{e}(t) Q \mathrm{e}(t) + \Delta u(t) R \Delta u(t)] dt \tag{5.29}$$

where F, Q and R are weighing matrices. The real output vector can correspond to the variation in the system considering the target input $\Delta v(t) = 0$. When terminal time $t_f = \infty$, terminal state of the system must reach equilibrium. In this case, the system performance index is often described as

$$J = \frac{1}{2}\int_{t_0}^{t_f} [\Delta y(t) Q \Delta y(t) + \Delta u(t) R \Delta u(t)] dt \tag{5.30}$$

The optimal control law can be expressed as

$$\Delta u^*(t) = -R^{-1} B^T P \Delta x(t) \tag{5.31}$$

where P should be positive definite matrix, and it should satisfy the Riccati equation

$$A^T P A + P A + C^T Q C - P B R^{-1} B^T P = 0 \tag{5.32}$$

Let $K = R^{-1} B^T P$. Assuming that P can be derived, K also can be calculated. This feedback gain matrix K can be approximated for different values of weighted coefficients Q and R in the vicinity of the operating points and at the same time system response at initial state $\Delta x(t_0) = [\ 0 \quad 0 \quad 10 \quad 0 \quad 0\ ]^T$ is also analyzed. As the system is SISO system, Q and R are also scalar. Here $Q = C^T * C$ and R can be chosen independently. Therefore, several cases for different values of R were considered. Case 1: Q=1 and R=3
$K = \begin{bmatrix} 4.75 \times 10^{-7} & 1.065 \times 10^{-6} & -0.402 & -5.5 \times 10^{-3} & -7.69 \times 10^{-5} \end{bmatrix}$ and the performance index J=1.36
Case 2: Q=1 and R=20
$K = \begin{bmatrix} 1.12 \times 10^{-7} & 2.43 \times 10^{-7} & -0.11 & -1.9 \times 10^{-3} & -3.45 \times 10^{-5} \end{bmatrix}$ and the performance index J=2.23
Case 3: Q=1 and R=30

$K = \begin{bmatrix} 7.75 \times 10^{-8} & 1.68 \times 10^{-7} & -0.071 & -1.34 \times 10^{-3} & -2.65 \times 10^{-5} \end{bmatrix}$ and the performance index J=2.78

The output response of the system for various values of R is shown in figure 5.1 below. For different values of R and Q being unchanged, as we increase the value of R, feedback matrix becomes lesser than before. Also, the response gets slower. From the below figure for $R = 3$, response is quick, but it has an undershoot. And therefore, appropriate value of R can be selected as 30 as it has fastest response with no undershoot and performance index J is also highest.

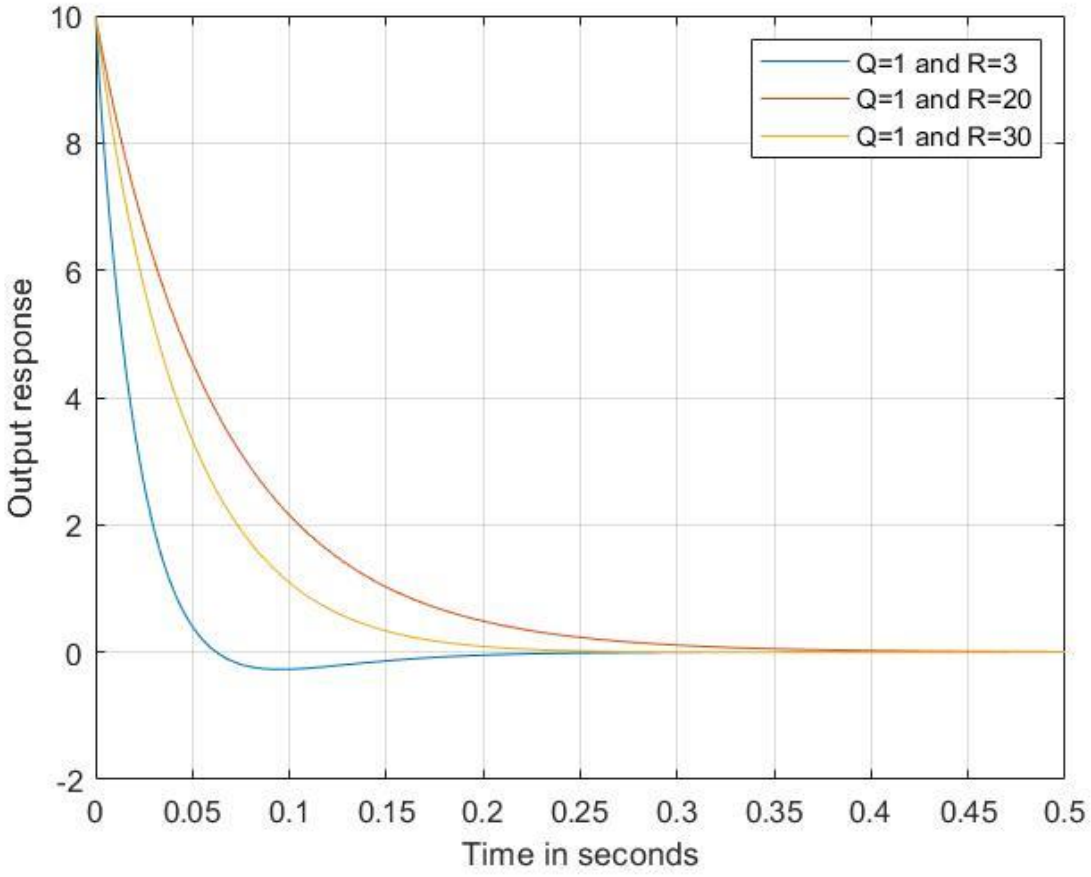

Figure 5.1. System response for various values of R

After implementation of this feedback matrix K, the step response of open loop and closed loop system were compared which is shown in figure 5.2 below. It can be clearly seen that there is a constant offset and to compensate this offset, we need an integral term. For

a unit step input, the system remains stable after 0.4 seconds for open loop system and 0.2 seconds for closed loop system and the change in output does not keep up with the input.

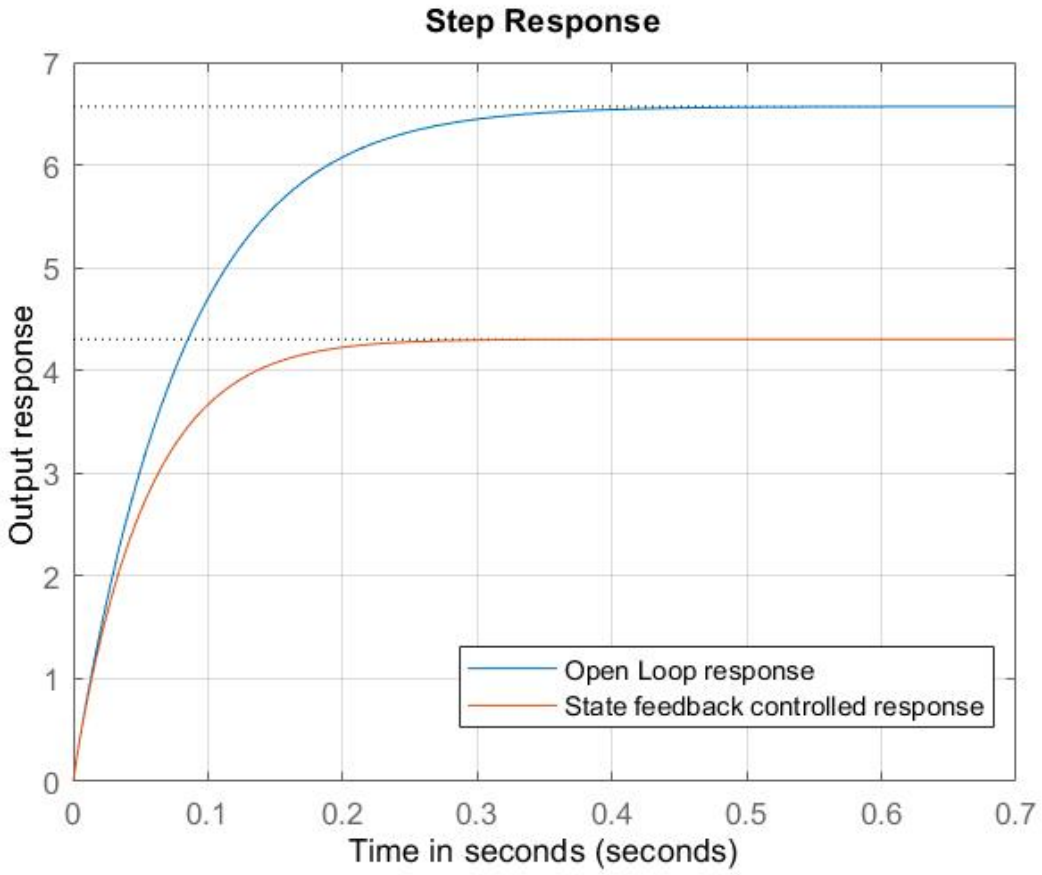

Figure 5.2. Controlled response after implementation of state feedback controller

To eliminate this static error, we need to introduce an integral term in between plant and error compensator. This can be discussed as follows

$$\begin{aligned} \Delta u &= -K\Delta x + K_{\mathrm{i}}\epsilon \\ \dot{\epsilon} &= \Delta v - y = \Delta v - C\Delta x \end{aligned} \tag{5.33}$$

where ϵ is the integrator output, K_{i} is integral gain and both are scalars.

Considering ϵ as a one of the states, the transient response of the system can be given [103] as

$$\begin{bmatrix} \Delta\dot{x} \\ \dot{\epsilon} \end{bmatrix} = \begin{bmatrix} A - BK & BK_{\mathrm{i}} \\ -C & 0 \end{bmatrix} \begin{bmatrix} \Delta x \\ \epsilon \end{bmatrix} + \begin{bmatrix} 0 \\ 1 \end{bmatrix} \Delta v \tag{5.34}$$

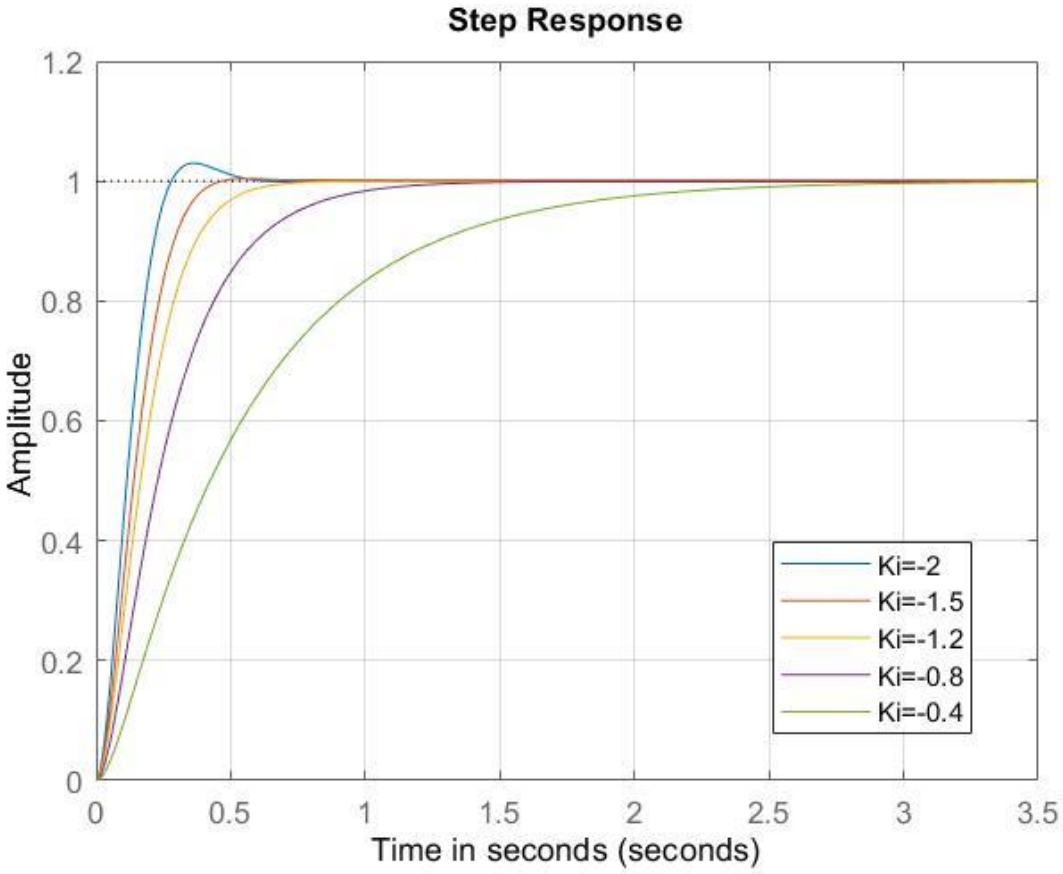

Figure 5.3. Controlled response after adding an integral term

Above figure 5.3 shows transient response for unit step input for the controlled system for various values of K_{i}. From the figure it can be inferred that as K_{i} decreases, output response time also decreases. When K_{i} goes below -1.5, overshoot appears and there is no further major change in the response time. Therefore K_{i}=-1.5 can be selected.

5.2 Soot State Space Model and Controller Design

As discussed in chapter 4 earlier, the soot prediction model comprises of two stages namely soot formation and oxidation. Here, we can consider mass of soot formation and oxidation as two states and derive a state space model accordingly.

The formation stage is expressed [90] as first state by rate of soot formation as

$$\dot{x}_1 = \dot{m}_{sf} = \frac{dm_{sf}}{dt} = C_{BS} \cdot \phi \cdot m_f \cdot P^{0.5} \cdot \exp\left(\frac{-E_{sf}}{RT}\right) \tag{5.35}$$

And oxidation stage is expressed [90] as second state by rate of oxidation as

$$\dot{x}_2 = \dot{m}_{SO} = \frac{dm_{SO}}{dt} = C_{SO} \cdot m_S \cdot Y_{O_2} \cdot P^{1.8} \cdot \exp\left(\frac{-E_{SO}}{RT}\right) \tag{5.36}$$

Let

$$A_1 = C_{BS} \cdot m_f \cdot P^{0.5} \cdot \exp\left(\frac{-E_{Sf}}{RT}\right) \text{ and } A_2 = C_{SO} \cdot Y_{O_2} \cdot P^{1.8} \cdot \exp\left(\frac{-E_{SO}}{RT}\right) \tag{5.37}$$

In this case, above expressions can be written as

$$\dot{x}_1 = A_1 u \dot{x}_2 = A_2 m_s = A_2 \left(x_1 - x_2\right) = A_2 x_1 - A_2 x_2 \tag{5.38}$$

The input to system can be considered as equivalence ratio which depends on oxygen fraction in intake manifold and output of the system is net soot output. Therefore,

$$u = \phi \text{ and } y = m_s = m_{sf} - m_{so} = x_1 - x_2 \tag{5.39}$$

So the overall state space model for soot system can be written as

$$\begin{aligned} \dot{x} = \begin{bmatrix} \dot{x}_1 \\ \dot{x}_2 \end{bmatrix} &= \begin{bmatrix} 0 & 0 \\ A_2 & -A_2 \end{bmatrix} \begin{bmatrix} x_1 \\ x_2 \end{bmatrix} + \begin{bmatrix} A_1 \\ 0 \end{bmatrix} u \\ y &= \begin{bmatrix} 1 & -1 \end{bmatrix} \begin{bmatrix} x_1 \\ x_2 \end{bmatrix} \end{aligned} \tag{5.40}$$

From the reference values considering test point conditions, A_1=162.7 and A_2=26.2

$$A = \begin{bmatrix} 0 & 0 \\ 26.2 & -26.2 \end{bmatrix} \text{ and } B = \begin{bmatrix} 162.7 \\ 0 \end{bmatrix} \tag{5.41}$$

With respect to the controllability criterion, the system is fully controllable if the controllability matrix $C_M = [\ B \quad AB \quad ... \quad A^{n-1}B\ ]$ is a full rank matrix.

Here,

$$C_M = \begin{bmatrix} B & AB \end{bmatrix} = \begin{bmatrix} 162.7 & 0 \\ 0 & 4260.8 \end{bmatrix} \tag{5.42}$$

has rank of 2 and is a full rank matrix. Therefore, system is fully controllable.

The open loop response of above system to unit step input is shown in below figure 5.5. Here, there is a constant offset which is compensated by using a simple PI controller with $K_p = 1$ and $K_\mathrm{i} = 26$. PID tuner app was used in MATLAB for this purpose as shown in below figure 5.4.

After implementation of PI controller, the closed loop response shows substantial enhancement in settling time as well as steady state output of the system.

5.3 Closure on the Chapter

This chapter describes state space modeling for both NOx and soot models. NOx model being highly intricate, and several differential equations govern the dynamics of the system, it is essential to validate their states before going for final estimation. This has been presented in next chapter with test case setup information. Soot state space model is comparatively simple, and the states are controllable. However, soot state space model is not observable and thus observer cannot be designed for the same. Next chapter describes the test setup and validation of the models for both steady state and transient test conditions.

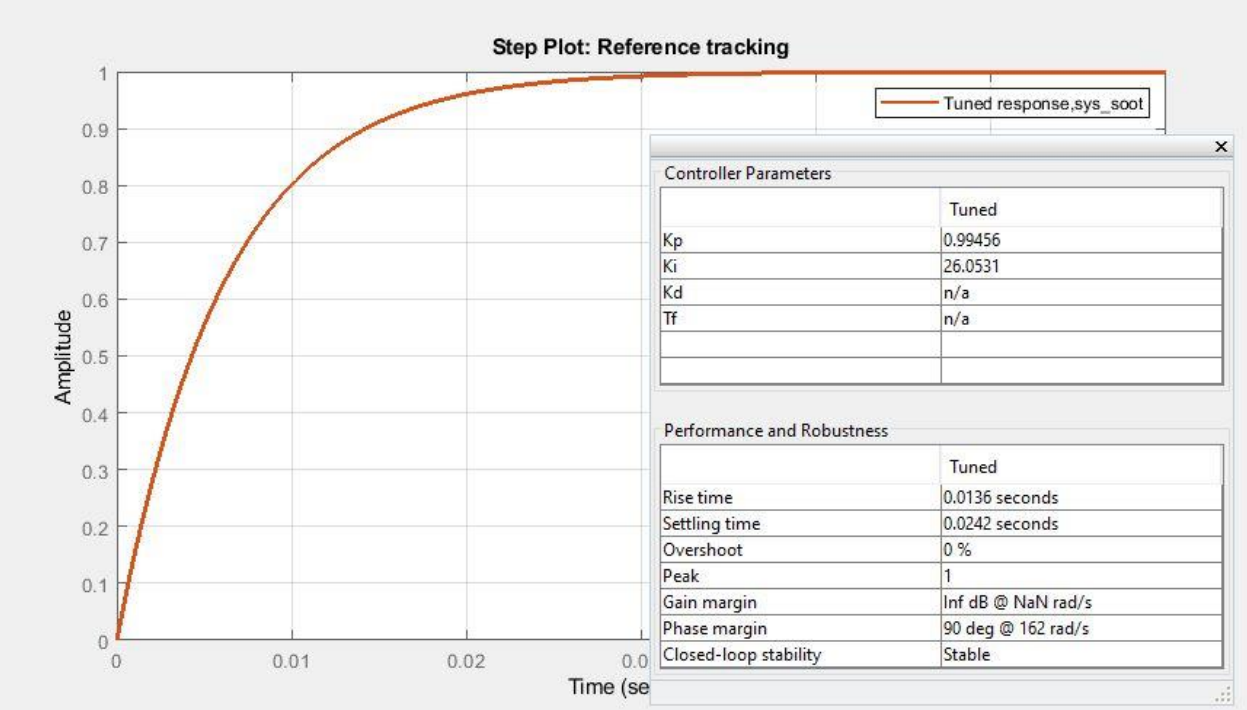

Figure 5.4. Determination of PI gains in PID tuner app

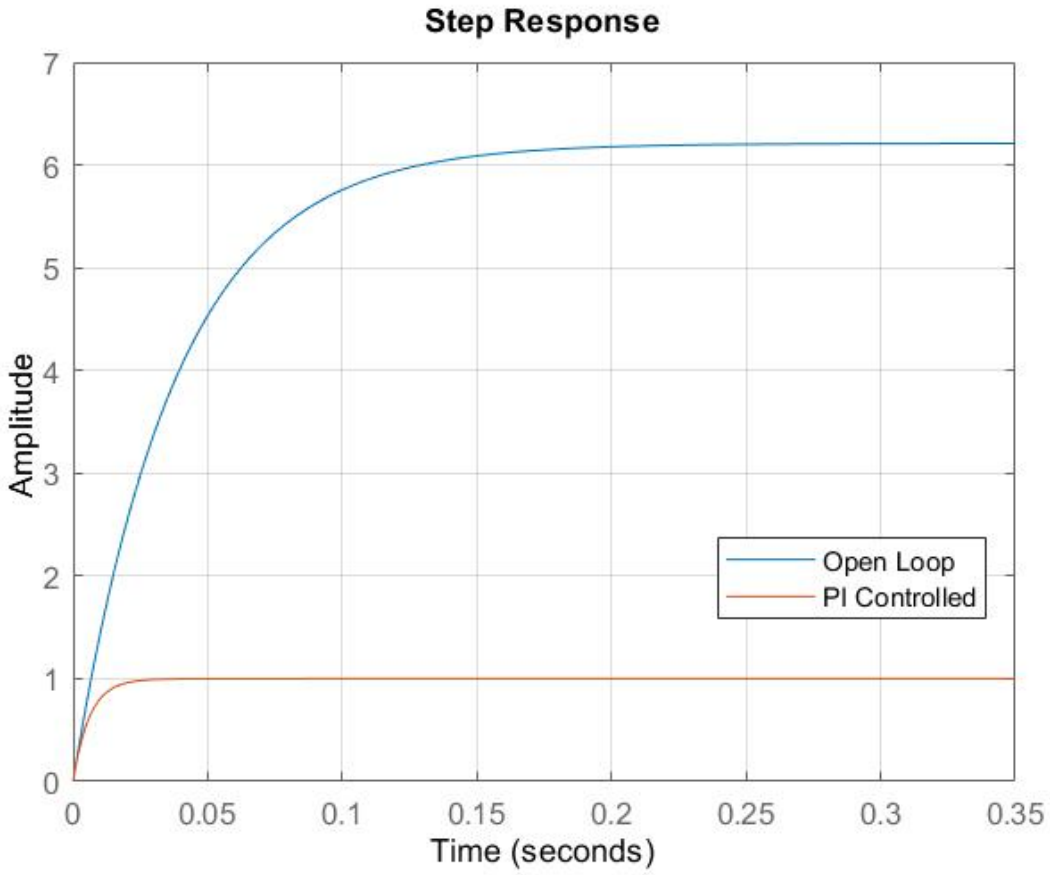

Figure 5.5. Closed loop-controlled response of system after PI controller implementation

6. TEST SETUP AND VALIDATION

The validation of proposed model is carried out with the data obtained from virtual model developed in GT-Suite. The test cases required to run both developed and GT-Suite model are discussed in this chapter to record the dynamic behavior of systems that closely aligns with the actual engine setup. The air fuel mixing model in Simulink is the integrated with emission models developed in Matlab to estimate engine out emissions (NOx and soot) to fulfil the objectives of this work. The detailed process of developing, preparing and validating proposed concept is discussed in subsequent sections.

6.1 Engine Consideration

The proposed approach highlights the application on all segments on diesel engines in both on and offroad applications. The engine under consideration is Cummins 6.7L turbo diesel engine equipped with EGR and turbocharger as a benchmark. One of the same models is already there at IUPUI as shown in figure 6.1 below, and all the physical measurements have been obtained from the same. Though the engine has been procured, the test cell is not operational and experimental validation could not be done. Considering it as a baseline, a GT-Power model was created which is displayed in Fig. 6.2. The technical data for this engine is mentioned in Table 6.1 [104].

Table 6.1. Specifications of Cummins 6.7L diesel engine

Parameter	**Value**
Engine Design	Inline 6 Cylinder DI Diesel
Bore	4.21” (106.9 mm)
Stroke	4.88” (124 mm)
Displacement	6.7 Liters
Compression ratio	17.3:1
Firing order	350-385 at 2800-3013 rpm
Torque	610-930 lb/ft at 1500-1700 rpm

Figure 6.1. Closed loop-controlled response of system after PI controller implementation

The results obtained from these developed models are needed to be validated with that of experimental setup in the test cell. A high-fidelity software GT-Suite is used to validate the results obtained from predictive models.

6.2 GT-Suite Model as a Reference

GT-Suite is an industry approved specification software tool used for simulation activities by majority of engine manufacturers and vehicle OEMs. It is used to predict the various performance variables of engine like volumetric efficiency, fuel consumption, turbocharger performance, power output, torque, airflow and many more subsystems variables on both time and crank angle degrees scale. Standalone and integrated GT-Suite models can be

utilized in a full system level simulation run that can be arranged to run to deliver accurate and co-simulation can also be carried out with other software tools as well as hardware platforms [105].

It also includes various solutions for modeling combustion and emissions. These solutions perform an important role for engine simulations to correctly forecast performance, fuel utilization and engine-out emissions. The developed models facilitate effective analysis at full and part load, as well as real-time efficient transient process for traditional and advanced combustion ideas.

GT-Suite presents an Advanced Combustion Toolset, a set of productivity tools that allows both enhanced model fidelity and quicker runtimes. It contains a state-of-the-art chemical kinetics solver that presents considerably better computational times, allowing use of more comprehensive mechanisms. The toolset also comprises of a pre-processing tool that calculates ignition delay time for mixtures of air, fuel, and residual gases using complete kinetics. This tool allows the user to generate custom correlations for ignition delay (CI) or knock (SI) that reflect the impact of pressure, temperature, equivalence ratio, residual gas fraction, fuel composition, etc. [106]. The developed GT-Suite model is shown in figure 6.2 below.

Tables 6.2 and 6.3 below denote the operational and dimensional parameters that were assumed to be default from GT-Power help pages and templates.

6.3 Stationary and Dynamic Testing Profiles

Figure 6.3 shows the performance curve of Cummins 6.7L engine indicating torque and power curve throughout the operating range of the engine. It describes the best possible working range for the engine under consideration which also infers that it is not advisable to operate this engine beyond the constraints in the performance curve. With this curve in consideration, three test cases were considered for steady speed testing in each low, medium and high load regions i.e. at 800, 1400 and 2300 rpm respectively. The constant VGT and EGR fraction input of 50% was considered as the initial test case. These inputs were

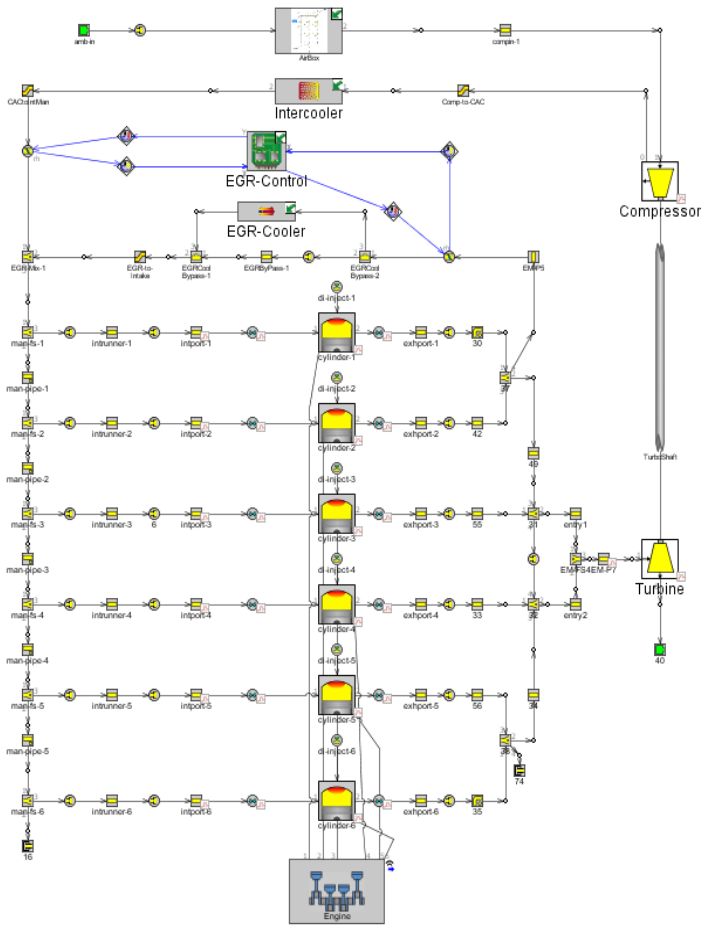

Figure 6.2. GT-Suite model for Cummins 6.7L diesel engine

implemented both on GT-Suite and developed prediction model and the output data for NOx and soot was obtained for validation purposes.

Further, to study the transient behavior of the system, step input change in the speed and load, was given from idling speed of 800 rpm to 1800 rpm at t = 15 seconds. This profile is used to capture the dynamic behavior of all subsystems in both GT-Suite and the proposed model. Fractions of the EGR and VGT actuators opening are considered to be fixed for avoiding complexity concerned in the actuator dynamics. A fixed sampling time of 10ms is devoted to record the output data from both GT-Suite and prediction model.

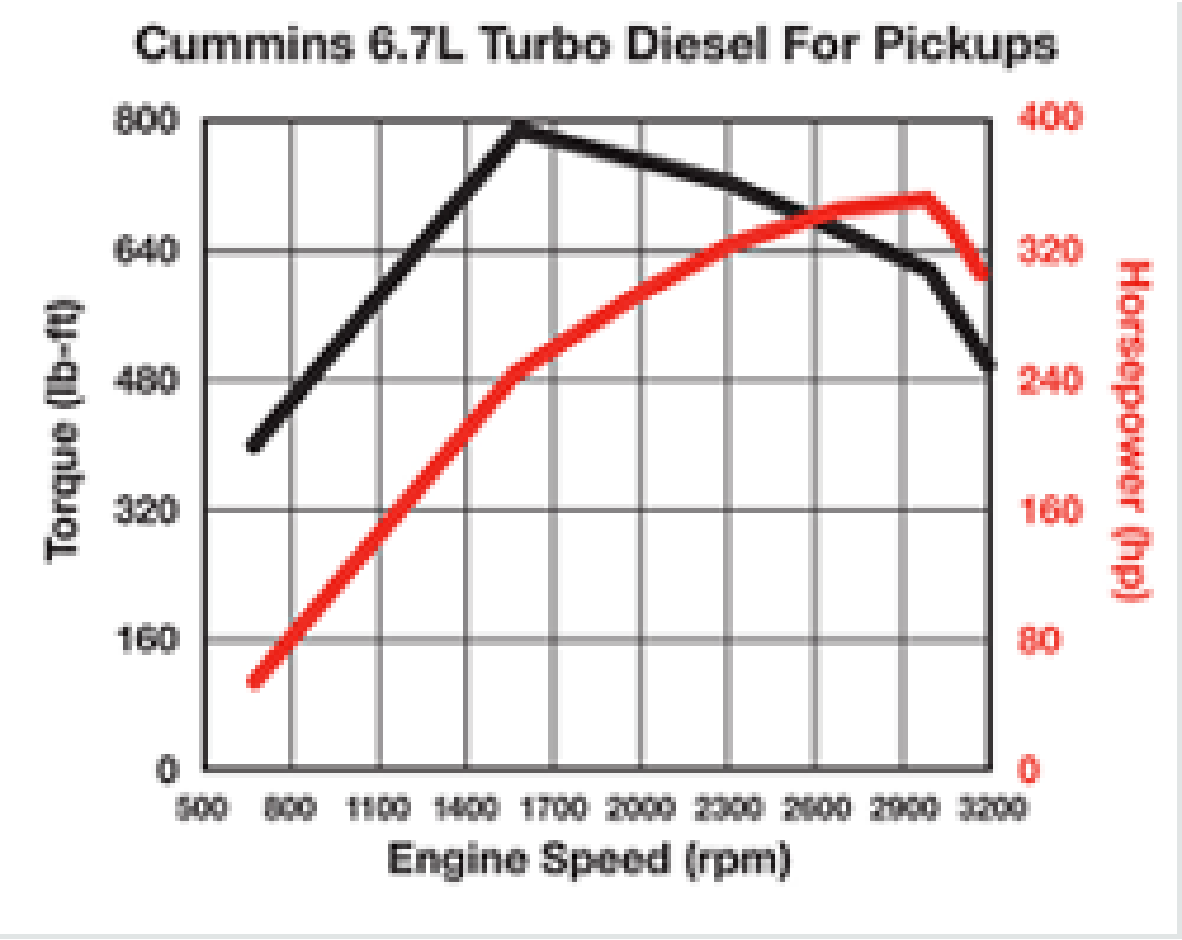

Figure 6.3. Cummins 6.7L Turbo Diesel Engine Torque and Horsepower data

6.4 Validation of NOx States

The states derived in the state space model are needed to be checked against reference data obtained from GT-Suite to ensure the appropriate dynamic behavior of the system. For this purpose, a step signal for speed was considered as an input from 800 rpm to 1500 rpm at t=15seconds. The data obtained from predictive models used in previous sections was used to calculate the state outputs and this output was compared with GT-Suite reference data. The data obtained in both the models have noise that needs to be filtered. Low pass filters have been used to better understand the comparison between reference and predicted data. However, using these filters for all the datasets has been avoided to retain the critical transient information during the step change. To compare the output results, as

an agreement between the predicted states by the proposed model and reference data from GT-Suite tool, root mean squared error was calculated by using the following equation.

$$RMSE = \sqrt{\sum_{\mathrm{i}=1}^{n} \frac{\hat{x}_{\mathrm{i}} - x_{\mathrm{i}}}{n}} \tag{6.1}$$

Where $\hat{x}_{\mathrm{i}}$ is the predicted model state value, x_{i} is the reference data value and n is the total number of datapoints. The values of RMSE for all states are summarized in the closure of this chapter.

6.4.1 Pressure in Intake Manifold

The pressure in intake manifold is a function of compressor output pressure and EGR outlet variables. Other parameters like intake manifold volume and temperature also have a significant impact on intake manifold pressure. Other details like compressor efficiency, EGR cooler temperature, nozzle valve area were also considered. As shown in figure 6.4 below, the state prediction shows a transient change at t=15s as step input is triggered. At this moment, the pressure momentarily drops below 1 bar and increases as engine speed is increased. The root mean square error (RMSE) for this comparison is 0.5136. The model output observes some delay due to the integrators and initial conditions involved in it. Due to these different initial conditions, the model observes significant tradeoff initially until the steady state is reached but agreement is more in next input change.

6.4.2 Pressure in Exhaust Manifold

The pressure in exhaust manifold is a result of intake manifold pressure and in-cylinder activities. The cylinder displacement and volumetric efficiency play critical role in the determination of exhaust manifold pressure. As shown in figure 6.5, at t = 15 seconds, where the step input is triggered, there is a sudden increase in exhaust pressure as there is increase in exhaust mass flow rate and a fixed volume of exhaust manifold. As a fact of comparison, RMSE for this state is around 0.3532. Initially, a large tradeoff is observed until t=3 seconds because of the different initial conditions of the prediction model.

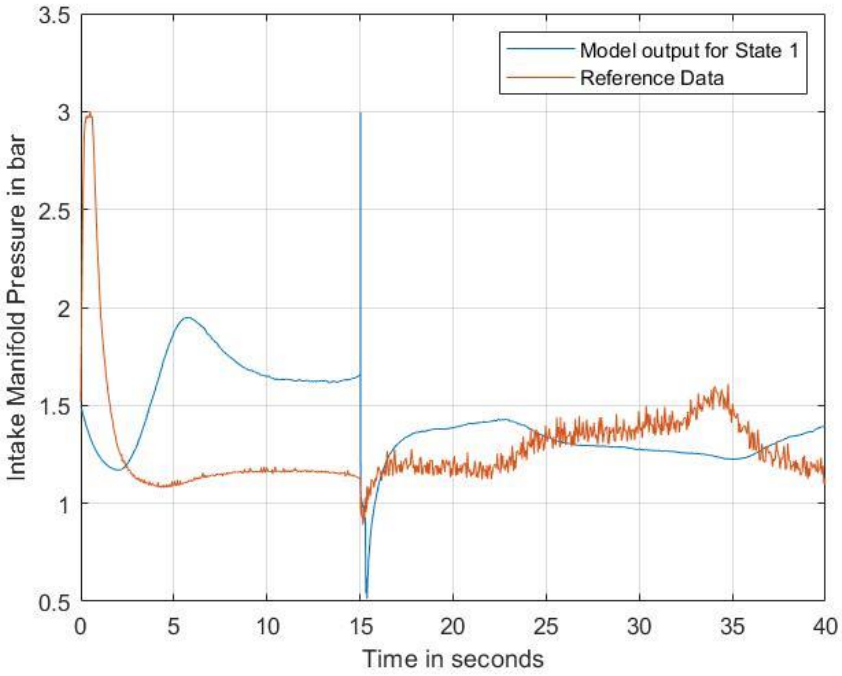

Figure 6.4. Validation of intake manifold pressure

6.4.3 Oxygen Fraction in Intake Manifold

The O_2 fraction in intake manifold is a function of oxygen fraction in air and exhaust manifold because of EGR. As shown in figure 6.6 the reference data having higher more resolution shows more deviations which can be further smoothed out using a filter. Here, a significant aspect to be noted is though there is change in input value at t=15 seconds, there is a delayed change in O_2 fraction because of the turbocharger inertia at t=18 seconds. Also, O_2 fraction is also a function of EGR and therefore, observes a slight delay when responding to transient change in the input. To calculate the agreement in between both of these results, RMSE lies around 0.0275.

6.4.4 Oxygen Fraction in Exhaust Manifold

The pressure difference in intake and exhaust manifolds and oxygen fraction in intake manifold are the two main influential factors in determining oxygen fraction in exhaust manifold. While it is also subject to the combustion chamber parameters, it is a measure of

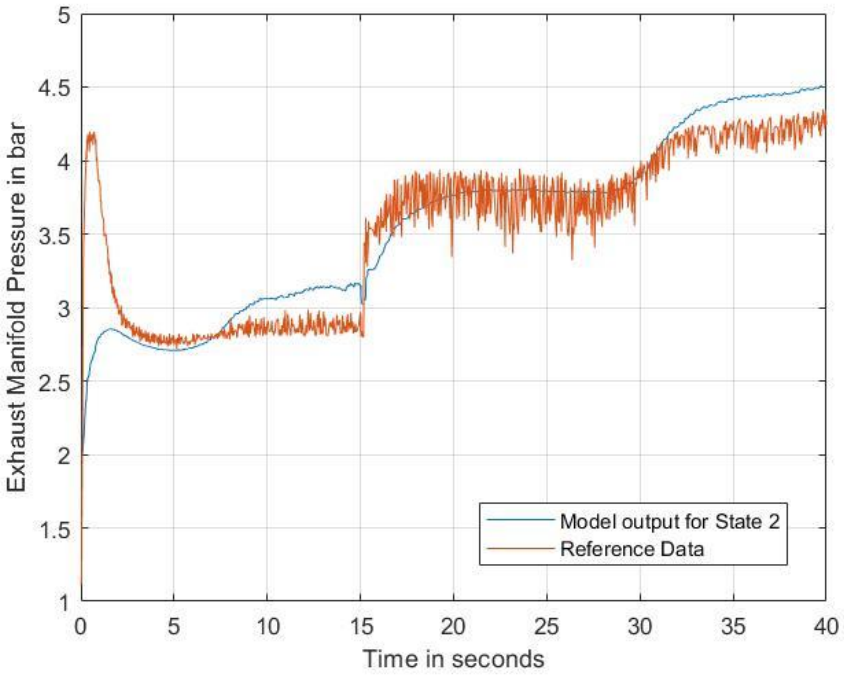

Figure 6.5. Validation of exhaust manifold pressure

how efficient the combustion process is. As shown in figure 6.7, there is a good agreement in between model prediction and reference data from GT-Suite and RMSE is 0.0137. At t=15 seconds, there is a slight delay before the state responds to the next change in the input due to the actuator dynamics and delay in the system.

6.4.5 Compressor Outlet Pressure

This state is purely dependent on the exhaust pressure and compressor efficiency as well as pressure ratio. As shown in figure 6.8, RMSE for this comparison is 0.4201 and it shows a fairly good agreement in between both of them.

6.5 NOx Model Results for Steady Speeds

Using the validated states as discussed in earlier section, the NOx prediction model is tested for steady state speeds of 800, 1400 and 2300 rpm. For the crank angle-based predictions, NOx output rises sharply as the pressure starts to build up and flame front

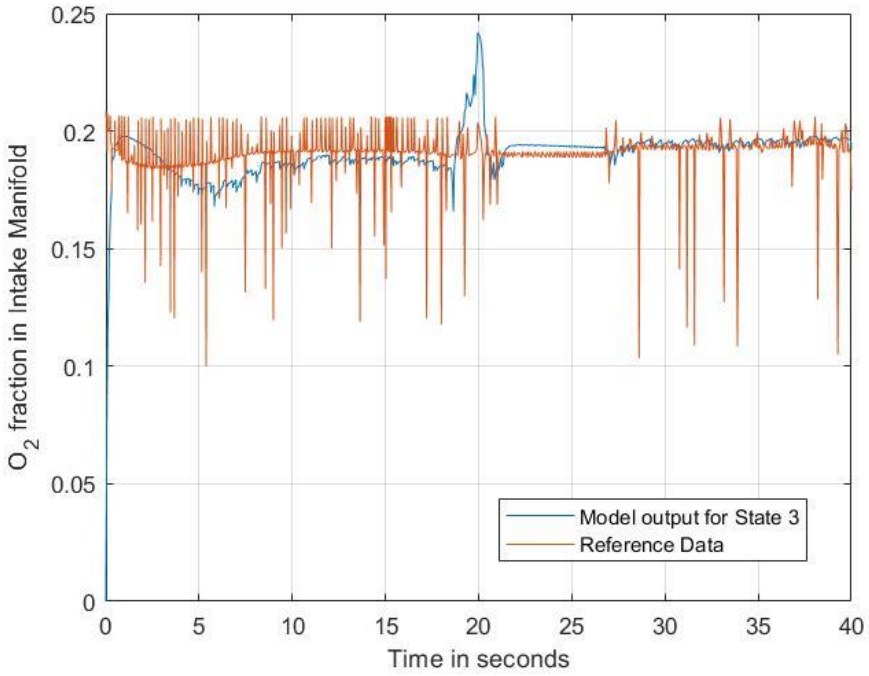

Figure 6.6. Validation of oxygen fraction in intake manifold

ignites. In the second phase of controlled diffusive combustion, NOx production takes place at different instances depending on the local air fuel ratios. As a reason, there is constant NOx formation until this phase occurs. In the last phase the NOx formation is quenched as there is less oxygen remaining and this leads to decrease in NOx amount.

At 800 rpm, there is a difference of around 31.52% in peak values for NOx with the uncontrolled model output and reference data. After implementation of state feedback controller this peak-to-peak error is reduced to 3.38% and steady state error is considerable reduced as shown in figure 6.9. RMSE for uncontrolled system is found to be 7.5509 which is way beyond acceptable limits. After the implementation of controller, it was found to be 0.4315.

At 1400 rpm, there is a difference of around 33.41% in peak values for NOx with the uncontrolled model output and reference data. This difference is highest among all test cases because of the higher torque values at this engine speed. After implementation of state feedback controller this this peak-to-peak error is reduced to 1.98% and steady state error

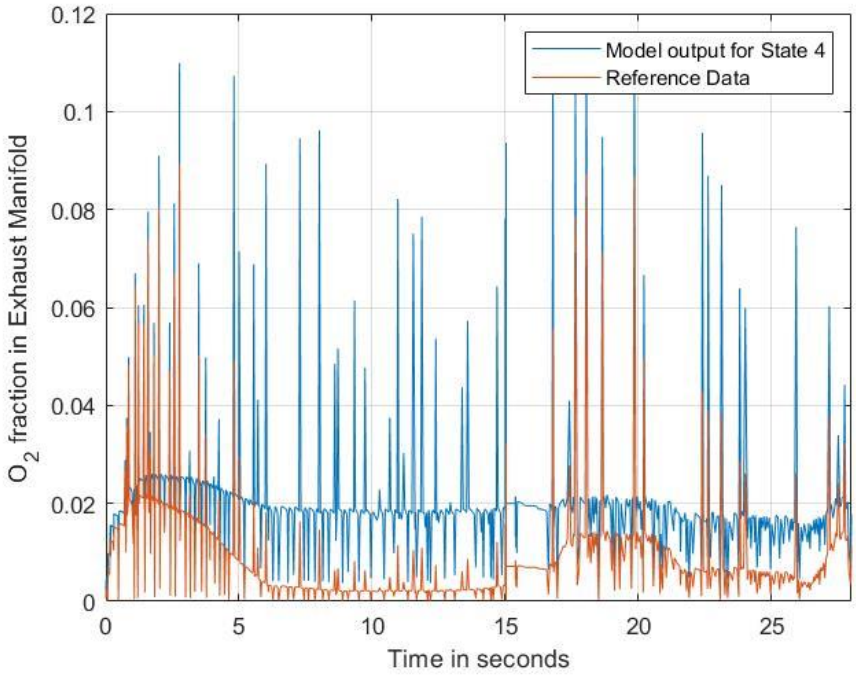

Figure 6.7. Validation of oxygen fraction in exhaust manifold

is considerable reduced as shown in figure 6.10. RMSE for uncontrolled system is found to be 6.6048 which is way beyond acceptable limits. After the implementation of controller, it was found to be 0.4199.

At 2300 rpm, there is a difference of around 32.07% in peak values for NOx with the uncontrolled model output and reference data. After implementation of state feedback controller this peak-to-peak error is reduced to 1.51% and steady state error is considerable reduced as shown in figure 6.11. RMSE for uncontrolled system is found to be 6.9373 which is way beyond acceptable limits. After the implementation of controller, it was found to be 0.4107.

6.6 NOx Model for Transient Profile

For the transient analysis of the proposed model, a step input was provided at t=12 seconds from 800 rpm to 1400 rpm and at t=22 seconds it resets to 800rpm. Again, at t=34 seconds, the input is again switched to 1400 rpm. In below figure 6.12, the reference data in

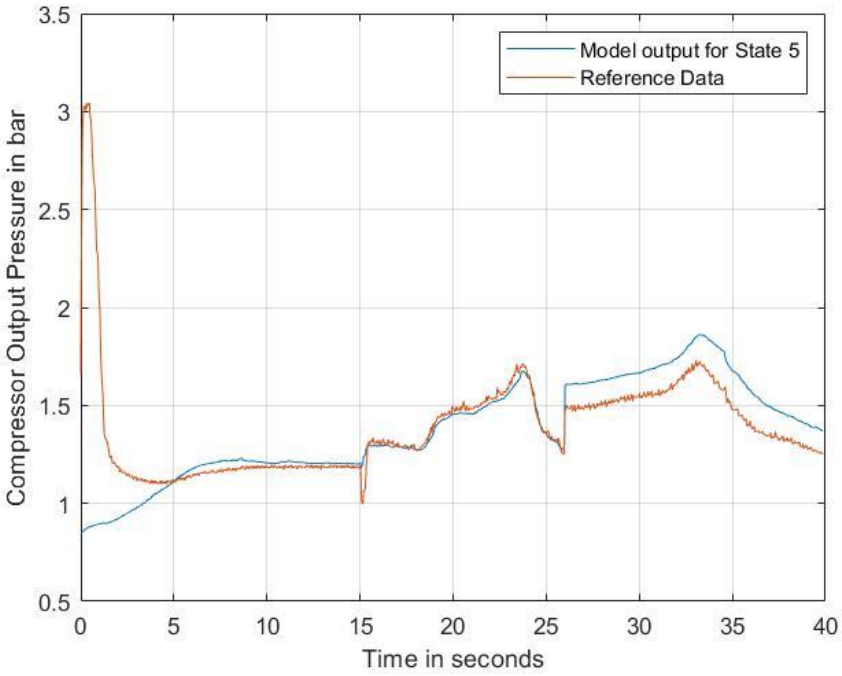

Figure 6.8. Validation of compressor outlet pressure

very noisy and thus it is filtered to capture the best possible dynamic response of the system and corresponding comparison is carried out.

As shown in figure 6.12 below, it shows a constant steady state error in amongst the proposed model output and reference data. This steady state error is eliminated in controlled system response highlighted by black line as we tuned the value of an integral term in the controller. As there is noise in the reference data, additional figure 6.13 was introduced to make this difference much clear.

The controlled response shows an excellent agreement with the reference data and RMSE for the same was found to be 0.5195. This is a significant improvement for uncontrolled model whose RMSE was found to be 2.8488. This proves the approach to derive the state space model and design the controller as highlighted in chapter 5.

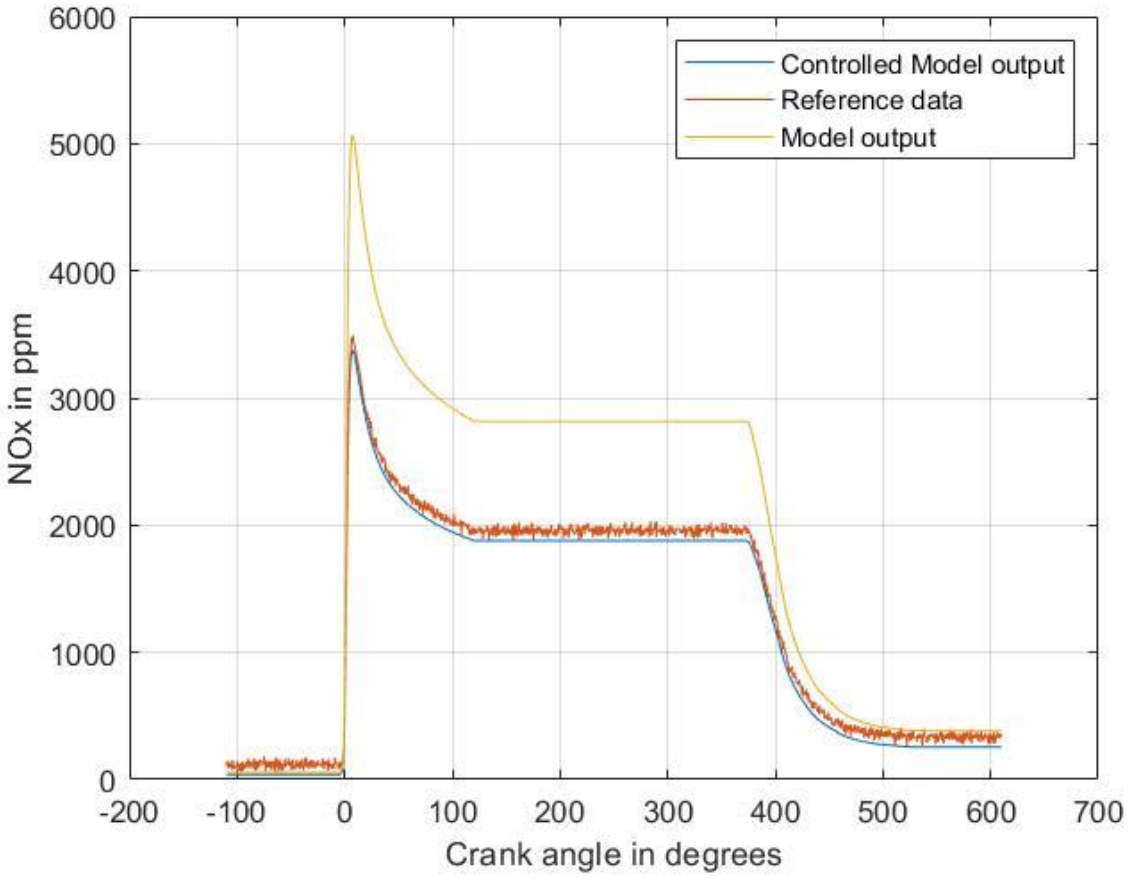

Figure 6.9. Comparison of NOx output at 800rpm

6.7 Soot Model Results

With respect to the soot model approach described in chapter 4 and its controller design in chapter 5, the soot prediction is considerably simple to achieve. However, though the controller is designed for soot model, the transient behavior cannot be tested as the reference data is not available through GT-Suite. Therefore, it is only validated for steady speed cases as shown below.

As shown in figure 6.14 below, the prediction model does not show any significant error in peak-to-peak values at 800 rpm. However, the model shows delayed output which is further compensated in a controlled response. RMSE for uncontrolled system is found to be 2.5508

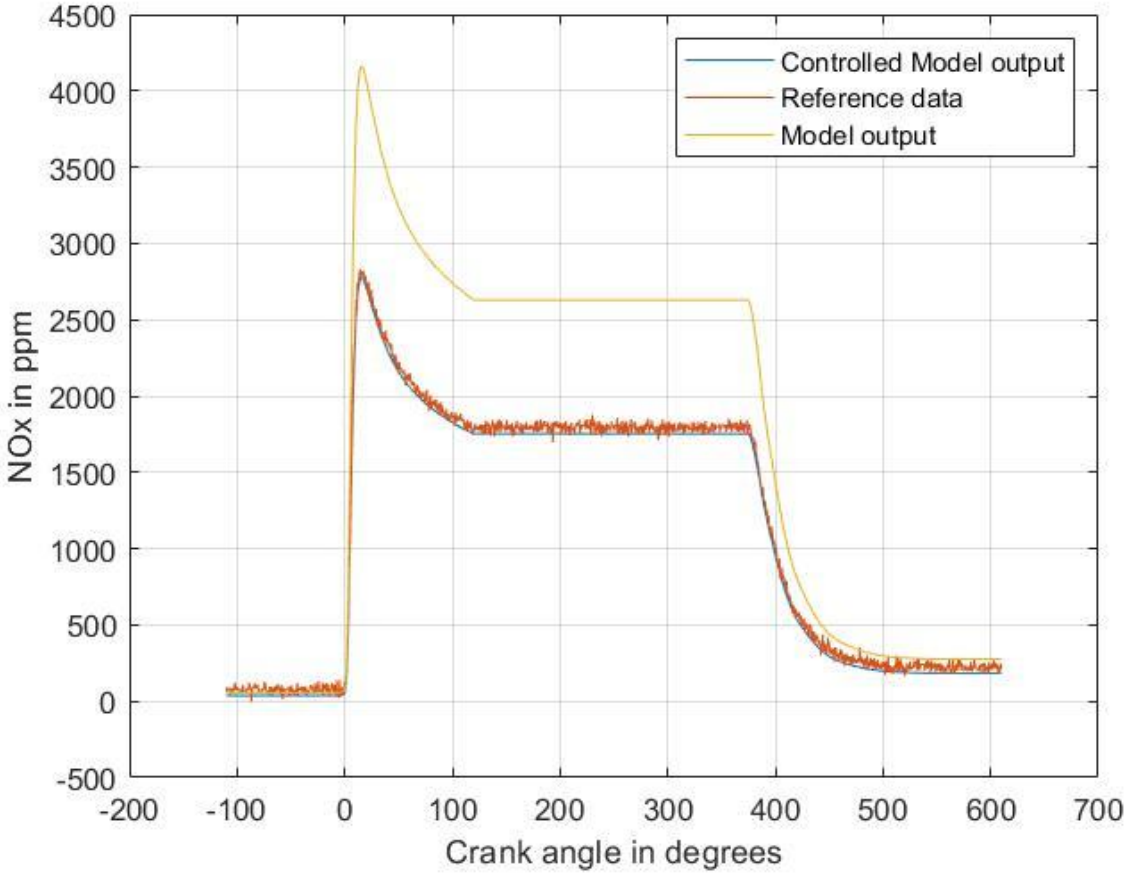

Figure 6.10. Comparison of NOx output at 1400rpm

which is way beyond acceptable limits. After the implementation of controller, it was found to be 0.0193.

With respect to figure 6.15 below, the prediction model output and reference data have a peak-to-peak error of 14.28% along with a delay in output at 1400 rpm. This is further compensated with a controlled response and both delay and peak to peak values are fairly close to each other. RMSE for uncontrolled system is found to be 3.7781 which is way beyond acceptable limits. After the implementation of controller, it was found to be 0.0387.

As shown in figure 6.16 below, the model output varies by a considerable margin with that of reference data. Also, the final steady state value of the soot is way higher. This is due to the less availability of oxygen at higher speeds and thus the oxidation of soot reduces. So more soot remains in the cylinder. With the controlled response, this error is

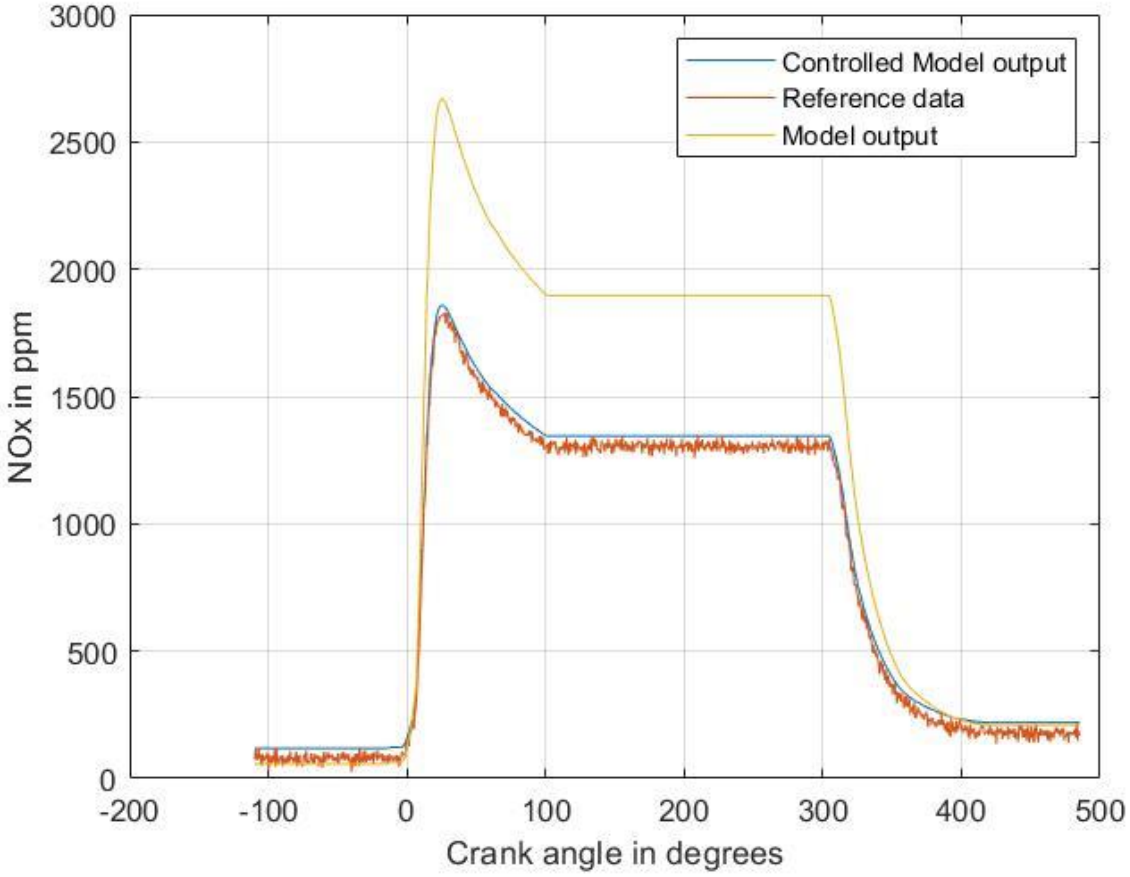

Figure 6.11. Comparison of NOx output at 2300rpm

also compensated considerably. RMSE for uncontrolled system is found to be 2.9874 which is way beyond acceptable limits. After the implementation of controller, it was found to be 0.0274.

6.8 Closure on the Chapter

A high-fidelity GT-Suite virtual model for Cummins 6.7L diesel engine has been developed to obtain the results as close to real engine setup. The parameters required for this model were referred from available datasheets and few were obtained by opening up the actual engine. This GT-Power model is set to run for various speed cases and benchmark results are obtained for both steady speed and transient conditions. Further, the data ob-

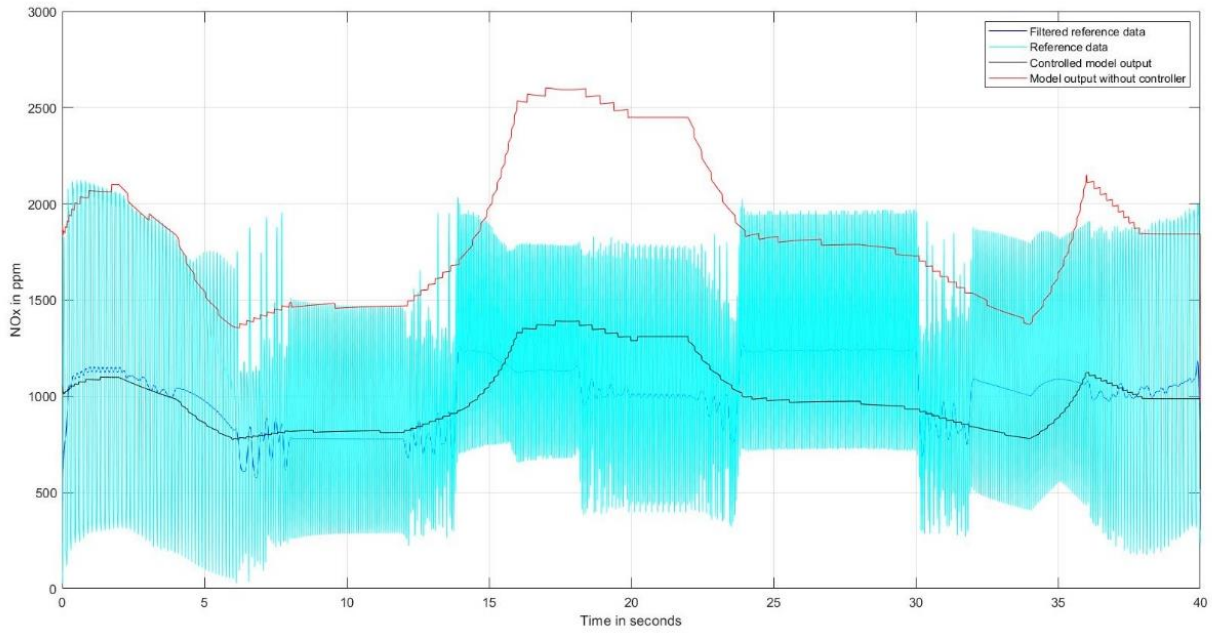

Figure 6.12. Comparison of NOx output for a transient input

tained from both uncontrolled and controlled NOx as well as soot model was compared with that of GT-Suite and RMSE was determined. It is found that RMSE for all the test cases is within acceptable limits, thus, proving the efficiency of designed controllers. Next chapter presents the conclusion and future aspects of this work.

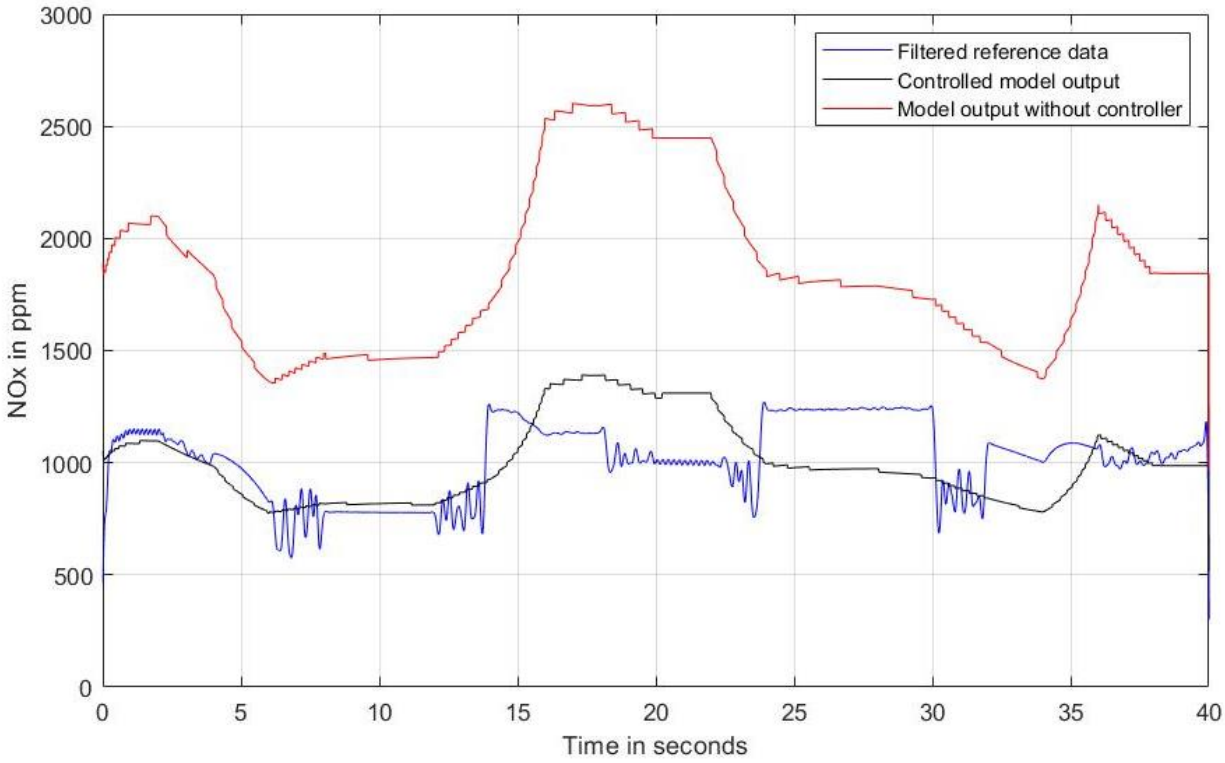

Figure 6.13. Comparison of filtered controlled data with reference

Table 6.2. Assumed parameters for analysis

Sr. No.	Parameter	Value
1	Airbox Intake pipe diameter	60mm
2	Airbox Intake pipe length	40mm
3	Maximum speed of compressor	26000rpm
4	Minimum efficiency of compressor	20%
5	Mean inlet diameter of compressor	60mm
6	Initial speed of compressor shaft	0rpm
7	Compressor shaft moment of Inertia	$2\times10^{-5}kg.m^2$
8	Rack position	0.5
9	Turbine Wheel diameter	57.69mm
10	Turbine Outlet diameter	74.25mm
11	Target EGR Fraction	0 to 0.35 %
12	Minimum EGR Valve Output	0
13	EGR cooler Mass Flow Rate	0.35778 kg/s
14	Coolant Composition	egl-5050
15	Coolant Temperature	373K
16	Coolant Pressure	2 bar
17	Inlet pipe diameter of EGR cooler	20mm
18	Inlet pipe length of EGR cooler	50mm
19	Outlet pipe diameter of EGR cooler	20mm
20	Outlet pipe length of EGR cooler	50mm
21	Inlet volume of intercooler	0.392699 L
22	Intercooler material	Steel
23	Imposed wall temperature for intercooler	325K
24	CAC Inlet diameter	7mm
25	CAC length	200mm
26	CAC Material	Steel
27	CAC Imposed wall temperature	325K
28	Injected mass of fuel	80 mg/pulse
29	Injected fuel temp	300K
30	Injection timing	-5 CAD
31	Injection duration	18 CAD
32	TDC clearnce height	0.5 mm
33	Wrist pin to crank offset	1 mm
34	Firing interval	120 CAD

Table 6.3. Assumed parameters for analysis

Component	Parameter	Unit	Section 1	Section 2	Section 3	Section 4	Section 5
CAC to intake manifold pipe geometry	Distance from						
Pipe Inlet	mm	0	45.3099	167.8721	348.5156	498.4448	
	Diameter	mm	50	50	50	50	50
	Radius of Bend	mm	0	0	69.87758	0	83.27418
	Angle of Bend	Degrees	0	0	100.4942	0	103.157
Compressor to CAC connecting pipe geometry	Distance from						
Pipe Inlet	mm	0	120.0597	312.021	362.0672	403.1696	
	Diameter	mm	50	50	50	50	50
	Radius of Bend	mm	0	79.67414	0	125.938	0
	Angle of Bend	Degrees	0	71.26013	0	22.76864	0

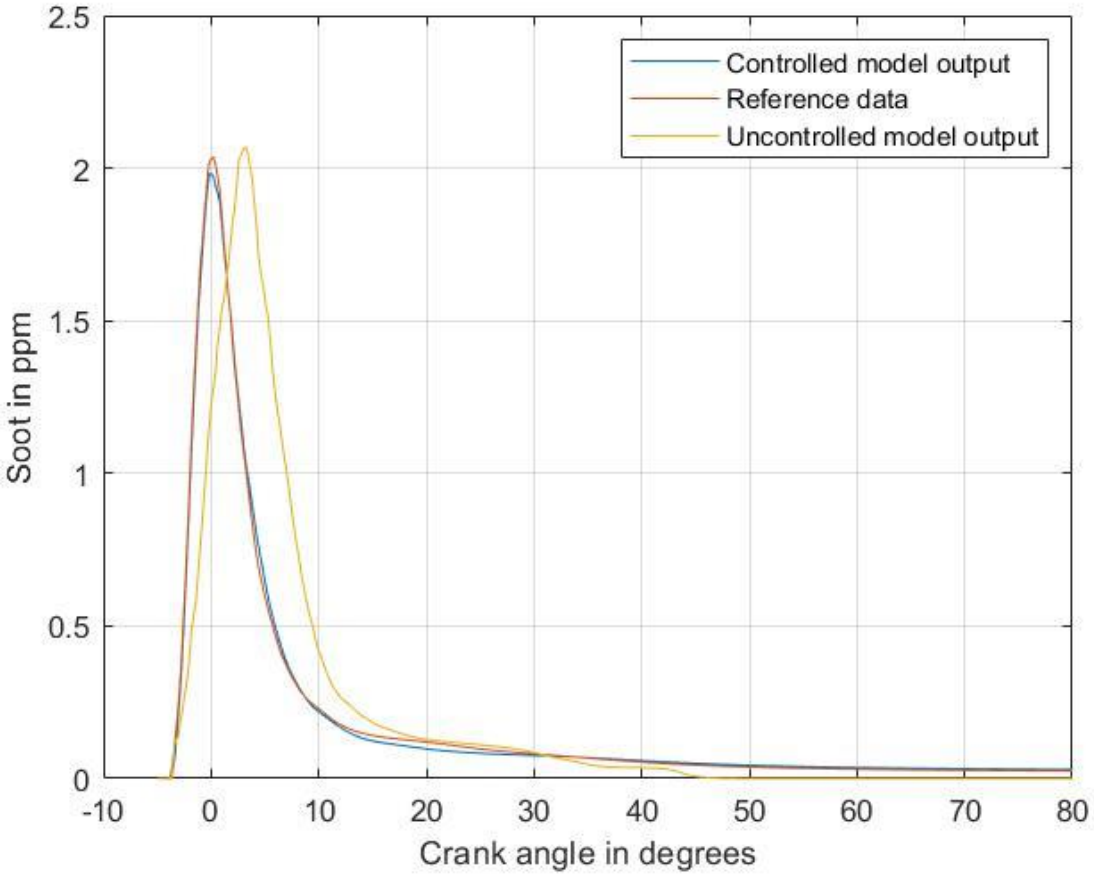

Figure 6.14. Comparison of filtered controlled data with reference

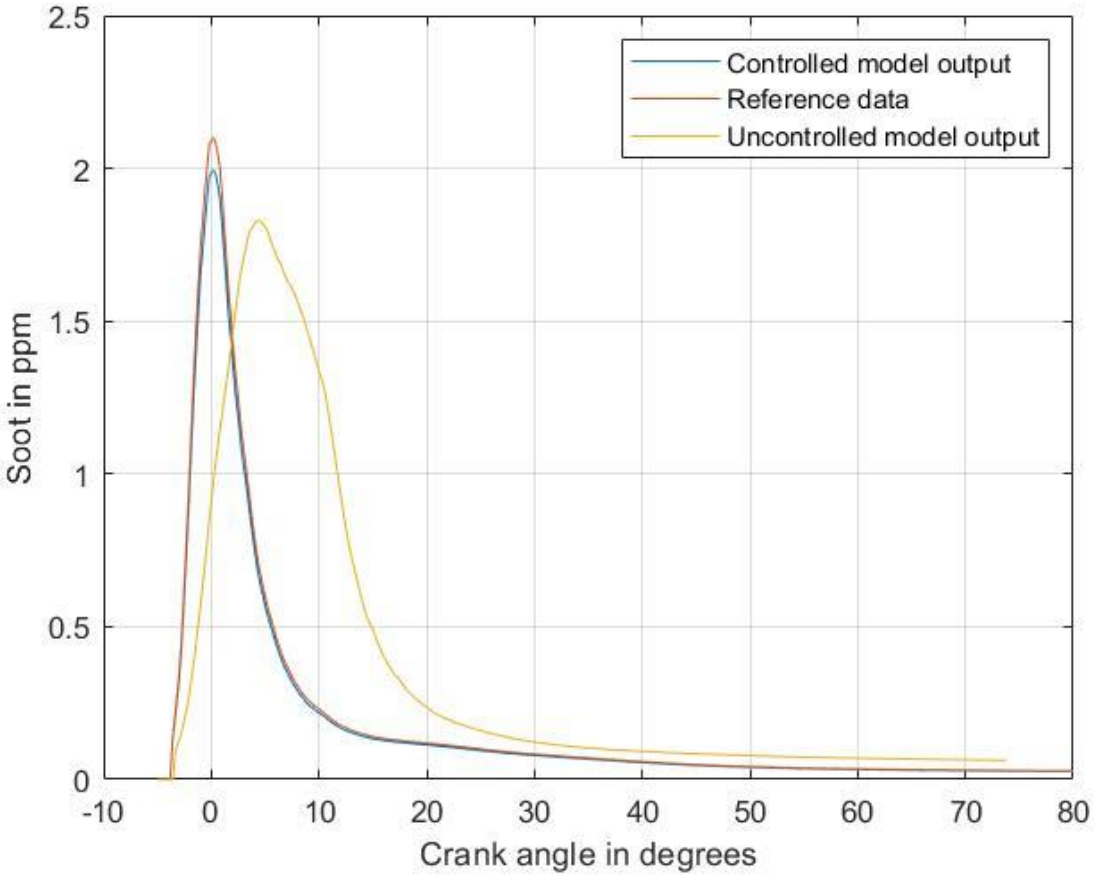

Figure 6.15. Comparison of filtered controlled data with reference

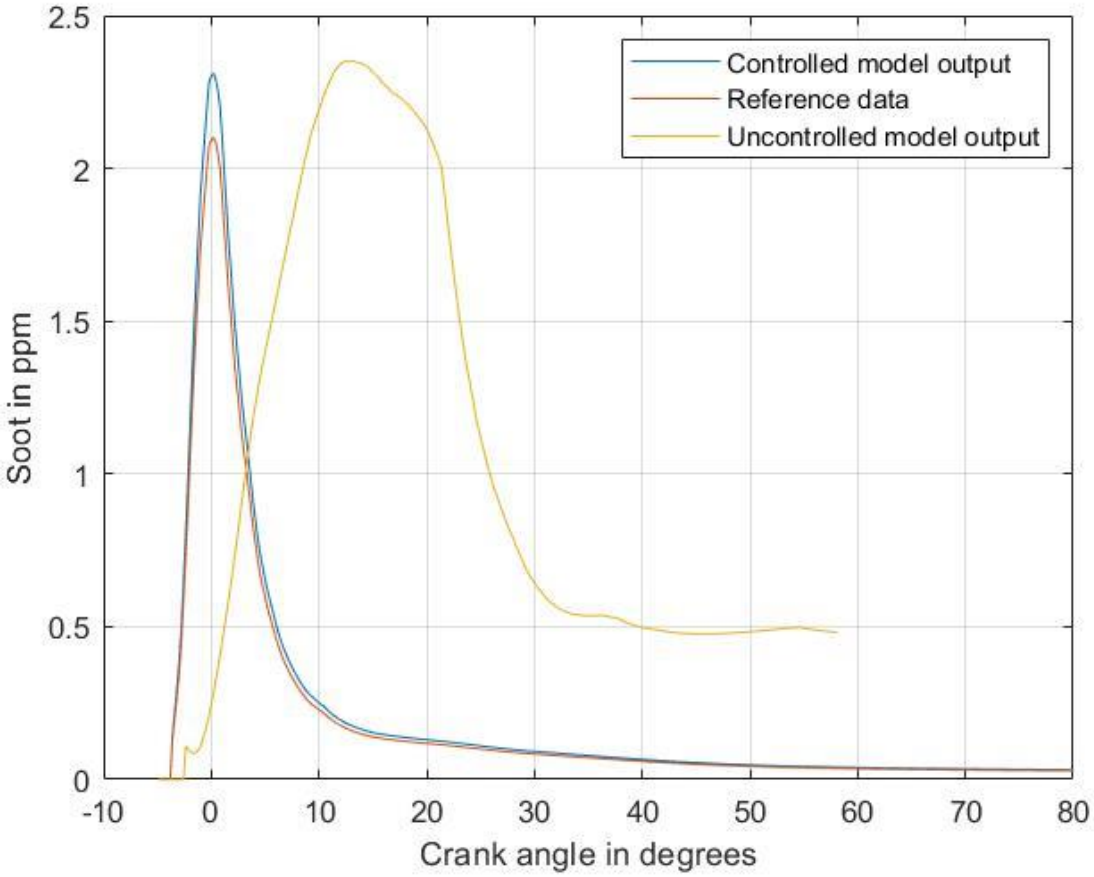

Figure 6.16. Comparison of filtered controlled data with reference

7. CONCLUSION AND FUTURE SCOPE

7.1 Conclusion

As a result of upcoming stringent emission norms for diesel engine out emissions by several regulatory organizations all over the world, engine systems and its development are becoming intricate and more demanding. To comply with these requirements, precise knowledge of relationships between in-cylinder processes and formation of emissions is very critical and is explored in detail in this work. The proposed approach introduces a method to develop physics-based modeling, prediction and validation to forecast several engine states required for formation engine out emissions like NOx and soot. Here, Cummins 6.7L turbocharged diesel engine is considered as application of interest. A high-fidelity virtual model is developed in GT-Suite as a benchmark and validation purposes. As a proof of concept towards proposed approach, the estimation models were developed for same engine in integration with turbocharger and EGR systems. The proposed model was set to be run on crank angle-based scale for steady speeds and time-based scale for transient testing conditions. Using the crank angle-based calculations, several subsystems of the combustion model were developed such as rate of heat release and mass fraction burnt.

Using the chemical processes occurring during the combustion process, a chemical equilibrium solver sub model was designed that considers thermochemistry of all species involved for converting chemical energy of fuel into useful work and exhaust gases. This subsystem gives in-cylinder conditions like concentrations of species of products and adiabatic temperature. Further, all these subsystems were integrated with extended zeldovich mechanism to find out engine out NOx.

For soot determination, Hiroyasu and Kadota methodology is implemented to find rate of soot formation and oxidation. Other key parameters like lift-off length, injector dimensions, fuel spray characteristics and equivalence ratio are the various subsystems of prime importance here.

Further, a state space model is derived for both NOx and soot models using a conventional derivation of key states and their outputs. The NOx model is simplified by eliminating its unnecessary states and it is considered as MIMO system. Further, it is linearized to ob-

tain its state space matrices and checked for controllability. The system for NOx was found to be both controllable and observable. Then a state feedback controller was designed to compensate the tradeoff between reference data and model output using quadratic performance index. For the soot state space model, the output response to unit step input was recorded based on which a PI controller was designed and implemented. All these models and controllers were designed and implemented using MATLAB and Simulink interface.

For the test setup in a steady state condition, three speeds were chosen each in a low, medium and high load ranges. For transient test case, a step change was provided at multiple instances. For all the test cases, the controlled response shows RMSE within acceptable limits. Few parameters show deviation of RMSE due to the difference in solvers used by GT-Suite and developed prediction models. The initial conditions for both models also have a significant impact on values of RMSE obtained. The developed model integrated with appropriate controller for NOx as well as soot yields an accuracy of around 2%. This is a significant increase from that of the uncontrolled prediction models which show around 32% of error. This enhancement in accuracy proves the use of proposed integrated approach. Also, RMSE for most of the predictions lies below 0.5 which shows good agreement of the controlled model with reference data.

The developed model for both NOx and soot integrated with control system approach has significant advantage over the reference model developed in GT-Suite. The time taken by GT-Suite model is significantly higher and thus are not suitable for real time application. On the contrary, the proposed approach uses a real time prediction of engine out emission and can readily be used in vehicles with minor modifications.

One of the advantages of this work is that it reduces dependency on statistical models that require lot of data, and they also require more experimentation as discussed in literature review. Therefore, the proposed approach can be used for the fast calibration and controller developments for several developments in the entire engine system. It can be either be used as a standalone simulation tool or integrated with the system level control architecture.

7.2 Future Scope

There is a good potential of this work for further development in the area of engine control, calibration, system architecture and framework design. This work forms a base for a new approach of deriving a state space model for an engine out emission for NOx and soot. This can be further extended to other emission contributors like UHC, CO, SOx, NO2, etc. Similar sort of physics-based models and their standalone control architectures can be derived to predict EO amount and reduce the dependency on physical sensors. Going ahead out of prediction, the validated models can also be used to reduce the engine out emissions which is a critical aspect given that upcoming norms are becoming stricter.

The current work is based on basic test cases for steady state and transient test cases. The actual test cases from WHSC or EPA can be used for testing these algorithms to make them more realistic and compliant. Also, increasing the dimensions of the model can provide more detailed prediction of the emissions and provide more flexibility in terms of control of various states.

This approach can be extended to be implemented practically on vehicle level with minor modifications. Usually, most of the data obtained by physical sensors is readily available through OBD port which can be easily set to be obtained at different sampling times. The complexity of this model can be further reduced by using this readily available data and using the predictive models for non-measurable signals like in-cylinder conditions. This will also reduce the load on ECU, reduce the computation time and provide accurate real time control of the system.

Also, this complex model was developed to eliminate the need of sensors and reduce redundancy of engine systems. With due experimental validation and calibration, this approach can be implemented on actual vehicle. This will not only enhance the computing performance of ECU, but also will save on hardware costs.

REFERENCES

[1] V. Franco, F. P. Sanchez, J. German, and P. Mock, "Real-world exhaust emissions from modern diesel cars," *communications*, vol. 49, pp. 847 129–102, 30 2014.

[2] M. Henningsson, P. Tunestål, and R. Johansson, "A virtual sensor for predicting diesel engine emissions from cylinder pressure data," *2012 IFAC Workshop on Engine and Powertrain Control, Simulation and Modeling*, vol. 45, pp. 424–431, 30 2012. DOI: https://doi.org/10.3182/20121023-3-FR-4025.00063.

[3] I. Arsie, D. Marra, C. Pianese, and M. Sorrentino, "Real-time estimation of engine nox emissions via recurrent neural networks," *IFAC Proceedings Volumes*, vol. 43, pp. 228–233, 7 2010. DOI: https://doi.org/10.3182/20100712-3-DE-2013.00117.

[4] D. J. Patterson and N. A. Henein, *Emissions from combustion engines and their control*. U.S. Department of Energy, 1981, ISBN: 5967871.

[5] J. B. Heywood, *Internal Combustion Engine Fundamentals*. McGraw-Hill, 1988, ISBN: 978-0070286375.

[6] M. K. Khair and H. Jääskeläinen, *Emission formation in diesel engines*. [Online]. Available: https://dieselnet.com/tech/diesel_emiform.php.

[7] J. A. Miller and C. T. Bowman, "Mechanism and modeling of nitrogen chemistry in combustion," *Progress in energy and combustion science*, vol. 15, pp. 287–338, 4 1989. DOI: https://doi.org/10.1016/0360-1285(89)90017-8.

[8] D. R. Tree and K. I. Svensson, "Soot processes in compression ignition engines," *Progress in energy and combustion science*, vol. 33, pp. 272–309, 3 2007. DOI: https://doi.org/10.1016/j.pecs.2006.03.002.

[9] H. Hiroyasu, T. Kadota, and M. Arai, "Development and use of a spray combustion modeling to predict diesel engine efficiency and pollutant emissions : Part 1 combustion modeling," *Bulletin of JSME*, vol. 26, pp. 569–575, 214 1983. DOI: https://doi.org/10.1299/jsme1958.26.569.

[10] R. Schubiger, K. Boulouchos, and M. Eberle, "Soot emission from diesel combustion," *MTZ worldwide*, vol. 63, pp. 2–5, 5 2002. DOI: https://doi.org/10.1007/BF03227537.

[11] M. Warth, P. Obrecht, A. Bertola, and K. Boulouchos, "Predictive phenomenological ci combustion modeling optimization on the basis of bio-inspired algorithms," *SAE transactions*, vol. 1, pp. 962–972, 1119 2005. DOI: https://doi.org/10.4271/2005-01-1119.

[12] K. Akihama, Y. Takatori, K. Inagaki, S. Sasaki, and A. M. Dean, "Mechanism of the smokeless rich diesel combustion by reducing temperature," *SAE transactions*, vol. 1, pp. 648–662, 655 2001. DOI: https://doi.org/10.4271/2001-01-0655.

[13] P. Kirchen, P. Obrecht, and K. Boulouchos, "Soot emission measurements and validation of a mean value soot model for common-rail diesel engines during transient operation," *SAE international journal of engines*, vol. 2, pp. 1663–1678, 1 2009. DOI: https://doi.org/10.4271/2009-01-1904.

[14] J. Bayer and D. E. Foster, "Zero-dimensional soot modeling," *SAE transactions*, vol. 112, pp. 1446–1458, 3 2003. DOI: https://doi.org/10.4271/2009-01-1904.

[15] P. Kožuch, "A phenomenological model for the combined nitrogen oxide and soot calculation in direct-injection diesel engines," *International Fuels Lubricants Meeting Exposition*, pp. 1663–1678, 1999. DOI: https://doi.org/10.4271/1999-01-1535.

[16] A. Westlund and H. E. Ångström, "Fast physical emission predictions for off-line calibration of transient control strategies," *SAE Technical Paper*, 2009. DOI: https://doi.org/10.4271/2009-01-1778.

[17] J. Nagle, "Oxidation of carbon between 1000-2000°C," *Proceedings of Fifth Carbon Conference*, pp. 154–164, 1962. DOI: https://doi.org/10.1016/B978-0-08-009707-7.50026-1.

[18] J. Schaeffler, D. Alberer, K. S. Oppenauer, and L. del Re, "Gray box diesel engine soot emission modeling based on two-color spectroscopy measurements," *SAE Technical Paper*, vol. 24, pp. 1663–1678, 205 2011. DOI: https://doi.org/10.4271/2011-24-0205.

[19] J. E. Dec, "A conceptual model of dl diesel combustion based on laser-sheet imaging," *SAE transactions*, vol. 106, pp. 1319–1348, 3 1997.

[20] D. Siebers and B. Higgins, "Flame lift-off on direct-injection diesel sprays under quiescent conditions," *SAE Transactions*, vol. 110, pp. 400–421, 2001. DOI: https://doi.org/10.4271/2001-01-0530.

[21] D. Kihas and M. R. Uchanski, "Engine-out nox models for on-ecu implementation: A brief overview," *SAE Technical Paper*, vol. 10, pp. 1297–1304, 3 2015. DOI: https://doi.org/10.4271/2015-01-1638.

[22] K. Muric, O. Stenlåås, P. Tunestål, and B. Johansson, "A study on in-cycle control of nox using injection strategy with a fast cylinder pressure based emission model as feedback," *SAE Technical Paper*, vol. 11, 2603 2013. DOI: https://doi.org/10.4271/2013-01-2603.

[23] C. Guardiola, V. Triantopoulos, P. Bares, S. Bohac, and A. Stefanopoulou, "Simultaneous estimation of intake and residual mass using in-cylinder pressure in an engine with negative valve overlap," *IFAC-PapersOnLine*, vol. 48, pp. 461–468, 11 2016. DOI: https://doi.org/10.1016/j.ifacol.2016.08.068.

[24] P. Elbert, C. Barro, A. Amstutz, C. Onder, and K. Boulouchos, "Emissionsoptimierter dieselmotor," *Informationstagung Motoren*, vol. 572, pp. 4–45, 2015.

[25] C. Wilhelmsson, P. Tunestål, B. Widd, R. Johansson, and B. Johansson, "A physical two-zone nox model intended for embedded implementation," *SAE Technical Paper*, vol. 1, 1509 2009. DOI: https://doi.org/10.4271/2009-01-1509.

[26] M. L. Traver, R. J. Atkinson, and C. M. Atkinson, "Neural network-based diesel engine emissions prediction using in-cylinder combustion pressure," *SAE transactions*, vol. 108, pp. 1166–1180, 4 1999. DOI: https://doi.org/10.4271/1999-01-1532.

[27] E. C. Çebi, G. Rottenkolber, and E. Uyar, "In-cylinder pressure based real-time estimation of engine-out particulate matter emissions of a diesel engine," *SAE Technical Paper*, vol. 1, 1440 2011. DOI: https://doi.org/10.4271/2011-01-1440.

[28] L. Guzzella and A. Amstutz, "Control of diesel engines," *IEEE Control Systems Magazine*, vol. 18, pp. 53–71, 5 1998. DOI: https://doi.org/10.1109/37.722253.

[29] H. C. Cho, S. Takase, Y. Shimizu, and J. H. Song, "P1. 6.1 impedancemetric nox sensor using ysz-based solid electrolyte attached with oxide receptor," *Proceedings IMCS*, pp. 1042–1045, 2012. DOI: https://doi.org/10.5162/IMCS2012/P1.6.1.

[30] S. Carstens and W. A. Majewski, *Nox sensors*. [Online]. Available: https://dieselnet.com/tech/sensors_nox.php.

[31] T. Martin, *Diesel nox sensor technology*. [Online]. Available: https://www.vehicleservicepros.com/collision-repair/on-the-shop-floor/article/21181404/diesel-nox-sensor-technology.

[32] R. Hammerle, "Urea scr and dpf system for diesel sport utility vehicle meeting tier ii bin 5," *8th Diesel Engine Emissions Reduction Conference*, pp. 25–29, 2002.

[33] Q. Song and G. Zhu, "Model-based closed-loop control of urea scr exhaust aftertreatment system for diesel engine," *SAE Transactionse*, vol. 1, pp. 102–110, 1287 2002. DOI: https://doi.org/10.4271/2002-01-0287.

[34] R. Mukundan, E. L. Brosha, C. Kreller, *et al.*, "Robust nitrogen oxide/ammonia sensors for vehicle on-board emissions control (no. la-ur-13-28922)," *US Department of Energy*, vol. GRA and I, pp. 102–110, GRA and I 2013. DOI: https://doi.org/10.2172/1107996.

[35] K. Muric, O. Stenlåås, P. Tunestål, and B. Johansson, "A study on in-cycle control of nox using injection strategy with a fast cylinder pressure based emission model as feedback," *SAE Technical Paper*, vol. 11, 2603 2013. DOI: https://doi.org/10.4271/2013-01-2603.

[36] D. Siegberg and M. Kilinc, "Thermal and chemical robustness of the smart nox-sensor," *Proceedings of the 12th CTI International Conference Exhaust Systems—Euro VI and Beyond—Focus on CO2 Reduction*, pp. 28–29, 2014.

[37] J. Bayer and D. E. Foster, "Zero-dimensional soot modeling," *SAE transactions*, vol. 112, pp. 1446–1458, 3 2003. DOI: https://doi.org/10.4271/2009-01-1904.

[38] Y. Kawamoto, Y. Todo, H. Shimokawa, K. Aoki, M. Kawai, and K. Ide, "Development of high accuracy nox sensor," *SAE Technical Paper*, vol. 1, 749 2019. DOI: https://doi.org/10.4271/2019-01-0749.

[39] D. Siegberg and M. Kilinc, "Thermal and chemical robustness of the smart nox-sensor," *Proceedings of the 12th CTI International Conference Exhaust Systems—Euro VI and Beyond—Focus on CO2 Reduction*, pp. 28–29, 2014.

[40] L. Y. Woo and R. S. Glass, "Nox sensor development (no. llnl-tr-418835)," *U.S. Department of Energy*, 2009.

[41] L. Guzzella and A. Amstutz, "Control of diesel engines," *IEEE Control Systems Magazine*, vol. 18, pp. 53–71, 5 1998. DOI: https://doi.org/10.1109/37.722253.

[42] C. Ericson, B. Westerberg, M. Andersson, and R. Egnell, "Modelling diesel engine combustion and nox formation for model based control and simulation of engine and exhaust aftertreatment systems," *SAE Technical Paper*, vol. 1, 687 2006. DOI: https://doi.org/10.4271/2006-01-0687.

[43] Y. Yildiz, A. M. Annaswamy, D. Yanakiev, and I. Kolmanovsky, "Spark ignition engine fuel-to-air ratio control: An adaptive control approach," *Control Engineering Practice*, vol. 18, pp. 1369–1378, 12 2010. DOI: https://doi.org/10.1016/j.conengprac.2010.06.011.

[44] C. Guardiola, J. Martín, B. Pla, and P. Bares, "Cycle by cycle nox model for diesel engine control," *Applied Thermal Engineering*, vol. 110, pp. 1011–1020, 2017. DOI: https://doi.org/10.1016/j.applthermaleng.2016.08.170.

[45] C. Atkinson and G. Mott, "Dynamic model-based calibration optimization: An introduction and application to diesel engines," *SAE technical paper*, vol. 1, 26 2005. DOI: https://doi.org/10.4271/2005-01-0026.

[46] E. Klampfl, J. Lee, D. Dronzkowski, and K. Theisen, "Engine calibration process optimization," *ICORES*, pp. 335–341, 2012. DOI: https://doi.org/10.5220/0003695603350341.

[47] I. Brahma and J. N. Chi, "Development of a model-based transient calibration process for diesel engine electronic control module tables-part 1: Data requirements, processing, and analysis," *International Journal of Engine Research*, vol. 13, pp. 77–96, 1 2012. DOI: https://doi.org/10.1177/1468087411424376.

[48] J. Asprion, O. Chinellato, and L. Guzzella, "A fast and accurate physics-based model for the nox emissions of diesel engines," *Applied energy*, vol. 13, pp. 221–233, 2013. DOI: https://doi.org/10.1016/j.apenergy.2012.09.038.

[49] S. Duraiarasan, R. Salehi, A. Stefanopoulou, S. Mahesh, and M. Allain, "Control-oriented physics-based nox emission model for a diesel engine with exhaust gas recirculation," *ASME Letters in Dynamic Systems and Control*, vol. 1, 1 2021. DOI: https://doi.org/10.1115/DSCC2019-9247.

[50] H. Cao, B. Y. Sun, and J. Duan, "Self-tuning pid controller of diesel engine based on fuzzy logic," *JOURNAL-DALIAN UNIVERSITY OF TECHNOLOGY*, vol. 40, pp. 465–469, 4 2000.

[51] J. Wahlström, L. Eriksson, and L. Nielsen, "Egr-vgt control and tuning for pumping work minimization and emission control," *IEEE transactions on control systems technology*, vol. 18, pp. 993–1003, 4 2009. DOI: https://doi.org/10.1109/TCST.2009.2031473.

[52] J. F. Arnold, N. Langlois, H. Chafouk, and G. Trémoulière, "Control of the air system of a diesel engine: A fuzzy multivariable approach," *2006 IEEE Conference on Computer Aided Control System Design, 2006 IEEE International Conference on Control Applications, 2006 IEEE International Symposium on Intelligent Control*, pp. 2132–2137, 2006. DOI: https://doi.org/10.1109/CACSD-CCA-ISIC.2006.4776970.

[53] M. Dabo, N. Langlois, and H. Chafouk, "Dynamic feedback linearization applied to asymptotic tracking: Generalization about the turbocharged diesel engine outputs choice," *2009 American Control Conference*, pp. 3458–3463, 2009. DOI: https://doi.org/10.1109/ACC.2009.5160404.

[54] X. Luo, S. Wang, B. de Jager, and F. Willems, "Cylinder pressure-based combustion control with multi-pulse fuel injection," *IFAC-PapersOnLine*, vol. 48, pp. 181–186, 15 2015. DOI: https://doi.org/10.1016/j.ifacol.2015.10.026.

[55] K. V. Nielsen, M. Blanke, and M. Vejlgaard-Laursen, "Nonlinear adaptive control of exhaust gas recirculation for large diesel engines," *IFAC-PapersOnLine*, vol. 48, pp. 254–260, 16 2015. DOI: https://doi.org/10.1016/j.ifacol.2015.10.289.

[56] S. Hong, I. Park, J. Chung, and M. Sunwoo, "Gain scheduled controller of egr and vgt systems with a model-based gain scheduling strategy for diesel engines," *IFAC-PapersOnLine*, vol. 48, pp. 109–116, 15 2015. DOI: https://doi.org/10.1016/j.ifacol.2015.10.016.

[57] Z. Yang, E. Winward, D. Zhao, and R. Stobart, "Three-input-three-output air path control system of a heavy-duty diesel engine," *IFAC-PapersOnLine*, vol. 49, pp. 604–610, 11 2016. DOI: https://doi.org/10.1016/j.ifacol.2016.08.088.

[58] S. Chen and F. Yan, "Decoupled, disturbance rejection control for a turbocharged diesel engine with dual-loop egr system," *IFAC-PapersOnLine*, vol. 49, pp. 619–624, 11 2016. DOI: https://doi.org/10.1016/j.ifacol.2016.08.090.

[59] I. Khalek and V. Premnath, "Particle sensor performance durability for obd applications beyond," *Proceedings of the CE-CERT Workshop*, vol. 11, 2013.

[60] M. B.Hopka, D.Bilby, and M. V. Nieuwstadt, "Evaluation of non-contiguous pm measurements with a resistive particulate matter sensor," *SAE International Journal of Engines*, vol. 10, pp. 1683–1690, 4 2017. DOI: https://doi.org/10.4271/2017-01-0952.

[61] M. B. Hopka, D. Bilby, and M. V. Nieuwstadt, "Evaluation of non-contiguous pm measurements with a resistive particulate matter sensor," *SAE International Journal of Engines*, vol. 10, pp. 1683–1690, 4 2017. DOI: https://doi.org/10.4271/2017-01-0952.

[62] A. Kondo, S. Yokoi, T. Sakurai, *et al.*, "New particulate matter sensor for on board diagnosis," *SAE International Journal of Enginess*, vol. 4, pp. 117–125, 1 2011. DOI: https://doi.org/10.4271/2011-01-0302.

[63] M. Moser and L. Leimkühler, "Simulative assessment of tolerance limits of new sensor concepts for controls and obd," *Proceedings of the 4th International Specialist Conference: Sensors for Exhaust Gas Aftertreatment and CO2 Reduction, Augsburg, Germany*, pp. 27–29, 2017.

[64] A. Sappok and L. Bromberg, "Development of radio frequency sensing for in-situ diesel particulate filter state monitoring and aftertreatment system control," *Internal Combustion Engine Division Fall Technical Conference*, vol. 56093, V001T04A004, 2013. DOI: https://doi.org/10.1115/ICEF2013-19199.

[65] A. Sappok, L. Bromberg, J. Parks, and V. Prikhodko, "Loading and regeneration analysis of a diesel particulate filter with a radio frequency-based sensor," *SAE Technical Paper*, vol. 1, pp. 1–18, 2126 2010. DOI: https://doi.org/10.4271/2010-01-2126.

[66] C. W. Vigild, S. C. Sorenson, and E. Hendricks, *The Internal Combustion Engine Modelling: Modelling, Estimation and Control Issues*. Ørsted, DTU, 2001, 2002, ISBN: 978-8-7879-5090-9.

[67] I. Kolmanovsky, P. Morall, M. V. Nieuwstadt, and A. Stefanopoulou, "Issues in modelling and control of intake flow in variable geometry turbocharged," *Chapman and Hall CRC research notes in mathematics*, pp. 436–445, 1999.

[68] S. Ahmed, M. Halesh, P. Aman, and V. Satish, "Modelling and simulation of virtual nox sensor for diesel engine using thermodynamic model," *IOP Conference Series: Materials Science and Engineering*, vol. 1189, pp. 12–38, 1 2021. DOI: https://doi.org/10.1088/1757-899X/1189/1/012038.

[69] P. M. Abelló, V. M. Iglesias, M. de los Santos López, and J. Álvarez-Flórez, "Real drive cycles analysis by ordered power methodology applied to fuel consumption, co2, nox and pm emissions estimation," *Frontiers of Environmental Science Engineering*, vol. 15, pp. 1–14, 4 2021. DOI: https://doi.org/10.1007/s11783-020-1296-z.

[70] P. Johnson, R. Chakrabarty, and B. Kumfer, "A modeling approach for soot formation in non-premixed flames with elevated stoichiometric mixture fraction," *Combustion and Flame*, vol. 229, p. 111 383, 2021. DOI: https://doi.org/10.1016/j.combustflame.2021.02.029.

[71] F. Jiang, M. Li, J. Wen, Z. Tan, and W. Zhou, "Optimization analysis of engine intake system based on coupling matlab-simulink with gt-power," *Mathematical Problems in Engineering*, vol. 2021, pp. 1–17, 2021. DOI: https://doi.org/10.1155/2021/6673612.

[72] M. Jadidi, L. D. Liddo, and S. Dworkin, "A long short-term memory neural network for the low-cost prediction of soot concentration in a time-dependent flame," *Energies*, vol. 14, p. 1394, 5 2021. DOI: https://doi.org/10.3390/en14051394.

[73] I. Umar, V. Nourani, and H. Gökçekuş, "A novel multi-model data-driven ensemble approach for the prediction of particulate matter concentration," *Environmental Science and Pollution Research*, vol. 28, pp. 49 663–49 677, 36 2021. DOI: https://doi.org/10.1007/s11356-021-14133-9.

[74] M. Koç and R. Şener, "Prediction of emission and performance characteristics of reactivity-controlled compression ignition engine with the intelligent software based on adaptive neural-fuzzy and neural-network," *Journal of Cleaner Production*, vol. 318, p. 128 642, 2021. DOI: https://doi.org/10.1016/j.jclepro.2021.128642.

[75] M. Rumaling, F. Chee, H. Chang, *et al.*, "Forecasting particulate matter concentration using nonlinear autoregression with exogenous input model," *Global Journal of Environmental Science and Management*, vol. 8, pp. 27–44, 1 2021. DOI: https://doi.org/10.22034/GJESM.2022.01.03.

[76] F. Kharroubi, M. Fertat, S. E. Hassani, and H. Ouahmane, "Design, simulation and control of a marine ship model's diesel engine using python and matlab/simulink," *Manufacturing Technology*, vol. 21, pp. 483–491, 4 2021. DOI: https://doi.org/10.21062/mft.2021.059.

[77] C. Ke, K. Han, Y. Huang, X. Wang, and S. Bai, "Neural network based nonlinear model predictive control for two-stage turbocharged diesel engine air-path system," *2021 33rd Chinese Control and Decision Conference (CCDC)*, 2021. DOI: https://doi.org/10.1109/CCDC52312.2021.9602515.

[78] V. K. Ahire, "Physics-based diesel engine model development calibration and validation for accurate cylinder parameters and nox prediction," *M.S. Thesis*, 2021. DOI: http://dx.doi.org/10.7912/C2/13.

[79] D. Singh, K. Pappacena, and J. L. Routbort, "Compact potentiometric O_2/nox sensor," *US DOE Annual Merit Review*, 2012.

[80] O. Brunel, F. Duault, B. Youssef, J. Lavy, and Y. Creff, "Smart soot sensor for particulate filter obd," *SAE International Journal of Passenger Cars – Electronic and Electrical Systems*, vol. 6, pp. 307–327, 1 2013. DOI: https://doi.org/10.4271/2013-01-1334.

[81] N. Miyamoto, H. Ogawa, and M. Nabi, "Approaches to extremely low emissions and efficient diesel combustion with oxygenated fuels," *International Journal of Engine Research*, vol. 1, pp. 71–85, 1 2000. DOI: https://doi.org/10.1243/1468087001545272.

[82] T. Kitamura, T. Ito, J. Senda, and H. Fujimoto, "Detailed chemical kinetic modeling of diesel spray combustion with oxygenated fuels," *SAE Transaction*, vol. 1, pp. 1560–1578, 1262 2001. DOI: https://doi.org/10.4271/2001-01-1262.

[83] T. Kitamura, T. Ito, J. Senda, and H. Fujimoto, "Mechanism of smokeless diesel combustion with oxygenated fuels based on the dependence of the equivalence ration and temperature on soot particle formation," *International Journal of Engine Research*, vol. 3, pp. 223–248, 4 2002. DOI: https://doi.org/10.1243/146808702762230923.

[84] J. Naber and D. Siebers, "Effects of gas density and vaporization on penetration and dispersion of diesel sprays," *SAE Technical Paper*, pp. 1–32, 1996. DOI: https://doi.org/10.4271/960034.

[85] D. Siebers, "Scaling liquid-phase fuel penetration in diesel sprays based on mixing-limited vaporization," *SAE Technical Paper*, vol. 1, pp. 1–28, 528 1999. DOI: https://doi.org/10.4271/1999-01-0528.

[86] R. Reitz and F. Bracco, "On the dependence of spray angle and other spray parameters on nozzle design and operating conditions," *SAE Technical Paper*, pp. 1–24, 1979. DOI: https://doi.org/10.4271/790494.

[87] N. Peters, *Turbulent combustion*. Cambridge University Press, Jan. 2010, ISBN: 978-0-5116-1270-1.

[88] D. Bradley, R. Hicks, M. Lawes, C. Sheppard, and R. Woolley, "The measurement of laminar burning velocities and markstein numbers for iso-octane–air and iso-octane–n-heptane–air mixtures at elevated temperatures and pressures in an explosion bomb," *Combustion and flame*, vol. 115, pp. 126–144, 1-2 1998. DOI: https://doi.org/10.1016/S0010-2180(97)00349-0.

[89] H. Hiroyasu and T. Kadota, "Models for combustion and formation of nitric oxide and soot in direct injection diesel engines," *SAE Technical Paper*, pp. 1–14, 1976. DOI: https://doi.org/10.4271/760129.

[90] M. Patterson, S. Kong, G. Hampson, and R. Reitz, "Modeling the effects of fuel injection characteristics on diesel engine soot and nox emissions," *SAE Technical Paper*, pp. 1–19, 1994. DOI: https://doi.org/10.4271/940523.

[91] A. Kazakov and D. Foster, "Modeling of soot formation during di diesel combustion using a multi-step phenomenological model," *SAE Technical Paper*, pp. 1–15, 1998. DOI: https://doi.org/10.4271/982463.

[92] V. Ahire, M. Shewale, and A. Razban, "A review of the state-of-the-art emission control strategies in modern diesel engines," *Archives of Computational Methods in Engineering*, vol. 28, pp. 4897–4915, 7 2021. DOI: https://doi.org/10.1007/s11831-021-09558-x.

[93] M. Shewale and A. Razban, "A control oriented soot prediction model for diesel engines using an integrated approach," *Proceedings of the ASME 2021 International Mechanical Engineering Congress and Exposition*, vol. 7A, pp. 1–5, 2021. DOI: https://doi.org/10.1115/IMECE2021-71502.

[94] M. Ammann, N. Fekete, L. Guzzella, and A. Glattfelder, "Model-based control of the vgt and egr in a turbocharged common-rail diesel engine theory and passenger car implementation," *SAE Technical Paper*, vol. 1, pp. 1–14, 0357 2003. DOI: https://doi.org/10.4271/2003-01-0357.

[95] C. Richard and R. Bishop, *Modern Control Systems*. Pearson, 2008, ISBN: 978-0-1344-0762-3.

[96] D. E. Kirk, *Optimal Control Theory: An Introduction*. Dover Publications, 2004, ISBN: 978-0-4864-3484-1.

[97] A. Ejiri, J. Sasaki, Y. Kinoshita, K. Shimotani, and R. Iizawa, "Transient control of air intake system in diesel engines," *Proceedings of SICE Annual Conference 2010*, pp. 503–508, 2010.

[98] L. Guzzella and C. Onder, *Introduction to Modeling and Control of Internal Combustion Engine Systems*. Springer, Jan. 2010, ISBN: 978-3-6421-0774-0.

[99] M. Jung, R. Ford, K. Glover, N. Collings, U. Christen, and M. Watts, "Parameterization and transient validation of a variable geometry turbocharger for mean-value modeling at low and medium speed-load points," *SAE Technical Paper*, vol. 1, pp. 1–16, 2729 2002. DOI: https://doi.org/10.4271/2002-01-2729.

[100] O. Storset, A. Stefanopoulou, and R. Smith, "Adaptive air charge estimation for turbocharged diesel engines without exhaust gas recirculation," *Journal of Dynamic Systems, Measurement, and Control*, vol. 126, pp. 633–643, 3 2004. DOI: https://doi.org/10.1115/1.1771691.

[101] X. An, B. Liu, F. Zhang, and G. Fu, "Simulation of the effect of intake charge oxygen concentration based egr on diesel engine performance," *Transactions of Chinese Society for Internal Combustion Engines*, vol. 31, pp. 115–119, 2 2013.

[102] J. Chauvin, G. Corde, and N. Petit, "Transient control of a diesel engine airpath," *2007 American Control Conference*, pp. 4394–4400, 2007. DOI: https://doi.org/10.1109/ACC.2007.4282942.

[103] K. Ogata, *Modern control engineering*. Pearson, 2010, ISBN: 978-0-1361-5673-4.

[104] Dieselhub. "6.7l cummins specs." (), [Online]. Available: http://www.cumminshub.com/67.html.

[105] G. Technologies. "Gt-power engine simulation software." (), [Online]. Available: https://www.gtisoft.com/gt-suite-applications/propulsion-systems/gt-power-engine-simulation-software/.

[106] G. Technologies. "Combustion and emissions." (), [Online]. Available: https://www.gtisoft.com/gt-suite-applications/propulsion-systems/combustion-and-emissions/.